University of Arkansas, Fayetteville
ScholarWorks@UARK

Theses and Dissertations

5-2013

On Chlorine Salts: Their Detection, Stability and Implications for Water on Mars and Europa

Jennifer Hanley
University of Arkansas, Fayetteville

Follow this and additional works at: http://scholarworks.uark.edu/etd

 Part of the Inorganic Chemistry Commons, Stars, Interstellar Medium and the Galaxy Commons, and the The Sun and the Solar System Commons

Recommended Citation
Hanley, Jennifer, "On Chlorine Salts: Their Detection, Stability and Implications for Water on Mars and Europa" (2013). *Theses and Dissertations*. 696.
http://scholarworks.uark.edu/etd/696

This Dissertation is brought to you for free and open access by ScholarWorks@UARK. It has been accepted for inclusion in Theses and Dissertations by an authorized administrator of ScholarWorks@UARK. For more information, please contact scholar@uark.edu, ccmiddle@uark.edu.

ON CHLORINE SALTS: THEIR DETECTION, STABILITY AND IMPLICATIONS FOR WATER ON MARS AND EUROPA

ON CHLORINE SALTS: THEIR DETECTION, STABILITY AND IMPLICATIONS FOR WATER ON MARS AND EUROPA

A dissertation submitted in partial fulfillment
of the requirements for the degree of
Doctor of Philosophy in Space and Planetary Sciences

By

Jennifer Hanley
Cornell University
Bachelor of Arts in Science of Earth Systems, 2006

May 2013
University of Arkansas

ABSTRACT

Chlorine salts (e.g. chlorides, chlorates and perchlorates) are an important factor in the stability of water on the surfaces of planetary bodies. Here we have shown that perchlorate and chlorate salts will lower the freezing point of water, allowing it to be liquid down to ~204 K. These salts will also slow down the evaporation rate, extending the lifetime of the liquid water solution. Chlorine salts have been detected on Mars, which has significant implications for the stability of water and hence its habitability. To study their effects on the stability of water on planetary surfaces, we need to first locate where these chlorine salts exist; this is typically done by remote sensing. To date, only anhydrous chlorides have been remotely detected, mostly due to the lack of hydrated chlorine salts in the spectral libraries used to identify features. To address this deficit, we measured reflectance spectra for numerous chlorine salts. Hydration bands were most common in near-infrared spectra, with band depth and width increasing with increasing hydration state. In the mid-infrared, oxychlorine salts exhibit spectral features due to Cl-O vibrations. We also investigated the spectral features of these salts at low temperature (80 K) to compare with remote sensing data of the outer satellites, specifically Europa. At low temperature, water bands become narrower and shallower than their room temperature counterparts. We show that chlorine salts do possess distinct spectral features that should allow for their detection by remote sensing, though care must be taken to acquire laboratory spectra of all hydrated phases at the relevant conditions (e.g. temperature, pressure) for the planetary body being studied.

This dissertation approved for recommendation
to the Graduate Council.

Dissertation Director:

_____
Dr. Vincent Chevrier

Dissertation Committee:

_____
Dr. John Dixon

_____
Dr. David Paul

_____
Dr. Larry Roe

DISSERTATION DUPLICATION RELEASE

I hereby authorize the University of Arkansas Libraries to duplicate this dissertation when needed for research and/or scholarship.

Agreed _____

Jennifer Hanley

Refused _____

Jennifer Hanley

ACKNOWLEDGMENTS

Portions of this work were funded by NASA's Mars Data Analysis Program Grant #NNX10AN81G. Other portions of the work were conducted at the Jet Propulsion Laboratory, California Institute of Technology, under contract of the National Aeronautics and Space Administration, through the Strategic University Research Partnership.

Special acknowledgements are given to: Dr. Vincent Chevrier for his role as my advisor; to Dr. J. Brad Dalton III for the use of his laboratory and extensive spectral knowledge; to Deanna Berget, Robert Adams, Chase Swaffer, Amir Francis and Holly Farris who were undergraduate interns in the Arkansas Center for Space and Planetary Sciences Research Experience for Undergraduates program, which is funded by a grant from the National Science Foundation, for project support; to Corey Jamieson; to Walter Graupner for technical assistance; and Scott Barrows for help with the spectral modeling.

And finally, a special thank you to all my friends, especially Scott Barrows, Edgard Rivera-Valentin and Patricia Gavin, who provided support and encouragement about the light at the end of the tunnel.

DEDICATION

This dissertation would not have been possible without the love and support of my entire family, but in particular my mom, who has been there for me every step of the way, with words of encouragement. I also could not have done this without Scott Barrows, who supported me in every way through this process. Thank you both.

TABLE OF CONTENTS

LIST OF FIGURES

LIST OF TABLES

LIST OF PAPERS

Chevrier, V. F., J. Hanley, and T. S. Altheide (2009), Stability of perchlorate hydrates and their liquid solutions at the Phoenix landing site, Mars, *Geophysical Research Letters*, 36, L10202, doi:10.1029/2009GL037497.

Hanley, J., V. F. Chevrier, D. J. Berget, and R. D. Adams (2012), Chlorate salts and solutions on Mars, *Geophysical Research Letters*, 39, L08201, doi:10.1029/2012GL051239.

1 Introduction

1.1 General Overview

Chlorine is expected to exist throughout the solar system and would be present on any body that has chondritic origins. Chlorine salts (e.g. chlorides, chlorates and perchlorates) would in turn occur on any body that has been altered by water in the past. For example, chlorides have even been found in martian meteorites (Sawyer et al., 2000).

These salts are important to the stability of water on the surfaces of planetary bodies. In their solid phase, they can be a reservoir of water, as hydration state can include up to 12 water molecules ($MgCl_2 \cdot 12H_2O$). Even more importantly, chlorine salts will lower the freezing point of water, allowing it to be liquid down to ~204 K (Hanley et al., 2012). They also slow down the evaporation rate, extending the lifetime of the liquid water solution.

To study their effects on the stability of water on planetary surfaces, we need to first locate where these chlorine salts exist. This is typically done by remote sensing. To date, only anhydrous chlorides have been remotely detected, mostly due to the lack of hydrated chlorine salts in the spectral libraries used to identify features.

In this dissertation, the specific effects of chlorine salts on the stability of water are investigated. Additionally, reflectance spectra are measured for numerous chlorine salts, showing that they do possess distinct spectral features that should allow for their detection by remote sensing.

1.1.1 Chlorine Salts on Mars

Chlorine has been ubiquitously detected on Mars, suggesting that its salts are important in understanding both the past and present stability of water. Chlorine is distributed globally on the martian surface (Figure 1-1) as detected by the Mars Odyssey Gamma Ray Spectrometer (GRS) (Keller et al., 2006). It is important to note, though, that this distribution is heterogeneous. From this it is unclear in what form the chlorine is present, but upper limits place the concentration at 1 wt% of the regolith. This is similar to values directly measured by various landed missions (Table 1-1): Vikings 1 and 2 (Clark et al., 1976), Pathfinder (Brückner et al., 2003; Wänke et al., 2001), Spirit (Gellert et al., 2004), Opportunity (Rieder et al., 2004) and Curiosity (Gellert et al., 2013).

Chlorides (Cl^-) and perchlorates (ClO_4^-) have been detected by Phoenix in the north polar plains (Hecht et al., 2009), and putatively by MSL at Gale Crater (Archer Jr. et al., 2013). Reanalysis of Viking data suggests perchlorates could have been present there as well (Navarro-González et al., 2010). Chlorates (ClO_3^-), which are almost as stable as perchlorates (Kang et al., 2006), are found on Earth everywhere that perchlorates exist (Rao et al., 2010), making them likely to be present on Mars as well (Hanley et al., 2012). Other oxidized chlorine salts, such as hypochlorites (ClO^-) and chlorites (ClO_2^-), may be present in limited quantities as precursors to the formation of perchlorate (Catling et al., 2010; Kang et al., 2006).

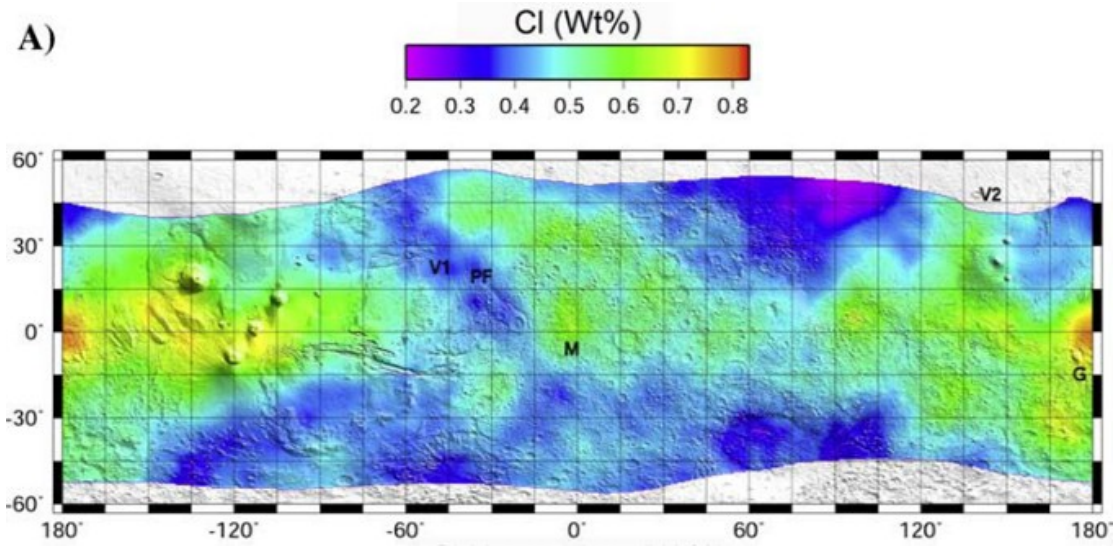

Figure 1-1. Distribution of equatorial and mid-latitude chlorine on Mars as detected by the Mars Odyssey GRS (Keller et al., 2006).

Table 1-1. Average measured concentrations (wt%) of chlorine at landing sites (Brückner et al., 2003; Clark et al., 1977; Clark et al., 1976; Gellert et al., 2013; Hecht et al., 2009; Rieder et al., 2004; Schmidt et al., 2008; Wänke et al., 2001). Note that Phoenix was the only lander to directly measure chloride and perchlorate concentrations, though Curiosity will be able to measure perchlorate if present.

	Chlorine	Chloride	Perchlorate
Curiosity	0.61-1.13	?	?
Phoenix	-	0.04	0.6
Spirit	0.2-1.94	-	-
Opportunity	0.33-0.68	-	-
Pathfinder	0.37-0.57	-	-
Viking 1	0.8 ± 0.3	-	-
Viking 2	0.6 ± 0.3	-	-

1.1.2 Chlorine Salts on Europa

Given its presumed chondritic composition, chlorine almost certainly exists on Europa. The idea of chlorine salts on icy satellites is extremely interesting with respect to the stability of water. Indeed, Europa is known to have other hydrated salts as part of its icy shell (McCord et al., 1998). Recent studies have acquired higher resolution spectral imaging of Europa's surface, finding new evidence to support the presence of magnesium sulfate on the trailing hemisphere (Brown and Hand, 2013), which is suggested to form by radiolysis of sulfur implantation from Io's torus. Since the feature associated with $MgSO_4$ is not seen on the leading hemisphere, it is suggested that the magnesium is originally brought to the surface as magnesium chloride. Given the supposed relative abundance of Na, K, and Mg in the subsurface ocean, the authors suggest that all three are associated with chloride on the leading hemisphere, but Na and K were preferentially sputtered off the surface at the same timescales as necessary to implant the sulfur; however, they were unable to detect the chloride salts because the spectra of the leading hemisphere was dominated by distorted water bands.

1.2 Effects of Chlorine Salts on the Stability of Water

Chlorine exists as an anion with various oxidation states ranging from -1 (Cl^-) to +7 (ClO_4^-). Between these exist three other oxyanions: hypochlorite (ClO^-), chlorite (ClO_2^-) and chlorate (ClO_3^-) (Table 1-2).

Chloride, perchlorate, and chlorate salts can all suppress the freezing temperature of water significantly, in some cases with a eutectic temperature down to 204 K (Altheide et al., 2009; Chevrier et al., 2009; Hanley et al., 2012). This is well below the mean annual surface temperature of Mars, and even below sub-polar temperatures during the summer (i.e. at the

Phoenix landing site), meaning that solutions of these salts would remain liquid for much of the day. Depending on the water vapor pressure, though, these solutions would likely be evaporating most of the day as well. For a few hours each day, at dawn and dusk, the temperature is above the eutectic, and the atmospheric water vapor pressure is higher than the saturation pressure of the solution, meaning that the liquid is neither frozen nor evaporating and therefore stable. Further exploring the stability of these salts in the presence of water would constrain the amount of liquid that has been present on the surface of Mars, and the longevity of such water.

Table 1-2. Oxidation states of chlorine (images from Wikimedia Commons).

Anion name	Chloride	Hypochlorite	Chlorite	Chlorate	Perchlorate
Formula	Cl^-	ClO^-	ClO_2^-	ClO_3^-	ClO_4^-
Oxidation state	-1	+1	+3	+5	+7
Structure		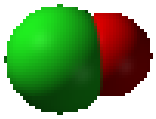	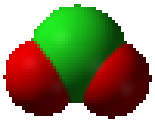	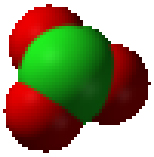	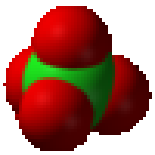

1.3 Detection

Anhydrous chloride salts are notoriously difficult to detect through remote sensing due to their lack of spectral features in the near-infrared (NIR) and mid-infrared (MIR). In fact, deposits of anhydrous chlorides have been seen in the southern highlands (Glotch et al., 2010; Osterloo et al., 2008; Ruesch et al., 2012), found *because of* their lack of spectral features. It is important to note, though, that there exist many stable hydrates of chlorine salts that could be detected by their hydration features, just as sulfates have been found. In fact, the dominant feature of all hydrated minerals in the NIR is that of water; therefore, many hydrated salts may be difficult to

distinguish from one another in mixed terrain. We have collected spectra for many of the chlorine salts that are likely to be on Mars.

1.3.1 Remote Sensing

Remote sensing by imaging spectroscopy is one of the most important ways to determine the composition of a planetary body. One particular technique is reflectance spectroscopy, which uses sunlight that has been scattered or reflected from a surface. In this context, spectral minima are representative of various absorption processes, based on the chemistry of the molecule. By comparing that spectrum with known laboratory spectra, it may be possible to find a match and determine which materials are present. Wavelengths for various features seen in reflectance spectroscopy of planetary surfaces are shown in Table 1-3.

Table 1-3. Ranges and types of spectral features commonly observed in remote sensing spectroscopy (Schmitt et al., 1998)

Range	Wavenumber	Wavelength	Types of features
FIR	~500 - 10 cm^{-1}	20 – 1000 μm	Pure rotational bands
MIR	4,000 – 500 cm^{-1}	2.5 – 20 μm	IR active fundamental bands (ro-vibrational), low order overtone and combinations modes
NIR	14,000 – 4,000 cm^{-1}	0.8 – 2.5 μm	Only overtone and combinations of fundamental bands
Vis	14,000 – 25,000 cm^{-1}	0.4 – 0.8 μm	Vibrational and electronic transitions
UV	> 25,000 cm^{-1}	< 0.4 μm	Electronic transitions

Three types of molecular physical processes cause spectral features typically seen in remote sensing data: electronic transitions, rotations and vibrations (Jensen, 2007). Electronic spectral features are generally due to vacant electron shells in transition metals, such as Fe. These are typically seen in the ultra-violet (UV) and visible (Vis) part of the spectrum. Rotation or vibration includes bending and stretching of bonds and is based on the bond energy.

Rotational features tend to occur in the far-infrared (FIR), while vibrational modes occur at lower wavelengths in the MIR. Overtones and combinations of these features are primarily seen in the NIR. For N molecules, there exist 3N-6 vibrational modes, or fundamentals. For instance, in H_2O there would be (3x3)-6 = 3 fundamentals. The characteristics of the normal vibration modes and the values of the permitted energy levels depend on the molecule's constituent atoms, their spatial geometry, and the magnitude of the binding forces between them (Hunt, 1977). In water, the three normal modes are designated v_1 (or v_{OH}, the symmetric OH stretch), v_2 (the HOH bend), and v_3 (the asymmetric OH stretch) (Crowley, 1991). Spectral features can also result from "overtones," which are integer multiples of the original mode, e.g. $2v_1$, caused by a double excitation, thus being released at double the energy (lower wavelength). Some vibrations can result in combination modes, which occur at the sum of the frequencies, e.g. $v_1 + v_3$ (Table 1-4). A rotational fundamental occurs in the gas phase at ~20 μm (Bayly et al., 1963). For this study, we are interested in liquid or solid water. The large shifts between phases are due to hydrogen bonding (Clark et al., 1990).

Table 1-4. Vibration, combination and overtone modes for water in gas, liquid and solid phases. Due to overlapping of various bands, some values must be approximated (Bayly et al., 1963; Clark et al., 1990; Cloutis et al., 2006; Hunt, 1977; Hunt et al., 1972).

Mode	Water Vapor	Liquid Water	Ice
v_1 (v_{OH})	2.738 μm	3.106 μm	3.105 μm
v_2	6.269 μm	6.08 μm	6.06 μm
v_3	2.663 μm	2.901 μm	2.941 μm
v_L	~20 μm		13 or 20 μm
$v_2 + v_3$	1.869 μm	~1.875 μm	1.96-2.05 μm
$2v_{OH}$	1.369 μm	1.553 μm	1.552 μm
$2v_2 + v_3$	1.439 μm	~1.454 μm	
$v_1 + v_3$	1.349 μm	~1.38 μm	
$v_1 + v_2 + v_3$	1.106 μm	1.135 μm	1.25 μm
$3v_{OH}$	0.913 μm	1.035 μm	1.035 μm
$2v_1 + v_3$	0.904 μm	~0.942 μm	1.04 μm

1.3.2 Spectral Analysis of Mars

The surface of Mars is currently being imaged in the NIR with two spectrometers: CRISM (Compact Reconnaissance Imaging Spectrometer) on board the Mars Reconnaissance Orbiter and OMEGA (Visible and Infrared Mineralogical Mapping Spectrometer) on board Mars Express. This study will focus primarily on the NIR spectra, as almost all of the vibration modes of water occur in this wavelength range (Table 1-4), and there exists a more complete spectral library in this range for future mineral identification.

1.3.3 Spectral Analysis of Europa

The surface of Europa has been imaged in the NIR with two spectrometers: NIMS (Near-Infrared Mapping Spectrometer) on board Galileo, and LEISA (Linear Etalon Imaging Spectral Array) on the New Horizons mission, during its Jupiter flyby. In the case of Europa, other factors must be taken into account other than simply looking at laboratory reflectance spectra. Temperature can influence the spectral reflectance of a material (Dalton et al., 2005; Pommerol and Schmitt, 2008). In general, the temperature effect is reversible within a given crystal phase. With colder temperatures, thermal contraction of the crystal shifts spectral features toward shorter wavelengths. Absorption bands shift up to 0.02-μm longer from 270 to 40 K, and band-width generally decreases with lower temperatures. In addition, hydrated salts appear to be more stable to the harsh radiation environment of Jupiter than pure water-ice (McCord et al., 2001), making it likely that hydrated salts are mixed with the water ice on Europa's surface.

1.4 Summary

Chlorine salts (chlorides, perchlorates and chlorates) are an important aspect of understanding the stability of water on Mars, as well as the potential habitability. Locating and identifying the types of chlorine salts present would help constrain both the current and past conditions; however, distinguishing hydrated chlorine salts from other hydrated minerals through remote sensing, especially when in a mixture, may prove difficult. The amount of chlorine salt that has been detected so far, mixed in the regolith, does not support large amounts of liquid water. Mixtures of chlorine and other salts, however, can lower the freezing temperature enough to support even lakes (Rivera-Valentin et al., 2013, Wray et al., 2011).

The purpose of this dissertation is to conduct a thorough investigation of the stability of chlorine salts in the presence of water, particularly in solution (Chapter 2 studies perchlorates (Chevrier et al., 2009) and Chapter 3 studies chlorates (Hanley et al., 2012)), as well as determine their NIR and MIR reflectance spectra in order to allow detection by remote sensing on other planets (Chapter 4 studies chloride spectra, Chapter 5 studies oxidized chlorine spectra, while Chapter 6 looks at all chlorine salts, but at low temperature).

1.5 References

Altheide, T., Chevrier, V., Nicholson, C., Denson, J., 2009. Experimental investigation of the stability and evaporation of sulfate and chloride brines on Mars. Earth and Planetary Science Letters. 282**,** 69-78.

Archer Jr., P. D., et al., 2013. Possible Detection of Perchlorates by Evolved Gas Analysis of Rocknest Soils: Global Implications. 44th Lunar and Planetary Science Conference. Lunar and Planetary Institute, Houston, pp. Abstract #2168.

Bayly, J. G., Kartha, V. B., Stevens, W. H., 1963. The absorption spectra of liquid phase H2O, HDO and D2O from 0·7 μm to 10 μm. Infrared Physics. 3**,** 211-222.

Brown, M. E., Hand, K. P., 2013. Salts and Radiation Products on the Surface of Europa. Astrophysical Journal. in press.

Brückner, J., Dreibus, G., Rieder, R., Wänke, H., 2003. Refined data of Alpha Proton X-ray Spectrometer analyses of soils and rocks at the Mars Pathfinder site: Implications for surface chemistry. Journal of Geophysical Research. 108**,** 8094.

Catling, D. C., et al., 2010. Atmospheric origins of perchlorate on Mars and in the Atacama. Journal of Geophysical Research. 115**,** E00E11.

Chevrier, V. F., Hanley, J., Altheide, T. S., 2009. Stability of perchlorate hydrates and their liquid solutions at the Phoenix landing site, Mars. Geophysical Research Letters. 36**,** L10202.

Clark, B. C., et al., 1977. The Viking X Ray Fluorescence Experiment: Analytical methods and early results. Journal of Geophysical Research. 82**,** 4577-4594.

Clark, B. C., et al., 1976. Inorganic Analyses of Martian Surface Samples at the Viking Landing Sites. Science. 194**,** 1283-1288.

Clark, R. N., King, T. V. V., Klejwa, M., Swayze, G. A., Vergo, N., 1990. High Spectral Resolution Reflectance Spectroscopy of Minerals. Journal of Geophysical Research. 95**,** 12653-12680.

Cloutis, E. A., et al., 2006. Detection and discrimination of sulfate minerals using reflectance spectroscopy. Icarus. 184**,** 121-157.

Crowley, J. K., 1991. Visible and Near-Infrared (0.4-2.5 μm) Reflectance Spectra of Playa Evaporite Minerals. Journal of Geophysical Research. 96**,** 16231-16240.

Dalton, J. B., Prieto-Ballesteros, O., Kargel, J. S., Jamieson, C. S., Jolivet, J., Quinn, R., 2005. Spectral comparison of heavily hydrated salts with disrupted terrains on Europa. Icarus. 177**,** 472-490.

Gellert, R., et al., 2013. Initial MSL APXS Activities and Observations at Gale Crater, Mars. 44th Lunar and Planetary Science Conference. Lunar and Planetary Institute, Houston, pp. Abstract #1432.

Gellert, R., et al., 2004. Chemistry of rocks and soils in Gusev Crater from the Alpha Particle X-ray Spectrometer. Science. 305**,** 829-832.

Glotch, T. D., Bandfield, J. L., Tornabene, L. L., Jensen, H. B., Seelos, F. P., 2010. Distribution and formation of chlorides and phyllosilicates in Terra Sirenum, Mars. Geophysical Research Letters. 37**,** L16202.

Hanley, J., Chevrier, V. F., Berget, D. J., Adams, R. D., 2012. Chlorate salts and solutions on Mars. Geophysical Research Letters. 39**,** L08201.

Hecht, M. H., et al., 2009. Detection of Perchlorate and the Soluble Chemistry of Martian Soil at the Phoenix Lander Site. Science. 325**,** 64-67.

Hunt, G. R., 1977. Spectral Signatures of Particulate Minerals in the Visible and Near Infrared. Geophysics. 42**,** 501-513.

Hunt, G. R., Salisbury, J. W., Lenhoff, C. J., 1972. Visible and near-infrared spectra of minerals and rocks: V. Halides, phosphates, arsenates and borates. Modern Geology. 3**,** 121-132.

Jensen, J. R., 2007. Remote Sensing of the Environment: An Earth Resource Perspective. Pearson Education, Inc.

Kang, N., Anderson, T. A., Andrew Jackson, W., 2006. Photochemical formation of perchlorate from aqueous oxychlorine anions. Analytica Chimica Acta. 567**,** 48-56.

Keller, J. M., et al., 2006. Equatorial and midlatitude distribution of chlorine measured by Mars Odyssey GRS. J. Geophys. Res. 111**,** E03S08.

McCord, T. B., et al., 1998. Salts on Europa's Surface Detected by Galileo's Near Infrared Mapping Spectrometer. Science. 280**,** 1242-1245.

McCord, T. B., et al., 2001. Thermal and radiation stability of the hydrated salt minerals epsomite, mirabilite, and natron under Europa environmental conditions. Journal of Geophysical Research. 106**,** 3311-3319.

Navarro-González, R., Vargas, E., de la Rosa, J., Raga, A. C., McKay, C. P., 2010. Reanalysis of the Viking results suggests perchlorate and organics at midlatitudes on Mars. Journal of Geophysical Research. 115**,** E12010.

Osterloo, M. M., et al., 2008. Chloride-Bearing Materials in the Southern Highlands of Mars. Science. 319**,** 1651-1654.

Pommerol, A., Schmitt, B., 2008. Strength of the H2O near-infrared absorption bands in hydrated minerals: Effects of particle size and correlation with albedo. Journal of Geophysical Research. 113**,** E10009.

Rao, B., et al., 2010. Natural Chlorate in the Environment: Application of a New IC-ESI/MS/MS Method with a Cl18O3- Internal Standard. Environmental Science & Technology. 44**,** 8429-8434.

Rieder, R., et al., 2004. Chemistry of Rocks and Soils at Meridiani Planum from the Alpha Particle X-ray Spectrometer. Science. 306**,** 1746-1749.

Rivera-Valentin, E. G., Chevrier, V., Marnocha, C., 2013. Journal of Geophysical Research. under review.

Ruesch, O., et al., 2012. Compositional investigation of the proposed chloride-bearing materials on Mars using near-infrared orbital data from OMEGA/MEx. Journal of Geophysical Research: Planets. 117.

Sawyer, D. J., McGehee, M. D., Canepa, J., Moore, C. B., 2000. Water soluble ions in the Nakhla martian meteorite. Meteoritics & Planetary Science. 35**,** 743-747.

Schmidt, M. E., et al., 2008. Hydrothermal origin of halogens at Home Plate, Gusev Crater. Journal of Geophysical Research: Planets. 113.

Schmitt, B., Quirico, E., Trotta, F., Grundy, W. M., 1998 Optical Properties of Ices from UV to Infrared. In: B. Schmitt, C. D. Bergh, M. Festou, (Eds.), Solar System Ices. Kluwer Academic Publishers, pp. 199-240.

Wänke, H., Brückner, J., Dreibus, G., Rieder, R., Ryabchikov, I., 2001. Chemical Composition of Rocks and Soils at the Pathfinder Site. Space Science Reviews. 96**,** 317-330.

Wray, J. J., et al., 2011. Columbus crater and other possible groundwater-fed paleolakes of Terra Sirenum, Mars. Journal of Geophysical Research: Planets. 116**,** E01001.

2 Stability of Perchlorate Hydrates and Their Liquid Solutions at the Phoenix Landing Site, Mars

2.1 Abstract

We studied the low-temperature properties of sodium and magnesium perchlorate solutions as potential liquid brines at the Phoenix landing site. We determined their theoretical eutectic values to be 236 ± 1 K for 52 wt% sodium perchlorate and 206 ± 1 K for 44.0 wt% magnesium perchlorate. Evaporation rates of solutions at various concentrations were measured under martian conditions, and range from 0.07 to 0.49 mm h^{-1} for $NaClO_4$ and from 0.06 to 0.29 mm h^{-1} for $Mg(ClO_4)_2$. The extrapolation to Phoenix landing site conditions using our theoretical treatment shows that perchlorate are liquid during the summer for at least part of the day, and exhibit very low evaporation rates. Moreover, magnesium perchlorate eutectic solutions are thermodynamically stable over vapor and ice during a few hours a day. We conclude that liquid brines may be present and even stable for short periods of time at the Phoenix landing site.

2.2 Introduction

NASA Phoenix landed on the surface of Mars on May 25, 2008, in the Vastitas Borealis plains at 68.22°N 234.25°E, a region dubbed "Green Valley", and performed an extensive set of physical and chemical analyses aimed at characterizing the history of water and potential habitability of the martian subsurface. While the direct observation of ice was an important discovery, a big surprise was the detection of the perchlorate ion ClO_4^- by the MECA (Microscopy, Electrochemistry, and Conductivity Analyzer) instrument [*Hecht et al.*, 2009; *Kounaves et al.*, 2009].

Perchlorate is a strongly oxidized ion (Cl in the +7 oxidation state) and is extremely rare on the surface of the Earth: its natural occurrences are limited to hyper arid environments such as the Atacama Desert in Chile where perchlorate is present as a few percent associated with nitrate deposits [*Ericksen*, 1981]. Although nitrates have not been detected, perchlorates are part of a saline alkaline paragenesis dominated by chlorine [*Kounaves et al.*, 2009], and may constitute a significant component in other regions where chlorides have been identified [*Osterloo et al.*, 2008]. In this case, the determination of perchlorate thermodynamic and kinetic properties would help elucidate the reactivity of the soil at the Phoenix landing site, and also the potential presence of liquid water [*Renno et al.*, 2009].

Therefore, we present a study of the stability of perchlorate solutions on Mars. We calculated the thermodynamic stability diagrams of two martian perchlorates relevant to Mars [*Marion et al.*, 2009]: sodium ($NaClO_4$) and magnesium ($Mg(ClO_4)_2$), in order to determine the conditions suitable for the formation of liquid solutions. We investigated the evaporation rates of these solutions as a function of temperature and concentration, to evaluate their resident times on the surface.

2.3 Methods

Solutions were made using D.I. water and sodium perchlorate ($NaClO_4.H_2O$, EMD product #SX0694-1) at concentrations 20, 30, 40 and 55 wt% (± 0.5%), and magnesium perchlorate ($Mg(ClO_4)_2$, Alfa Aesar product #11636) at concentrations 20, 30, 40 and 49 wt% (± 0.5%). Evaporation rates of the perchlorate solutions were measured in our 0.6 m^3 Mars simulation chamber [*Chevrier and Altheide*, 2008; *Sears and Chittenden*, 2005; *Sears and Moore*, 2005] under 7 ± 0.01 mbar of pure CO_2 at temperatures ranging from 255 K to 275 K

(Table 2-1). The atmosphere was first evacuated from the chamber by lowering the pressure under 0.06 mbar. The chamber was then filled with pure CO_2 to atmospheric pressure and cooled below 273 K. Once filled with CO_2, the chamber was opened and the sample placed on a loading analytical balance. The platform supporting the balance set-up was then lowered into the chamber, the lid sealed, and the pressure pumped down to 7 mbar. Once the pressure reached 7 mbar, we waited 20 min to accommodate the instruments to the new conditions. Then we started recording mass, temperature (chamber and sample), pressure, and relative humidity (Table 2-1). The pressure was maintained at 7.00 ± 0.01 mbar during the whole experiment and the atmosphere was continuously exchanged to maintain the relative humidity (RH) below 1%.

2.4 Stability Diagrams and Eutectic Determination

Vapor pressure of liquid solutions are controlled by temperature and composition. Therefore, we calculated the stability diagram of Mg and Na-perchlorates as a function of concentration and temperature. Such diagrams are also useful to determine the hydration state of the salt depending on temperature. Perchlorate solubility data are scarce and most thermodynamic parameters (Gibbs free energy and enthalpy) are unknown. Therefore, we used theoretical calculations and adjusted the thermodynamic parameters to obtain the best fit of existing data. We determined the eutectic temperature and concentration for each salt, by calculating the theoretical intercept between the liquid-ice liquidus (concentration below the eutectic) and the liquidus of the salt hydrate (concentration above the eutectic). The activities of ions and water were calculated using the Pitzer ion interaction model [*Pitzer*, 1991].

The calculations require the hydration state of the salt at the eutectic. $NaClO_4$ possesses three degrees of hydration: 0, 1 and 2 [*Chretien and Kohlmuller*, 1966], whereas $Mg(ClO_4)_2$ has

five hydration states: 0, 2, 3, 4 and 6 [*Dobrynina et al.*, 1980; *Krivtsov et al.*, 1989; *Smith et al.*, 1924; *Willard and Smith*, 1922]. All the details of the calculations, approximations, and parameters are presented in the section 2.10.1 of the supplementary materials.

The results of the calculations indicate that the eutectic of $NaClO_4$ is 236 ± 1 K for 52 wt% concentration (Figure 2-1A), whereas the eutectic of $Mg(ClO_4)_2$ is 206 ± 1 K for 44.0 wt% (Figure 2-1B). Both values are very close to previous determinations: 239 K for $NaClO_4$ [*Chretien and Kohlmuller*, 1966], and 204.5 K [*Marion et al.*, 2009; *Pestova et al.*, 2005] or 206 K [*Dobrynina et al.*, 1980] for $Mg(ClO_4)_2$. Mg-perchlorate remains liquid at much lower temperatures than Na-perchlorate and has one of the lowest observed eutectics, close to ferric sulphate (205 K according to Chevrier and Altheide, 2008). The transition from sodium perchlorate dihydrate to the monohydrate occurs at 259.9 K, which in turns transforms into the anhydrous form at 326.3 K (Figure 2-1A). Experimental data and calculations indicate that $Mg(ClO_4)_2.6H_2O$ appears stable over a large range of temperatures (Figure 2-1B, Dobrynina *et al.*, 1980). Thermal analyses indicate only one transition to the trihydrate phase at around 420-434 K [*Mikuli et al.*, 1998; *Willard and Smith*, 1922] or the 4-hydrate at 409 K [*Dobrynina et al.*, 1980]. The 2 and 4 hydrates are obtained through dehydration [*Besley and Bottomley*, 1969; *Krivtsov et al.*, 1989], or direct precipitation [*Dobrynina et al.*, 1980].

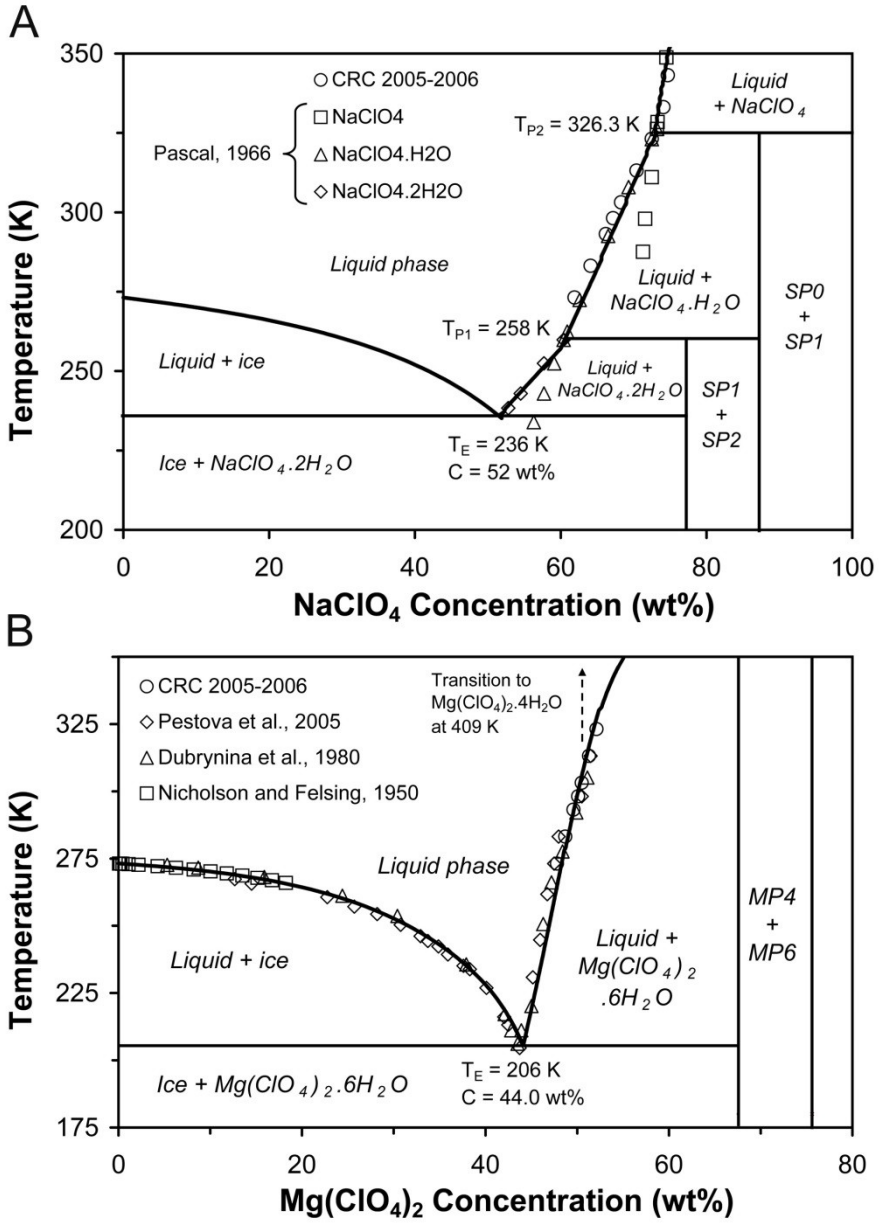

Figure 2-1. Stability diagrams of **(A)** sodium and **(B)** magnesium perchlorate solutions, as a function of temperature and salt concentration. Thick lines indicate calculated equilibrium lines (see supplementary materials for methods of calculation). The symbols indicate data gathered from various sources. T_E is the eutectic point, T_P are the peritectic points. Sodium perchlorate data are from [*Chretien and Kohlmuller*, 1966; *CRC*, 2005-2006] and magnesium perchlorate data from [*CRC*, 2005-2006; *Dobrynina et al.*, 1980; *Nicholson and Felsing*, 1950; *Pestova et al.*, 2005].

2.5 Evaporation Results

We determined the evaporation rates of perchlorate solutions exposed to 7.00 ± 0.01 mbar of CO_2 at temperatures between 255 K and 275 K (Figure 2-2). Evaporation rates were calculated by dividing the mass loss data by the surface area of the sample and its density (Table 2-1). Evaporation rates of $NaClO_4$ solutions range from 0.07 to 0.49 mm h^{-1}, and from 0.06 to 0.29 mm h^{-1} for $Mg(ClO_4)_2$ brines. The error on the evaporation rate results from the error on the regression line (< 5%), the incertitude of the balance (0.01 g), and the error on the measurement of the density. The 1σ error is generally below 10% and we use this value as a standard error. Our data show that the evaporation rate is dependent on the temperature of the liquid. For example, the 40 wt% $NaClO_4$ solutions drops from 0.37 mm h^{-1} at 267 K to 0.11 mm h^{-1} at 256.5 K, i.e. a factor 3 over a range of 10 K (Figure 2-2A). Similarly the 49 wt% $Mg(ClO_4)_2$ shows a factor 3 decrease over 12 K. This is in agreement with our previous studies [*Chevrier and Altheide*, 2008; *Sears and Chittenden*, 2005], and is mostly related to the temperature dependency of the saturation vapor pressure of water, which controls the density gradient between the surface and the atmosphere [*Ingersoll*, 1970].

As we previously observed for other salts [*Chevrier and Altheide*, 2008], the evaporation rate also depends on the salt concentration: at 266 K, the 20 wt% $NaClO_4$ solution evaporates at 0.49 mm h^{-1} and at 0.14 mm h^{-1} for the 55 wt% sample. Magnesium perchlorate solutions show similar behavior: at 264 K, the 20 wt% $Mg(ClO_4)_2$ solution evaporates at 0.29 mm h^{-1}, compared to 0.07 mm h^{-1} for 49 wt% (Figure 2-2B).

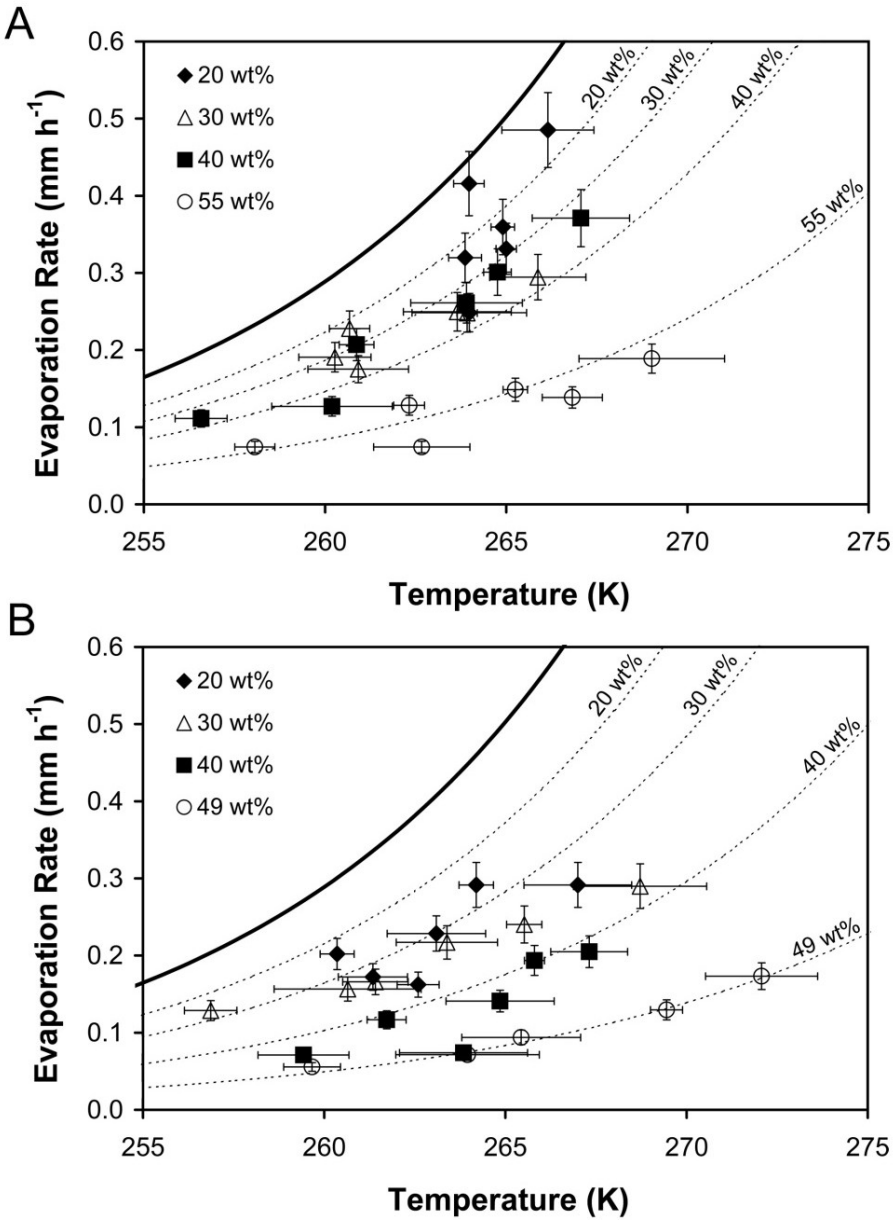

Figure 2-2. Evaporation rates of **(A)** sodium and **(B)** magnesium perchlorates as a function of sample temperature for various concentrations. The thick black curve is the theoretical line for evaporation of supercooled liquid water [Murphy and Koop, 2005]. Each dashed line represents the theoretical evaporation rate of liquid solutions with concentrations of perchlorate corresponding to experimental values (see sec 2.10.2 for methods of calculations).

2.6 Discussion

At martian surface conditions, the mono- and dihydrate sodium perchlorates and the magnesium perchlorate hexahydrate are the most relevant phases. Magnesium perchlorate is highly hygroscopic, but this is valid only for the trihydrate form [*Smith et al.*, 1924; *Willard and Smith*, 1922]. Its temperature of formation (~420 to 434 K) is too high for the surface of Mars, even in the equatorial regions, and it is probable that the hexahydrate is the most stable form. Other hydration states, 4 and 2, may be possible in low humidity conditions [*Krivtsov et al.*, 1989]. Large variations of humidity could induce variations in hydration state of magnesium perchlorate, in a similar way as for magnesium sulfate [*Vaniman et al.*, 2004]. However, further work on the effect of humidity would be necessary to determine the stability on these hydrates.

To determine the formation conditions of liquids at the Phoenix landing site, we compared the eutectic temperatures of each perchlorate to the temperatures during the coldest and warmest days [*Hudson et al.*, 2009]. Results show that sodium perchlorate is liquid for about 8 hours only during the warmest day, whereas magnesium perchlorate remains liquid for nearly 18 hours during the warmest day and 12 hours during the coldest (Figure 2-3A). Thus, the presence of metastable liquids at the Phoenix landing site is possible.

Using our model [*Chevrier and Altheide*, 2008], we calculated the evaporation rates of saturated perchlorate solutions at the Phoenix landing site during the coldest and warmest summer days [*Hudson et al.*, 2009], using smoothed temperature data (Figure 2-3A). The evaporation rates are also dependent on the total pressure and on the humidity in the atmosphere. We used the water vapor measured by the Thermal and Electrical Conductivity Probe TECP onboard Phoenix [*Hudson et al.*, 2009] and averaged the data using a Gaussian fit (Figure 2-3B), allowing us to calculate the average humidity at any time of the day. Using the LMD Mars

Global Circulation Model GCM, we determined the total pressure [*Forget et al.*, 1999] to be ~ 8 mbar at L_S 90-120, almost identical to the values measured by Phoenix [*Taylor et al.*, 2009]. Contrary to the total pressure, the water partial pressure determined from the LMD-GCM is very different from the measured value. The GCM values appear nearly constant while the measured values show variations of two orders of magnitude (Figure 2-3B). Since the GCM does not include regolith-atmosphere coupling, this suggests that the humidity is controlled by the regolith.

Integration of the evaporation rates over a full day shows that ~80 μm of $Mg(ClO_4)_2$ or $NaClO_4$ would evaporate during the warmest day (Figure 2-3C). The difference in the water activity 0.69 for $NaClO_4$ and 0.54 for $Mg(ClO_4)_2$, results in a slightly higher saturation pressure on $NaClO_4$ brine than on a brine of $Mg(ClO_4)_2$ (Figure 2-3B). Sodium perchlorate is frozen for a large part of the day, while magnesium perchlorate remains liquid for much longer, and thus could evaporate for longer durations (Figure 2-3C). On the coldest day, $NaClO_4$ is completely frozen (Figure 2-3A), while $Mg(ClO_4)_2$ remains frozen during almost half the day. The cumulative evaporation rate of $Mg(ClO_4)_2$ is only 4 μm (Figure 2-3C), due to the strong dependency of the evaporation rate on temperature.

The effect of humidity on the evaporation rate is almost negligible; evaporation of the solutions in a completely dry atmosphere results in a difference of only ~1 μm per day. Most of the evaporation occurs during the warmer periods, when the water pressure on the surface is several orders of magnitude higher than the atmospheric water vapor. Since the evaporation rate is a linear function of the humidity, but an exponential function of the temperature (through the saturation pressure), the humidity does not show large enough variations (Figure 2-3B) to affect the evaporation rate.

The more significant effect of humidity occurs during the evening or the early morning, when the equilibrium water vapor on the surface of the liquid drops under the atmospheric humidity (Figure 2-3B). For $Mg(ClO_4)_2$, the liquid temperature is above the freezing temperature (206 K) but under the temperature at which the equilibrium water vapor is above the atmospheric vapor (~215 K, Figure 2-3C), allowing the liquid to be thermodynamically stable between 6 and 7 PM and between 8 and 10 AM. Interestingly, these periods correspond exactly to the observations by Phoenix of large variations of dielectric permittivity [*Zent et al.*, 2009]. Moreover, the liquid is paradoxically stable during the coldest day, since high temperatures during the warmest day result in continual evaporation (Figure 2-3C). For sodium perchlorate, the frozen period is much longer than the liquid stability period (Figure 2-3C), and thus liquid is never stable with respect to ice or vapor, but only frozen or evaporating.

The presence of liquids in the regolith, even in low concentrations could have had significant effects on the stickiness of the soil, depending on the day (warm / cold) and the hour. Salts stable at very low-temperatures often show high viscosities at temperatures close to their eutectics [*Chevrier et al.*, 2009], as verified for strontium perchlorate [*Pestova et al.*, 2005]. Yet, application to magnesium perchlorate remains to be verified by experimental measurements.

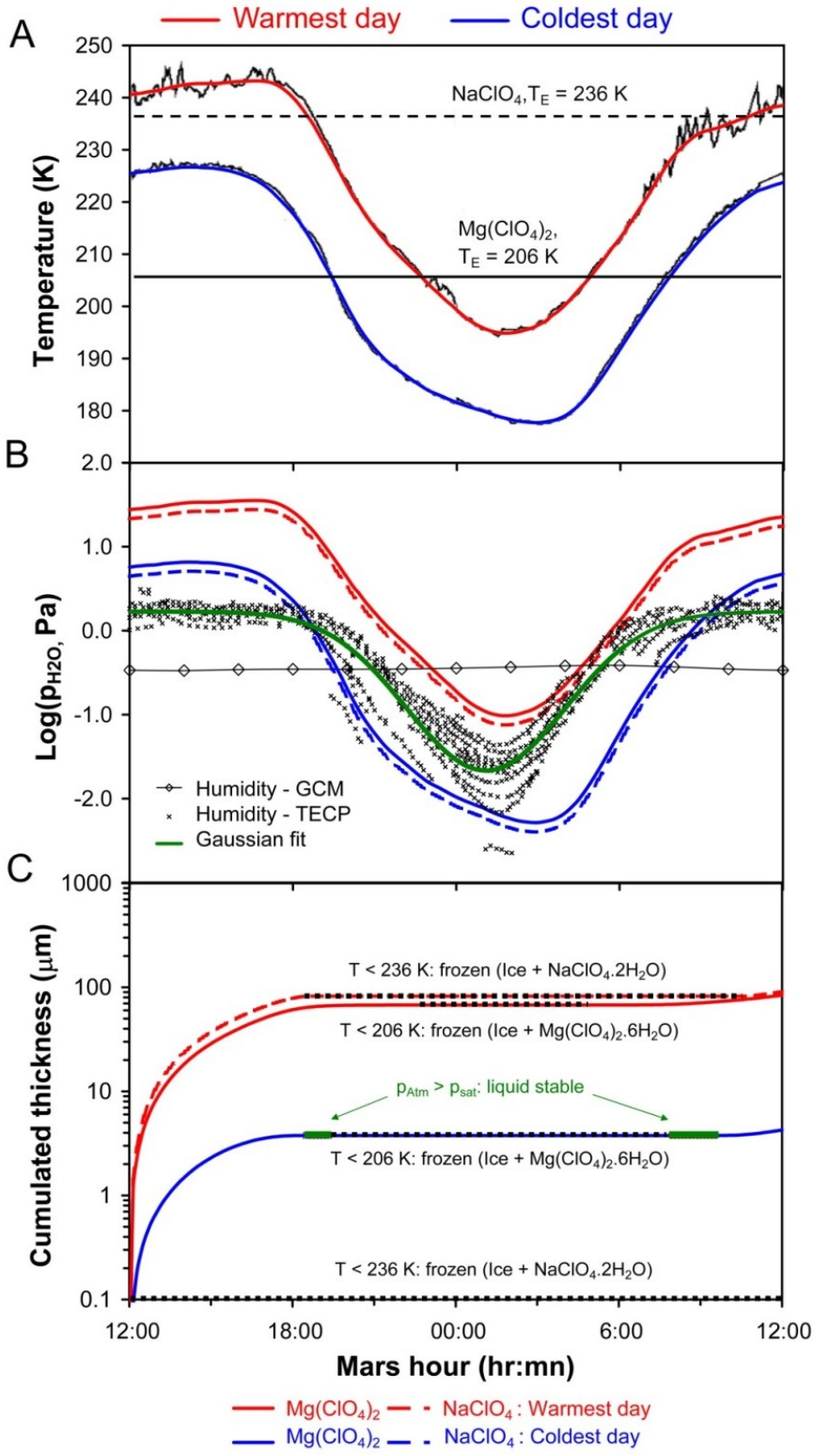
A
Warmest day
Coldest day
Temperature (K)
NaClO4,TE = 236 K
Mg(ClO4)2,
TE = 206 K
B
Log(pH2O, Pa)
Humidity - GCM
Humidity - TECP
Gaussian fit
C
Cumulated thickness (μm)
T < 236 K: frozen (Ice + NaClO4.2H2O)
T < 206 K: frozen (Ice + Mg(ClO4)2.6H2O)
pAtm > psat: liquid stable
T < 206 K: frozen (Ice + Mg(ClO4)2.6H2O)
T < 236 K: frozen (Ice + NaClO4.2H2O)
12:00
18:00
00:00
6:00
12:00
Mars hour (hr:mn)
Mg(ClO4)2 — NaClO4 : Warmest day
Mg(ClO4)2 — NaClO4 : Coldest day

Figure 2-3. Stability of magnesium and sodium perchlorate solutions at the Phoenix landing site. **(A)** Temperatures of the coldest and warmest days as a function of time as measured by the Phoenix lander (black curves), adapted from [Hudson et al., 2009]. The superimposed red and blue curves are smoothed curves of the data, used for the calculations of evaporation rates. The two horizontal lines represent the eutectic temperatures for Na and Mg perchlorates (Fig. 2-1). Temperatures are often above the eutectic for both salts during several hours of the day, allowing liquids to form. **(B)** Logarithm of the water vapor pressure as a function of the time of day. The small crosses are the humidity data as measured by the Thermal and Electrical Conductivity Probe TECP [*Hudson et al.*, 2009]. The thick green line is the Gaussian fit on the water vapor data used to calculate the evaporation rates. The thin line with diamonds is the water vapor calculated using the Global Circulation Model [*Forget et al.*, 1999]. Notice the strong difference between the TECP measurements and the GCM, indicating strong coupling of water vapor between the soil and the atmosphere. The thick blue and red lines are the equilibrium vapor pressures above the solutions during the coldest and warmest days, respectively – dashed for sodium perchlorate and solid for magnesium perchlorate – calculated using the equation for supercooled water [*Murphy and Koop*, 2005] and the activity of water [*Pitzer*, 1991]. **(C)** Logarithm of cumulative thickness of evaporated solution for each salt (dashed line: $NaClO_4$, solid line: $Mg(ClO_4)_2$, top red lines for the warmest day and bottom blue lines for the coldest day). Superimposed thick dotted black lines indicate the periods where the temperature is under the eutectic, and thus where liquid is frozen. The thick superimposed green lines on the Mg-perchlorate during the coldest day is the period during which the equilibrium water vapor pressure is under the ambient pressure in the atmosphere, and thus where condensation occurs instead of evaporation. This indicates that liquid is thermodynamically stable.

2.7 Conclusions

We have studied the stability of liquid solutions of sodium and magnesium perchlorates on the surface of Mars, using a combination of experimental measurements and thermodynamic and kinetic calculations. Magnesium and sodium perchlorate liquids are metastable during the day, due to low eutectic temperatures, although magnesium perchlorate is more stable due to its much lower eutectic temperature, 206 K versus 236 K for sodium perchlorate. Despite the very low evaporation rates of liquids, which possibly allow them to last several days, their metastability at longer timescales requires a replenishing process such as seasonal high humidity or deliquescence during periods of high obliquity. Indeed, during limited periods of time in the

evening and early morning, eutectic solutions of magnesium perchlorate are thermodynamically stable and could actually form and reabsorb the water lost during the evaporation periods, explaining the humidity swings. In contrast, sodium perchlorate eutectic solutions are never stable. Therefore, the liquid indirectly observed by Phoenix, if present may be a eutectic solution of magnesium perchlorate.

2.8 Acknowledgements

We thank Derek Sears, Giles Marion and Michael Hecht for the discussion on the stability and nature of perchlorates at the Phoenix landing site. We also thank Chris McKay and an anonymous reviewer for helping improve our manuscript.

2.9 References

Besley, L. M., and G. A. Bottomley (1969), The water vapour equilibria over magnesium perhclorate hydrates, *J. Chem. thermodynamics*, *1*(1), 13-19.

Chevrier, V., and T. S. Altheide (2008), Low Temperature Aqueous Ferric Sulfate Solutions on the Surface of Mars, *Geophys. Res. Lett.*, *35*(L22101), doi: 10.1029/2008GL035489.

Chevrier, V., R. Ulrich, and T. S. Altheide (2009), Viscosity of Liquid Ferric Sulfate Solutions and Application to the Formation of Gullies on Mars, *J. Geophys. Res.*, *In press*.

Chretien, A., and R. Kohlmuller (1966), Perchlorate de Sodium, in *Nouveau Traite de Chimie Minerale, Vol 2 (#1), Sodium and Lithium*, edited by P. Pascal, pp. 344-354, Masson & Cie, Paris, France.

CRC (2005-2006), *CRC Handbook of Chemistry and Physics, 86th Edition*, CRC Press, Taylor & Francis Group Boca Raton, Florida.

Dobrynina, T. A., A. M. Chernyshova, N. A. Akhapkina, and V. Y. Rosolovskii (1980), Fusion diagram of the magnesium perchlorate-water system, *Russian Journal of Inorganic Chemistry*, *25*, 2233-2236.

Ericksen, G. E. (1981), Geology and origin of the Chilean nitrate deposits, *Geological Survey Professional Paper #1188*.

Forget, F., F. Hourdin, R. Fournier, C. Hourdin, O. Talagrand, M. Collins, S. R. Lewis, P. L. Read, and J. P. Huot (1999), Improved general circulation models of the Martian atmosphere from the surface to above 80 km, *J. Geophys. Res.*, *104*(E10), 24,155-124,175.

Hecht, M. H., D. C. Catling, B. C. Clark, L. DeFlores, K. Gospodinova, J. Kapit, S. P. Kounaves, D. W. Ming, R. C. Quinn, S. J. West, and S. M. M. Young (2009), Perchlorate in Martian soil: Evidence and implications, *LPSC*, *XL*(2420).

Hudson, T. L., A. Zent, M. H. Hecht, S. Wood, and D. Cobos (2009), Near-surface humidity at the Phoenix landing site as measured by the Thermal and Electrical Conductivity Probe (TECP), *LPSC*, *XL*(#1804).

Ingersoll, A. P. (1970), Mars: Occurrence of liquid water, *Science*, *168*(3934), 972-973.

Kounaves, S. P., D. Catling, B. C. Clark, L. DeFlores, K. Gospodinova, M. H. Hecht, J. Kapit, D. W. Ming, and R. C. Quinn (2009), Aqueous carbonate chemistry of the martian soil at the Phoenix landing site, *LPSC*, *XL*(2489).

Krivtsov, N. V., Z. K. Nikitina, and V. Y. Rosolovs (1989), Thermochemical properties of anydrous and hydrated alkaline-earth metal and magnesium perchlorates, *Russian Chemical Bulletin*, *38*(9), 1817-1822.

Marion, G. M., D. C. Catling, M. Claire, and K. J. Zahnle (2009), Modeling aqueous perchlorate chemistries with application to Mars, *LPSC*, *XL*(1959).

Mikuli, E., A. Migdal-Mikuli, and J. Mayer (1998), Phase transitions in crystalline [M(H2O)6](ClO4)2 (M=Mg, Mn, Fe, Co, Ni, Cu, Zn, Cd and Hg), *J. Thermal. Anal.*, *54*(1), 93-102.

Murphy, D. M., and T. Koop (2005), Review of the vapour pressures of ice and supercooled water for atmospheric applications, *Quart. J. R. Meteor. Soc.*, *131*, 1539-1565.

Nicholson, D. E., and W. A. Felsing (1950), The Determination of the Activity Coefficients of the Alkaline Earth and Magnesium Perchlorates from Freezing Point Data, *J. Amer. Chem. Soc.*, *72*(10), 4469-4471.

Osterloo, M. M., V. E. Hamilton, J. L. Bandfield, T. D. Glotch, A. M. Baldridge, P. R. Christensen, L. L. Tornabene, and F. S. Anderson (2008), Chloride-Bearing Materials in the Southern Highlands of Mars, *Science*, *319*, 1651-1654.

Pestova, O. N., L. A. Myund, M. K. Khripun, and A. V. Prigaro (2005), Polythermal study of the systems $M(ClO_4)_2$-H_2O (M^{2+} = Mg^{2+}, Ca^{2+}, Sr^{2+}, Ba^{2+}), *Russian Journal of Applied Chemistry*, *78*(3), 409-413.

Pitzer, K. S. (1991), Chapter 3. Ion interaction approach: theory and data correlation, in *Activity coefficients in Electrolyte Solutions. 2nd Edition*, edited by K. S. Pitzer, pp. 75-154, CRC Press.

Renno, N. O., B. J. Bos, D. C. Catling, B. C. Clark, L. Drube, D. Fisher, W. Goetz, S. F. Hviid, H. U. Keller, J. F. Kok, S. P. Kounaves, K. Leer, M. Lemmon, M. B. Madsen, W. Markiewicz, J. Marshall, C. P. McKay, M. Mehta, M. Smith, P. H. Smith, C. Stoker, and S. M. M. Young (2009), Physical and thermodynamical evidence for liquid water on Mars, *LPSC*, *XL*(1440).

Sears, D. W. G., and J. D. Chittenden (2005), On laboratory simulation and the temperature dependence of evaporation rate of brine on Mars, *Geophys. Res. Lett.*, *32*(L23203), doi: 10.1029/2005GL024154.

Sears, D. W. G., and S. R. Moore (2005), On laboratory simulation and the evaporation rate of water on Mars, *Geophys. Res. Lett.*, *32*(L16202), doi: 10.1029/2005GL023443.

Smith, G. F., M. Brown, and J. F. Ross (1924), Magnesium perchlorate trihydrate. Its use as drying agent for steel and organic combustion analysis, *Industrial and Engineering Chemistry*, *16*(1), 20-22, doi: 10.1021/ie50169a006.

Taylor, P. A., W. Weng, C. Cook, C. Dickinson, A. Akingunola, J. Polkko, and H. Kahanpää (2009), Pressure data from the Phoenix landing site, *LPSC*, *XL*(1868).

Vaniman, D. T., D. L. Bish, S. J. Chipera, C. I. Fialips, J. W. Carey, and W. C. Feldman (2004), Magnesium sulphate salts and the history of water on Mars, *Nature*, *431*, 663-665.

Willard, H. H., and G. F. Smith (1922), The preparation and properties of magnesium perchlorate and its use as a drying agent, *J. Amer. Chem. Soc.*, *44*(10), 2255-2259.

Zent, A. P., T. L. Hudson, M. H. Hecht, D. Cobos, and S. E. Wood (2009), Mars regolith thermal and electrical properties: Initial results of the Phoenix Thermal and Electrical Conductivity Probe (TECP), *LPSC XL*(1125).

2.10 Supplemental Material

2.10.1 Determination of Eutectic Temperature and Concentrations

We calculated the stability diagrams using a combination of theoretical calculations and data analysis. In this paper we are mostly interested in the eutectic temperature. This temperature corresponds to the intersection of the equilibrium line between water ice and liquid solution and the equilibrium line between the salt hydrate and the solution.

The first step is to determine the water ice – liquid curve. For any solution, the activity of water is determined from the eutectic temperature by integrating the Gibbs-Helmholtz equation between the freezing temperature for pure water (273.16 K) and the eutectic temperature of the solution. [*Stokes*, 1991]:

$$\ln\left(a_{H_2O}\right) = \frac{\Delta H_f^0}{R}\left(\frac{1}{T_0} - \frac{1}{T}\right) + \frac{\Delta C_P}{R}\left(\ln\left(\frac{T_0}{T}\right) + \frac{T_0}{T} - 1\right) \tag{2.1}$$

where ΔH^0_f is the latent heat of fusion (ΔH^0_f = 6003.9 J mol^{-1}) at the eutectic temperature, T_0 = 273.16 K and ΔC_P is the specific heat capacity, which in the case of eq. (2.1) is supposed to remain constant with temperature. However, in this case ΔC_P is unknown, and is also probably itself a function of the temperature. Therefore we adopted an alternative approach and simplified eq. (2.1) into:

$$T_E = \frac{1}{\frac{1}{T_0} - \frac{R \ln a_{H_2O}}{\Delta H_f}} \tag{2.2}$$

where this time ΔH_f is the temperature dependent enthalpy of fusion, which can be rewritten as:

$$\Delta H_f = \frac{R\left(T_E - T_0\right)\ln a_{H_2O}}{T_E \cdot T_0} \tag{2.3}$$

However, since T_E is *a priori* unknown, we used an empirical fit to determine the variation of ΔH_f with the thermodynamic activity of water a_{H2O} [*Chevrier and Altheide*, 2008]:

$$\begin{aligned}\Delta H_f = {} & 3.34768 + \frac{1.85714}{1 + \exp\left[\frac{a_{H_2O} - 0.53822}{0.05031}\right]} + 1.85921 \cdot a_{H_2O} \\ & + 2.51524 \cdot a_{H_2O}^2 - 1.72933 \cdot a_{H_2O}^3\end{aligned} \tag{2.4}$$

Using the Pitzer model we calculated the water activity (see section 2.10.3), which is in turn converted into freezing point depression using eq. (2.2). Then the temperature is represented as a

function of the concentration used to calculate the water activity. The result is the equilibrium line between the water ice and the liquid solution in Figure 2-1. This method does not contain any adjustable parameter. It also shows that the control on the freezing point is only the water activity.

To determine the salt equilibrium lines, we need the hydration state of each salt at the eutectic. For this purpose we used solubility results from the literature, which unfortunately are very scarce: [*Chretien and Kohlmuller*, 1966; *CRC*, 2005-2006] for $NaClO_4$ and [*CRC*, 2005-2006; *Dobrynina et al.*, 1980; *Nicholson and Felsing*, 1950; *Pestova et al.*, 2005] for $Mg(ClO_4)_2$. Along each equilibrium line, the reaction between the salt hydrate and the solution can be written as follows [*Altheide et al.*, 2009]:

$$N_{\upsilon^+}^{z^+} X_{\upsilon^-}^{z^-} .nH_2O \leftrightarrow \upsilon^+ N^{z^+} + \upsilon^- X^{z^-} + nH_2O \tag{2.5}$$

where *NX* is the salt, *n* the number of water molecules in the structure of the salt, z^+ and z^- are the charges of the ions, and υ^+ and υ^- are the number of ions in the salt formula. The thermodynamic reaction constant *K* for dissolution (eq. 2.5) is defined as:

$$K(T) = \left(a_{N^{z+}}\right)^{\upsilon^+} \left(a_{X^{z-}}\right)^{\upsilon^-} \left(a_{H_2O}\right)^n \tag{2.6}$$

where *a* is the activity of each ion and water in the solution. This leads to the equation determining the activity of water at equilibrium [*Altheide et al.*, 2009]:

$$a_{H_2O} = \left[\frac{K}{\left(a_{N^{z+}}\right)^{\upsilon^+} \left(a_{X^{z-}}\right)^{\upsilon^-}} \right]^{\frac{1}{n}} \tag{2.7}$$

Then, using the Pitzer model, we can relate the activity of water to the activity of each ion at equilibrium (see section 2.10.3), leading to the complete equation for determining water activity:

$$a_{H_2O} = \left[\frac{K(T)}{\left(\upsilon^+ \times \upsilon^-\right)\left[m_{NX} \exp\left[-55.51 \frac{\ln a_{H_2O}}{m_{NX}\left(\upsilon^+ + \upsilon^-\right)} - 1 \right] \right]^{\left(\upsilon^+ + \upsilon^-\right)}} \right]^{\frac{1}{n}} \tag{2.8}$$

where m_{NX} is the molality of the salt, and υ^+, υ^- are the number of ions in the salt formula. The constant *K(T)* is determined as a function of the temperature using the Van't Hoff equation:

$$K(T) = \exp\left[\frac{-\Delta G^0_{298K,1bar}}{RT} \right] \exp\left[-\frac{\Delta H^0_{298K,1bar}}{R} \left(\frac{1}{T} - \frac{1}{298.15} \right) \right] \tag{2.9}$$

where $\Delta G^0_{298K,1bar}$ is the Gibbs free energy of dissolution of the salt and $\Delta H^0_{298K,1bar}$ its enthalpy of dissolution (Table 2-2) at saturation. The transcendental eq. (2.8) is solved numerically for each value of *T*, giving the molality m_{NX} and then the concentration. The advantage of this method is the possibility to calculate $\Delta G^0_{298K,1bar}$ and $\Delta H^0_{298K,1bar}$ when they are unknown, which happens very often for hydrates of rare salts such as perchlorates (Table 2-2). Finally, we determine the eutectic temperature and concentration from the intercept of both curves. All curves fit very well the data. This is especially important for the ice – solution equilibrium lines, which are calculated without any adaptive parameter. For the salt – solution equilibrium we adapted $\Delta G^0_{298K,1bar}$ and $\Delta H^0_{298K,1bar}$ to fit the data from other authors. Therefore, we estimate the eutectic conditions to be: C = 52 ± 1 wt% and 236 ± 1 K for $NaClO_4$ and 44.0 ± 0.5 wt% and 206 ± 1 K for $Mg(ClO_4)_2$.

2.10.2 Determination of Evaporation Rates

The evaporation rate *E* (in mm h^{-1}) was determined from mass loss (in grams) using the formula:

$$E = \frac{\Delta m / \Delta t \, S}{\rho_{sol}} \tag{2.10}$$

where $\Delta m/\Delta t$ is the mass loss rate, S is the surface area (cm^2) of the sample and ρ_{sol} is the density (g cm^{-3}) of the solution. It has been previously demonstrated that the evaporation rate of liquid water in the martian atmosphere is well described by a diffusion equation (Fick's theory) modified by the buoyancy of water molecules into the heavier CO_2 atmosphere [*Ingersoll*, 1970; *Sears and Chittenden*, 2005]:

$$E = 0.17 D_{H_2O/CO_2} \frac{a_{H_2O}\rho_{sat} - \rho_{Atm}}{\rho_{sol}} \left[\frac{\Delta\rho / \rho \, g}{\nu^2} \right]^{\frac{1}{3}} \tag{2.11}$$

where $D_{H2O/CO2}$ is the interdiffusion coefficient of $H_2O_{(g)}$ and $CO_{2(g)}$, a_{H2O} is the activity of water in the solution, ρ_{sat} is the saturation density of water vapor in equilibrium with pure liquid water, ρ_{Atm} is the atmospheric water vapor density, ρ_{sol} is the density of the solution, $\Delta\rho/\rho$ is the difference of density of the gas mixture between the surface of the liquid and the atmosphere, g is the gravity acceleration, and ν is the kinematic viscosity of CO_2. Temperature has a strong effect on the saturation pressure p_{sat} (in bars) of water through the following equations:

for liquid water [*Murphy and Koop*, 2005]:

$$p_{sat,liq} = 10^{-5} \exp\left[\begin{array}{l} 54.842763 - \dfrac{6763.22}{T} - 4.210\ln(T) + 0.000367T \\ + \tanh\left[0.0415(T - 218.8)\right] \times \left(\begin{array}{l} 53.878 - \dfrac{1331.22}{T} \\ - 9.44523\ln(T) + 0.014025T \end{array} \right) \end{array} \right] \tag{2.12}$$

and for water ice [*Murphy and Koop*, 2005]:

$$p_{sat,ice} = 10^{-5} \exp\left[9.550426 - \frac{5723.265}{T} + 3.53068\ln(T) - 0.00728332T \right] \tag{2.13}$$

From the saturation pressure, the gas density ρ_{sat} is defined as follows:

$$\rho_{sat} = \frac{p_{sat} M_{H_2O}}{RT} \tag{2.14}$$

Similarly, the water atmospheric density is defined as:

$$\rho_{Atm} = \frac{p_{Atm} M_{H_2O}}{RT} \tag{2.15}$$

While our experiments were ran in a completely dry atmosphere (Table 2-1), and thus $p_{Atm} = 0$, humidity varies strongly in the atmosphere of Mars, as measured by the Phoenix lander [*Hudson et al.*, 2009]. We replotted the data from Hudson *et al.* (2009) and for the calculations, we used a Gaussian fit of the data (green curve in Figure 2-3B), for which the equation is provided below:

$$\log(p_{Atm}) = \log(p_0) + \frac{A}{w} \exp\left[-2\left(\frac{t - t_0}{w} \right)^2 \right] \tag{2.16}$$

where $\log(p_{Atm}) = 0.2229 \pm 0.0157$, $A = -11.0646 \pm 0.2287$, $w = 5.8452 \pm 0.1003$ and $t_0 = 13.1051 \pm 0.0368$. While being entirely empirical, this fits provides a very good approximation of the characteristic distribution of the data, with relatively constant values during the day, and a decrease peak during the night, centered on 1 AM.

The relative density difference between the surface (ρ_{surf}) and the atmosphere (ρ_{atm}), $\Delta\rho/\rho$ is defined as:

$$\frac{\Delta\rho}{\rho} = \frac{\rho_{atm} - \rho_{surf}}{\rho_{surf}} = \frac{\left(a_{H_2O} p_{sat} - p_{Atm}\right)\left(M_{CO_2} - M_{H_2O}\right)}{P M_{CO_2} - a_{H_2O} p_{sat}\left(M_{CO_2} - M_{H_2O}\right)} \tag{2.17}$$

where P is the total atmospheric pressure, M_{H2O} and M_{CO2} are the molecular masses of water and CO_2, respectively. In the previous equation, the densities are for the gas mixture, and not only the water as in the density difference in eq. (2.11).

In addition, the kinetic parameters are also temperature dependant. The diffusion coefficient is defined as follow [*Boynton and Brattain*, 1929]:

$$D_{H_2O/CO_2} = 1.387 \times 10^{-5} \left(\frac{T}{273.15} \right)^{\frac{3}{2}} \left(\frac{1}{P} \right) \tag{2.18}$$

In this case P is in bar. The kinetic viscosity ν is defined as follows [*Crane*, 1988]:

$$\nu = 1.48 \times 10^{-5} \frac{RT}{M_{CO_2} P} \left(\frac{240 + 293.15}{240 + T} \right) \left(\frac{T}{293.15} \right)^{\frac{3}{2}} \tag{2.19}$$

where R is the ideal gas constant. All data necessary to calculate the evaporation rates are summarized in Table 2-1.

2.10.3 Determination of Water Activity Using the Pitzer Model

High concentrations of perchlorate create strong interactions between ions and water molecules. The kinetic eq. (2.9) includes the liquid water activity (a_{H2O}), which can be calculated using the Pitzer ion interaction model [*Grenthe and Plyasunov*, 1997; *Pitzer*, 1991]. This model accounts for electrostatic, non-specific, long-range interactions, as described by the Debye-Hückel theory, but also includes terms of short-range non-electrostatic interactions that become effective at very high concentrations. In this case the formula of the electrolyte is modeled as $N^{z+}{}_{\upsilon+}X^{z-}{}_{\upsilon-}$, where z^+ and z^- are the charges of the ions and υ^+, υ^- are the number of ions in the salt formula. In the case of $NaClO_4$, $z^+ = 1$, $\upsilon^+ = 1$, $z^- = 1$, and $\upsilon^- = 1$, and for $Mg(ClO_4)_2$, $z^+ = 2$, $\upsilon^+ = 1$, $z^- = 1$, and $\upsilon^- = 2$. The activity of water is calculated through the following equation:

$$\ln(a_{H_2O}) = \frac{-\Phi_{H_2O} \sum_k m_k}{55.10} \tag{2.20}$$

where m_k is the molality of the ion k in the solution (in mol kg^{-1}). The osmotic coefficient Φ_{H2O} is calculated as follows [*Pitzer*, 1991]:

$$\Phi_{H_2O} - 1 = |z_+ z_-| f + m_{NX}\left(\frac{2\upsilon_+\upsilon_-}{\upsilon_+ + \upsilon_-}\right)B_{NX} + m_{NX}^2\left(\frac{2(\upsilon_+\upsilon_-)^{\frac{3}{2}}}{\upsilon_+ + \upsilon_-}\right)C^{\phi} \tag{2.21}$$

where m_{NX} is the molality of the salt, B_{NX} and C_{NX} are constants representing specific interactions between the ions in the solution, and f is the extended form of the Debye-Hückel coefficient equivalent to:

$$f = -\frac{A\sqrt{I_m}}{1 + b\sqrt{I_m}} \tag{2.22}$$

Here A is the temperature-dependent Debye-Hückel coefficient:

$$A = 0.13422 \times \left(0.0368329 \times T - 14.62718 \times \ln(T) - \frac{1530.1474}{T} + 80.40631\right) \tag{2.23}$$

where b is a universal parameter with a value of 1.2 $kg^{1/2}$ $mol^{-1/2}$ and I_m is the ionic strength calculated as:

$$I_m = \frac{1}{2}\sum_{i=1}^{n} m_i z_i^2 \tag{2.24}$$

The value of B_{NX} and C_{NX} are calculated using the following equations:

$$B_{NX} = \beta^{(0)} + \beta^{(1)} \exp\left(-2\sqrt{I_m}\right) \tag{2.25}$$

with all the parameters presented in Table 2-3. The activity of ions in the solution is similarly calculated using the following formula:

$$a_k = m_k \times \exp\left[|z_+ z_-| f + m_{NX}\left(\frac{2\upsilon_+\upsilon_-}{\upsilon_+ + \upsilon_-}\right)B_{NX} + m_{NX}^2\left(\frac{2(\upsilon_+\upsilon_-)^{\frac{3}{2}}}{\upsilon_+ + \upsilon_-}\right)C^{\phi}\right] \tag{2.26}$$

2.10.4 References

Altheide, T. S., V. Chevrier, C. Nicholson, and J. Denson (2009), Experimental Investigation of the Stability and Evaporation of Sulfate and Chloride Brines on Mars, *Earth Planet. Sci. Lett.*, *In press*.

Boynton, W. P., and W. H. Brattain (1929), Interdiffusion of gases and vapors, *International Critical Tables*, *5*.

Chevrier, V., and T. S. Altheide (2008), Low Temperature Aqueous Ferric Sulfate Solutions on the Surface of Mars, *Geophys. Res. Lett.*, *35*(L22101), doi: 10.1029/2008GL035489.

Chretien, A., and R. Kohlmuller (1966), Perchlorate de Sodium, in *Nouveau Traite de Chimie Minerale, Vol 2 (#1), Sodium and Lithium*, edited by P. Pascal, pp. 344-354, Masson & Cie, Paris, France.

Crane (1988), Flow of fluids through valves, fittings, and pipe, in *Technical Paper No. 410*, edited, Crane Company, Joliet, Il.

CRC (2005-2006), *CRC Handbook of Chemistry and Physics, 86th Edition*, CRC Press, Taylor & Francis Group Boca Raton, Florida.

Dobrynina, T. A., A. M. Chernyshova, N. A. Akhapkina, and V. Y. Rosolovskii (1980), Fusion diagram of the magnesium perchlorate-water system, *Russian Journal of Inorganic Chemistry*, *25*, 2233-2236.

Grenthe, I., and A. Plyasunov (1997), On the use of semiempirical electrolyte theories for the modeling of solution chemical data, *Pure and Applied Chemistry*, *69*(5), 951-958.

Hudson, T. L., A. Zent, M. H. Hecht, S. Wood, and D. Cobos (2009), Near-surface humidity at the Phoenix landing site as measured by the Thermal and Electrical Conductivity Probe (TECP), *LPSC*, *XL*(#1804).

Ingersoll, A. P. (1970), Mars: Occurrence of liquid water, *Science*, *168*(3934), 972-973.

Krivtsov, N. V., Z. K. Nikitina, and V. Y. Rosolovs (1989), Thermochemical properties of anydrous and hydrated alkaline-earth metal and magnesium perchlorates, *Russian Chemical Bulletin*, *38*(9), 1817-1822.

Murphy, D. M., and T. Koop (2005), Review of the vapour pressures of ice and supercooled water for atmospheric applications, *Quart. J. R. Meteor. Soc.*, *131*, 1539-1565.

Nicholson, D. E., and W. A. Felsing (1950), The Determination of the Activity Coefficients of the Alkaline Earth and Magnesium Perchlorates from Freezing Point Data, *J. Amer. Chem. Soc.*, *72*(10), 4469-4471.

Pestova, O. N., L. A. Myund, M. K. Khripun, and A. V. Prigaro (2005), Polythermal study of the systems $M(ClO_4)_2$-H_2O (M^{2+} = Mg^{2+}, Ca^{2+}, Sr^{2+}, Ba^{2+}), *Russian Journal of Applied Chemistry*, *78*(3), 409-413.

Pitzer, K. S. (1991), Chapter 3. Ion interaction approach: theory and data correlation, in *Activity coefficients in Electrolyte Solutions. 2nd Edition*, edited by K. S. Pitzer, pp. 75-154, CRC Press.

Sears, D. W. G., and J. D. Chittenden (2005), On laboratory simulation and the temperature dependence of evaporation rate of brine on Mars, *Geophys. Res. Lett.*, *32*(L23203), doi: 10.1029/2005GL024154.

Smith, G. F., M. Brown, and J. F. Ross (1924), Magnesium perchlorate trihydrate. Its use as drying agent for steel and organic combustion analysis, *Industrial and Engineering Chemistry*, *16*(1), 20-22, doi: 10.1021/ie50169a006.

Stokes, R. H. (1991), Chapter 1. Thermodynamics of solutions, in *Activity coefficients in Electrolyte Solutions. 2nd Edition*, edited by K. S. Pitzer, pp. 1-28, CRC Press.

Willard, H. H., and G. F. Smith (1922), The preparation and properties of magnesium perchlorate and its use as a drying agent, *J. Amer. Chem. Soc.*, *44*(10), 2255-2259.

Table 2-1. Data obtained during evaporation experiments of perchlorate solutions.

Concentration (g g^{-1})	Run Time (min)	Density (g cm^{-3})	Slope	Evaporation Rate (mm h^{-1})	Avg. Sample Temp (K)	Avg. Chamber Temp (K)	Avg Rh (%)	Total Pressure (mbar)
$Mg(ClO_4)_2$								
0.2	60	1.126	0.0176	0.292	267.0 ± 1.5	277.5 ± 0.8	0.3	7.01 ± 0.01
0.2	60	1.126	0.0176	0.292	264.2 ± 0.5	277.5 ± 0.8	0.2	7.00 ± 0.01
0.2	60	1.126	0.0138	0.229	263.1 ± 1.4	269.0 ± 0.7	0.5	7.00 ± 0.01
0.2	60	1.126	0.0122	0.202	260.4 ± 0.5	268.9 ± 0.7	0.3	7.00 ± 0.01
0.2	60	1.126	0.0098	0.162	262.6 ± 0.6	259.9 ± 0.3	1.2	7.00 ± 0.01
0.2	60	1.126	0.0104	0.172	261.3 ± 1.0	259.6 ± 0.2	0.8	7.01 ± 0.04
0.3	60	1.203	0.0187	0.290	268.7 ± 1.8	277.0 ± 0.5	0.4	7.00 ± 0.01
0.3	60	1.203	0.0155	0.240	265.5 ± 0.5	277.0 ± 0.6	0.3	6.99 ± 0.00
0.3	60	1.203	0.0140	0.217	263.4 ± 1.4	268.2 ± 0.3	0.4	6.99 ± 0.01
0.3	60	1.203	0.0107	0.166	261.4 ± 0.9	268.2 ± 0.3	0.3	6.99 ± 0.00
0.3	60	1.203	0.0101	0.157	260.7 ± 2.0	260.2 ± 0.6	0.6	7.00 ± 0.00
0.3	60	1.203	0.0083	0.129	256.9 ± 0.7	260.2 ± 0.6	0.3	7.01 ± 0.01
0.4	60	1.310	0.0144	0.205	267.3 ± 1.1	275.6 ± 0.5	0.2	7.00 ± 0.01
0.4	60	1.310	0.0136	0.194	265.8 ± 0.3	276.5 ± 0.2	0.1	7.00 ± 0.01
0.4	60	1.310	0.0099	0.141	264.9 ± 1.5	268.8 ± 1.6	0.4	7.00 ± 0.01
0.4	60	1.310	0.0082	0.117	261.7 ± 0.5	268.8 ± 1.6	0.2	7.00 ± 0.01
0.4	60	1.310	0.0052	0.074	263.9 ± 1.8	260.2 ± 0.5	0.8	7.00 ± 0.01
0.4	60	1.310	0.0050	0.071	259.4 ± 1.3	259.9 ± 0.5	0.3	6.99 ± 0.01
0.49	60	1.410	0.0131	0.173	272.1 ± 1.6	277.1 ± 0.2	0.1	7.00 ± 0.01
0.49	60	1.410	0.0098	0.130	269.5 ± 0.4	277.1 ± 0.3	0.0	7.00 ± 0.01
0.49	90	1.410	0.0071	0.094	265.4 ± 1.6	269.2 ± 1.4	0.2	6.99 ± 0.01
0.49	60	1.410	0.0054	0.071	264.0 ± 2.0	260.2 ± 1.0	0.6	7.00 ± 0.01
0.49	60	1.410	0.0042	0.056	259.7 ± 0.8	260.1 ± 1.0	0.3	7.01 ± 0.03
$NaClO_4$								
0.2	60	1.126	0.0293	0.485	266.2 ± 1.3	277.3 ± 0.6	0.5	7.00 ± 0.01
0.2	60	1.126	0.0251	0.416	264.0 ± 0.4	277.3 ± 0.6	0.3	7.00 ± 0.01
0.2	60	1.126	0.0150	0.248	264.0 ± 1.6	268.6 ± 1.0	0.3	7.00 ± 0.01
0.2	60	1.126	0.0200	0.331	265.0 ± 0.3	268.6 ± 0.4	0.4	7.00 ± 0.01
0.2	60	1.126	0.0217	0.359	264.9 ± 0.3	260.2 ± 1.0	0.8	7.00 ± 0.01
0.2	60	1.126	0.0193	0.320	263.9 ± 0.5	259.7 ± 1.0	0.7	7.00 ± 0.01
0.3	60	1.203	0.0190	0.295	265.9 ± 1.3	276.4 ± 0.8	0.3	7.00 ± 0.01
0.3	60	1.203	0.0160	0.248	263.9 ± 0.3	277.2 ± 0.8	0.2	7.00 ± 0.01
0.3	60	1.203	0.0161	0.250	263.7 ± 1.5	267.8 ± 0.7	0.6	7.00 ± 0.01
0.3	60	1.203	0.0147	0.228	260.7 ± 0.6	267.7 ± 0.7	0.3	7.00 ± 0.01
0.3	60	1.203	0.0113	0.175	260.9 ± 1.4	259.6 ± 0.9	0.3	7.00 ± 0.01
0.3	60	1.203	0.0123	0.191	260.3 ± 1.0	259.6 ± 0.9	0.1	7.00 ± 0.01
0.4	60	1.307	0.0260	0.371	267.1 ± 1.3	277.2 ± 0.6	0.4	6.99 ± 0.01
0.4	60	1.307	0.0211	0.301	264.8 ± 0.4	277.2 ± 0.5	0.3	6.99 ± 0.00
0.4	60	1.307	0.0183	0.261	263.9 ± 1.5	268.0 ± 0.8	0.2	6.99 ± 0.00
0.4	60	1.307	0.0145	0.207	260.9 ± 0.5	268.0 ± 0.7	0.1	6.99 ± 0.00
0.4	60	1.307	0.0089	0.127	260.2 ± 1.7	258.5 ± 0.6	0.7	7.00 ± 0.01
0.4	60	1.307	0.0078	0.111	256.6 ± 0.7	258.5 ± 0.7	0.2	7.00 ± 0.01
0.55	60	1.481	0.0150	0.189	269.0 ± 1.3	278.1 ± 1.0	0.3	7.00 ± 0.01
0.55	60	1.481	0.0110	0.139	266.8 ± 0.4	278.1 ± 1.0	0.1	7.00 ± 0.00
0.55	60	1.481	0.0118	0.149	265.3 ± 1.3	266.8 ± 0.3	0.7	7.00 ± 0.01
0.55	60	1.481	0.0102	0.128	262.3 ± 0.6	266.9 ± 0.4	0.4	7.00 ± 0.00
0.55	60	1.481	0.0059	0.074	262.7 ± 2.0	258.9 ± 0.8	0.3	7.00 ± 0.03
0.55	60	1.481	0.0059	0.074	258.1 ± 0.8	258.7 ± 0.8	0.0	7.00 ± 0.01

Table 2-2. Thermodynamic parameters used or determined for the stability diagrams.

Compound	$\Delta G^0_{298K,1bar}$ **(kJ mol^{-1})**	***K* (298K)**	$\Delta H^0_{298K,1bar}$ **(kJ mol^{-1})**
$NaClO_4$	-16.8	877.8	1.6
$NaClO_4.H_2O$	-13.7	255.0	9.0
$NaClO_4.2H_2O$	-13.0	189.5	12.5
$Mg(ClO_4)_2.6H_2O$	-20.0	3200.0	5.4

Table 2-3. Binary Pitzer coefficient values for sodium and magnesium perchlorates [Pitzer, 1991].

Parameter	$\beta^{(0)}$	$\beta^{(1)}$	C^{ϕ}
$NaClO_4$	0.0554	0.2755	-0.00118
$Mg(ClO_4)_2$	0.4961	2.0085	0.00958

3 Chlorate Salts and Solutions on Mars

3.1 Abstract

Chlorate (ClO_3^-) is an intermediate oxidation species between chloride (Cl^-) and perchlorate (ClO_4^-), both of which were found at the Phoenix Landing Site by the Wet Chemistry Lab (WCL). The chlorate ion is almost as stable as perchlorate, and appears to be associated with perchlorate in most terrestrial reservoirs (e.g. Atacama and Antarctica). It is possible that chlorate contributed to the ion sensor response on the WCL, yet was masked by the strong perchlorate signal. However, very little is known about chlorate salts and their effect on the stability of water. We performed evaporation rate experiments in our mars simulation chamber, which enabled us to determine the activity of water for various concentrations. From this we constructed solubility diagrams for $NaClO_3$, $KClO_3$, $Mg(ClO_3)_2$ and $Ca(ClO_3)_2$, and determined the Pitzer parameters for each salt. Chlorate salt eutectic temperatures range from 270 K ($KClO_3$) to 204 K ($Mg(ClO_3)_2$). Modeling the addition of chlorate to the initial WCL solutions shows that it precipitates in concentrations comparable to other common salts, such as gypsum and epsomite, and implies that chlorates may play an important role in the wet chemistry on Mars.

3.2 Introduction

The recent discovery of perchlorates (ClO_4^-) by Phoenix (Hecht et al., 2009) has triggered a high interest for this ion that is rare on the surface of Earth. Although once thought only to be present in the hyper-arid Atacama Desert in Chile, natural perchlorate salts have since been found in other arid regions, such as the U.S. Southwest and most recently the Antarctic Dry Valleys (Kounaves et al., 2010c). It is thought that although perchlorate deposition occurs globally (Rajagopalan et al., 2008), it only concentrates in dry locations due to its propensity for

dissolving in water. Since perchlorate salts are so hygroscopic, any water present in the soil would be accumulated by the perchlorate salt, whether by adsorption or deliquescence. On Mars, pressure and temperature prevent pure liquid water from being stable on the surface (Ingersoll, 1970; Sears and Moore, 2005); however, perchlorate solutions have very low eutectics that favor the potential formation of liquid water on the surface of Mars (Chevrier et al., 2009; Cull et al., 2010; Rennó et al., 2009; Zorzano et al., 2009).

The mechanisms by which such a highly oxidized ion may form, especially on Mars, remain largely unknown. Between chloride (Cl^-, chlorine oxidation state -1) and perchlorate (ClO_4^-, chlorine ox. state +7), three other ions exist: hypochlorite ClO^- (ox. state +1), chlorite ClO_2^- (ox. state +3) and chlorate ClO_3^- (ox. state +5). Formation of ClO_4^- must include formation of these intermediate ions, and potentially other species (e.g. ClO_2), though the specific processes remain unclear. Perchlorate has been shown to be produced from O_3 or UV mediated oxidation of theses intermediate chlorine species. Isotopic analysis has indicated that possible reaction pathways include atmospheric oxidation of aerosols via UV, and/or reaction of strong oxidants like H_2O_2 or O_3 (Catling et al., 2010; Dasgupta et al., 2005; Jackson et al., 2010; Rao et al., 2010a). Other lines of evidence including laboratory experiments and modeling also support ClO_4^- formation in aqueous systems of oxychlorine solutions (Kang et al., 2006; Kang et al., 2009).

Therefore, these ions may be present (and undetected) at the Phoenix landing site as intermediate species of the processes leading to perchlorates, or formed during their decomposition (Copperthwaite and Lloyd, 1977). Of the intermediate species, ClO_3^- is the most stable (Chevrier and Hanley, 2009; Kang et al., 2006), making it likely that chlorate is present on

Mars along with perchlorate. Rao *et al.* (2010b) demonstrate that in all terrestrial samples containing perchlorate, chlorate was also detected at a concentration ratio of ~1:1 (mg/kg).

To further understand the intermediate ions leading to the formation of perchlorate, we have started a detailed investigation of the thermodynamic properties of chlorate salts. We have studied sodium, potassium, magnesium and calcium chlorates, but focused on $NaClO_3$ and $Mg(ClO_3)_2$ as the most relevant to the Phoenix chemistry (Chevrier et al., 2009; Marion et al., 2010).

3.3 Detection on Mars

The perchlorate ion was detected by the Wet Chemistry Lab (WCL) onboard the Phoenix lander (Hecht et al., 2009). Ions in solution (including ClO_4^-) were measured by a sensor array of electrochemically based ion-selective electrodes (ISE) (Kounaves et al., 2009). One drawback to this method is that while each sensor is selective, it is not specific, and careful modeling must be utilized to rule out interference from other ions. Results from the WCL were surprising at first; although the sensor was designed to detect nitrate (NO_3^-), the intensity of the signal was too high to be attributable to nitrate. Because that particular sensor is also sensitive, in relative order, to $SO_4^{2-} \leq F^- \leq Cl^- \leq Br^- \leq NO_3^- \leq ClO_3^- \leq I^- \leq ClO_4^- \leq SCN^-$, as described by the Hofmeister series, *Kounaves et al.* (2010a) concluded that ClO_4^- must be responsible for the signal. Detection sensitivities for ClO_3^- are on a similar order of magnitude for nitrate (~1-to-100 compared to ClO_4^-), meaning that ClO_4^- would overwhelm that anion signal as well. However, this does not preclude other anions, such as NO_3^- or ClO_3^-, from being present.

3.4 Methods

3.4.1 Magnesium Chlorate Synthesis

Magnesium chlorate was synthesized by mixing stoichiometric ratios of magnesium sulfate ($MgSO_4$ anhydrous, BDH product #0246-5006) and barium chlorate ($Ba(ClO_3)_2 \cdot H_2O$, Alfa Aesar product #A10128) according to (Mellor, 1922). $MgSO_4$ and $Ba(ClO_3)_2$ were separately dissolved in D.I. water on a stirplate then slowly added together. Since $BaSO_4$ is highly insoluble, it quickly precipitates, leaving Mg^{2+} and ClO_3^- in solution. After centrifuging the solution twice to separate the residual $BaSO_4$, the $Mg(ClO_3)_2$ solution is placed under continuous vacuum at 60°C (333 K) until all the water has evaporated.

3.4.2 Evaporation Rates

Solutions were made using D.I. water and sodium chlorate ($NaClO_3$, Alfa Aesar product #14267) at concentrations 20, 30, 40 and 50 wt% (±0.5%), and magnesium chlorate ($Mg(ClO_3)_2$) at concentrations 10, 20, 30, 40 and 50 wt% (±0.5%). Evaporation rates of the chlorate solutions were measured in our 0.6 m^3 Mars simulation chamber (Chevrier et al., 2009; Sears and Moore, 2005) under 7.00 ± 0.01 mbar of pure CO_2 at temperatures ranging from 255 to 275 K (Table 3-1). We recorded mass, temperature (chamber and sample), pressure, and relative humidity (Table 3-1). The atmosphere was continuously exchanged to maintain the relative humidity (RH) below 1%.

3.5 Results

3.5.1 Evaporation Experiments

At temperatures between 256 and 267 K, evaporation rates of sodium chlorate (Figure 3-1A) range from 0.141 mm h^{-1} (50 wt% at 258 K) to 0.443 mm h^{-1} (20 wt% at 264 K). At temperatures between 256 and 269 K, evaporation rates of magnesium chlorate (Figure 3-1B) range from 0.051 mm h^{-1} (50 wt% at 260 K) to 0.889 mm h^{-1} (10 wt% at 269 K). Similar to results with other salts, the evaporation rate is dependent both directly on the temperature and inversely on the concentration of the solution (Chevrier and Altheide, 2008; Chevrier et al., 2009). For instance, the evaporation rate of a 50 wt% $NaClO_3$ solution ranges from 0.141 to 0.325 mm h^{-1} over a temperature range of 9 K. The evaporation rate is also dependent on chlorate concentration: at 265 K, the 20 wt% sodium chlorate evaporates at 0.443 mm h^{-1} while the 50 wt% evaporates at 0.284 mm h^{-1}.

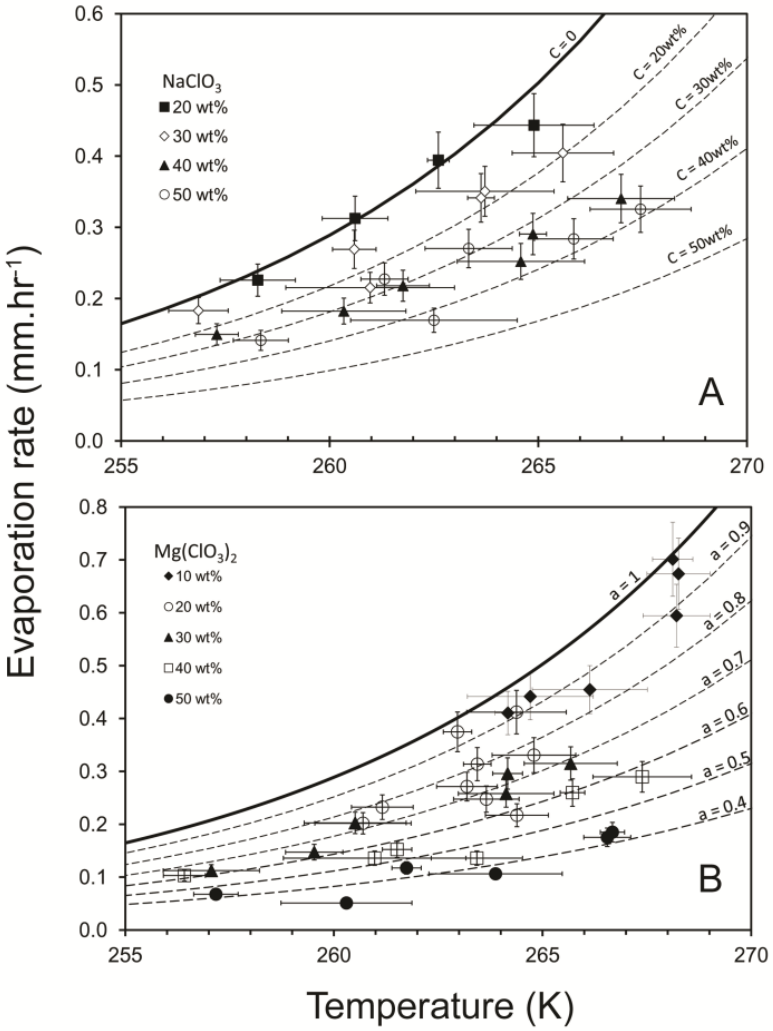

Figure 3-1. Evaporation rates of **(A)** $NaClO_3$ and **(B)** $Mg(ClO_3)_2$ as a function of sample temperature shown for various concentrations. Dashed lines are theoretical evaporation rates for each concentration, calculated from a modified Ingersoll (1970) equation and Pitzer (1991) model. The solid line is for pure supercooled liquid water (Murphy and Koop, 2005).

3.6 Discussion

3.6.1 Activity of Water

The Pitzer method for determining the activity of water takes into account various thermodynamic parameters and ion interactions, such as charge, stoichiometric ratios and concentration. However, the Pitzer parameters used in thermodynamic models do not exist for many of these chlorine oxyanions. Since the evaporation rate is a function of the water activity, we can use our experimental results to solve the evaporation equation for the activity of water at a given concentration (Figure 3-2). From the activity of water versus concentration, we can solve the Pitzer equations and determine the parameters for each cation – anion pair (Table 3-2, see sec 3.10.2) (Chevrier and Altheide, 2008; Pitzer, 1991).

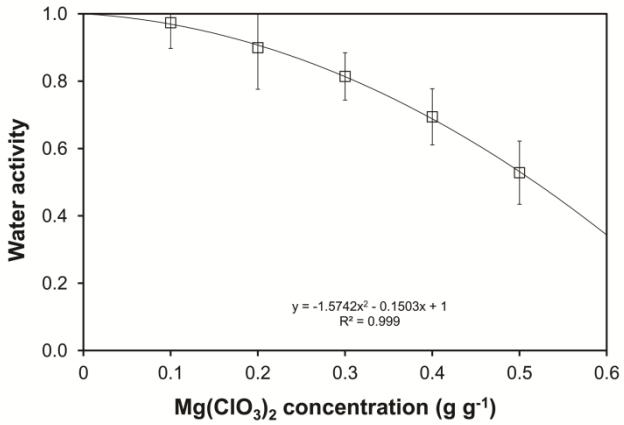

Figure 3-2. Activity of water for various $Mg(ClO_3)_2$ solution concentrations, calculated by solving our modified Ingersoll equation for brine evaporation rate (Chevrier and Altheide, 2008; Chevrier et al., 2009). Error bars are given by standard deviation of the data (Table 3-1).

3.6.2 Stability Diagrams

There is a clear lack of thermodynamic data for the various species of oxidized chlorine, especially those associated with magnesium. From the literature and our own data, we have constructed stability diagrams of chlorate salts for the four major cations present at the Phoenix landing site: $NaClO_3$, $KClO_3$, $Mg(ClO_3)_2$ and $Ca(ClO_3)_2$, as shown in Figure 3-3. Solubility data come from the *CRC* (2005-2006) and *Linke* (1965). Theoretical calculations for the $NaClO_3$ and $KClO_3$ liquidus lines come from (Pitzer, 1991). There was an absence of Pitzer parameters for Mg^{2+}, Ca^{2+}, and H^+, each paired with ClO_3^-, therefore we calculated them from the available data as described above (Table 3-2).

$NaClO_3$ (Figure 3-3A) and $KClO_3$ (Figure 3-3B) do not form any hydrates, as expected from their high eutectics of 250 K and 270 K, respectively. On the other hand, $Mg(ClO_3)_2$ (Figure 3-3C) forms three hydrates (2, 4 and 6 H_2O), which correspond exactly to the hydrates of Mg-perchlorate. $Ca(ClO_3)_2$ (Figure 3-3D) also forms three known hydrates (2, 4 and 6 H_2O), in contrast to Ca-perchlorate which forms four hydrates (2, 4, 6 and 8 H_2O). It is interesting to note that the eutectic temperatures for $Ca(ClO_3)_2$ and $Mg(ClO_3)_2$ are quite low: 232 K and 204 ± 3K, respectively.

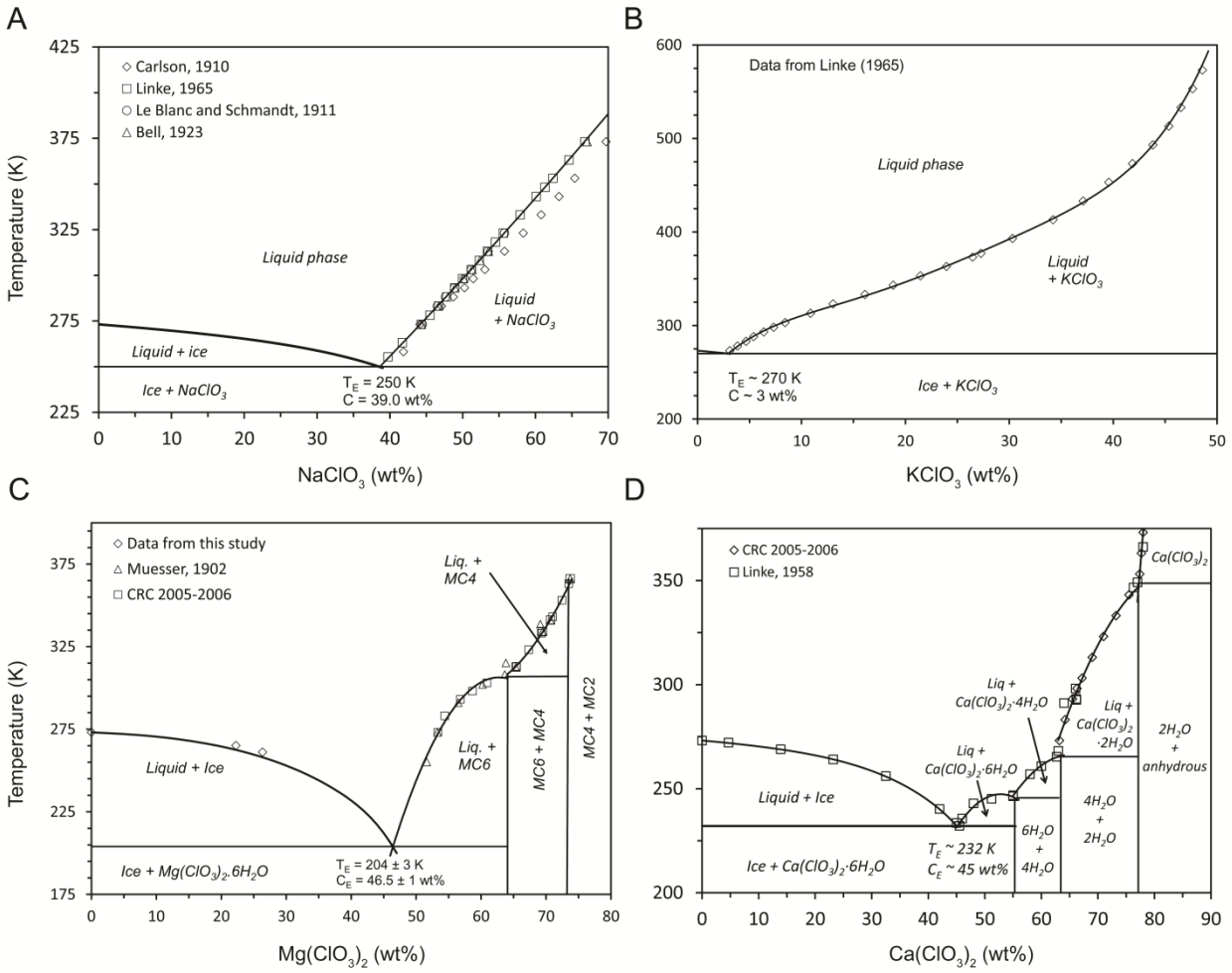

Figure 3-3. Stability diagrams of (A) sodium chlorate, (B) potassium chlorate, (C) magnesium chlorate, and (D) calcium chlorate. Solubility data come from (CRC, 2005-2006; Linke, 1965). In (A) and (B), the ice-line is from theoretical calculations (Pitzer, 1991). Potassium chlorate (B) has a very high eutectic temperature (270 K), not much lower than pure water. In (C) additional data are from the evaporation experiments (Fig. 3-1B). Lines are calculated from the calculated Pitzer parameters (Table 3-2). Magnesium chlorate (C) has the lowest eutectic of these four salts, at 204 ± 3 K. Note the lack of hydrates for $NaClO_3$, and $KClO_3$, while $Mg(ClO_3)_2$ and $Ca(ClO_3)_2$ have multiple hydrates. Interestingly, $Mg(ClO_3)_2$ has the same number and type of hydrates as $Mg(ClO_4)_2$.

3.6.3 Modeling WCL Solutions

Knowing the Pitzer parameters allows us to model the possible salt assemblages at the Phoenix landing site. We updated the PRQPITZ database used by the Geochemist's Workbench® software package to include the Pitzer parameters for each of these chlorate salt pairs, in addition to other salts species and ion couples previously described in the literature and relevant to Mars (Marion et al., 2010). Then we modeled the salt composition resulting from the evaporation of the solution measured by the WCL. Initial conditions were taken from Kounaves *et al.* (2010b) to include the sulfate ion. We used chlorate as the charge balance (i.e. initial concentration = 2.25 mM), and ran a model evaporating 1 kg of water at 7°C, with an initial pH of 7.7 and a fixed calcite concentration of 4.5 wt%, corresponding to 45 g in the simulation (see Table 3-3 for initial composition). As water is removed from the system, the ion concentrations initially increase, but then decrease as salts reach saturation (Figure 3-4A). As the solution becomes more concentrated, the activity of water decreases, which in turn means the freezing temperature of the solution is depressed (Chevrier and Altheide, 2008; Chevrier et al., 2009). The results (Figure 3-4B) show a variety of salts precipitating; the sulfates gypsum, mirabilite, and epsomite were among the first to precipitate, along with magnesite and $KClO_3$, while magnesium chlorate, halite and bischofite were the last. However, based on total amount precipitated, the most prevalent salts were $Mg(ClO_3)_2 \cdot 6H_2O$, epsomite, and gypsum, in that order. Since the model uses ClO_3^- to maintain electroneutrality, the apparently high amounts of precipitating chlorates partly result from a charge imbalance of the initial system as defined from literature data (i.e. 2.25 mM initial ClO_3^- concentration versus 4.9 determined by the model once equilibrated with carbonates). Therefore, other anions may also be present, yet undetected, in the regolith; chlorates in particular would be a major influence on the stability of liquid water on the surface

of Mars, due to their low eutectic temperatures and evaporation rates. Since this model was run at 7°C in an evaporation scenario, it does not necessarily reflect the original salt assemblage which is probably in equilibrium with the much lower temperature at the surface. However, in most cases, only the hydration state of the salt assemblages is affected by lower temperatures (Marion et al., 2010). Nevertheless, future work will include further modeling of the WCL solution. Extending our new database to FREZCHEM will allow us to compare evaporation between the two models, as well as run freezing scenarios, giving us the best possible picture to determine exactly which species will precipitate. An entire paper will be devoted to detailed modeling of the salt assemblages, as well as the effect on freezing point depression.

3.7 Conclusions

Given the presence of both chloride (Cl^-) and perchlorate (ClO_4^-), it is likely that other oxidized chlorine species would be present at the Phoenix landing site. ClO_3^- is almost as stable as perchlorate, and may be present (yet undetected) at the Phoenix landing site. Evaporation rates of chlorate solutions decrease with increasing concentration and decreasing temperature, as predicted by previous studies of concentrated salt solutions. Eutectic temperatures for chlorate solutions range from 270 K ($KClO_3$) to 204 K ($Mg(ClO_3)_2$).

Currently, magnesium perchlorate has one of the lowest known eutectic temperatures for any brine, which, along with its low evaporation rates, suggests that it should be the dominant liquid phase at the Phoenix landing site (Chevrier et al., 2009). However, $Mg(ClO_3)_2$ has a eutectic temperature very similar to Mg-perchlorate, suggesting that it may in fact play a role in the water cycle at the Phoenix landing site. These chlorate species, as well as other oxidized

chlorine compounds, require further study and modeling as they have intermediate eutectic temperatures that could potentially affect martian surface geochemistry.

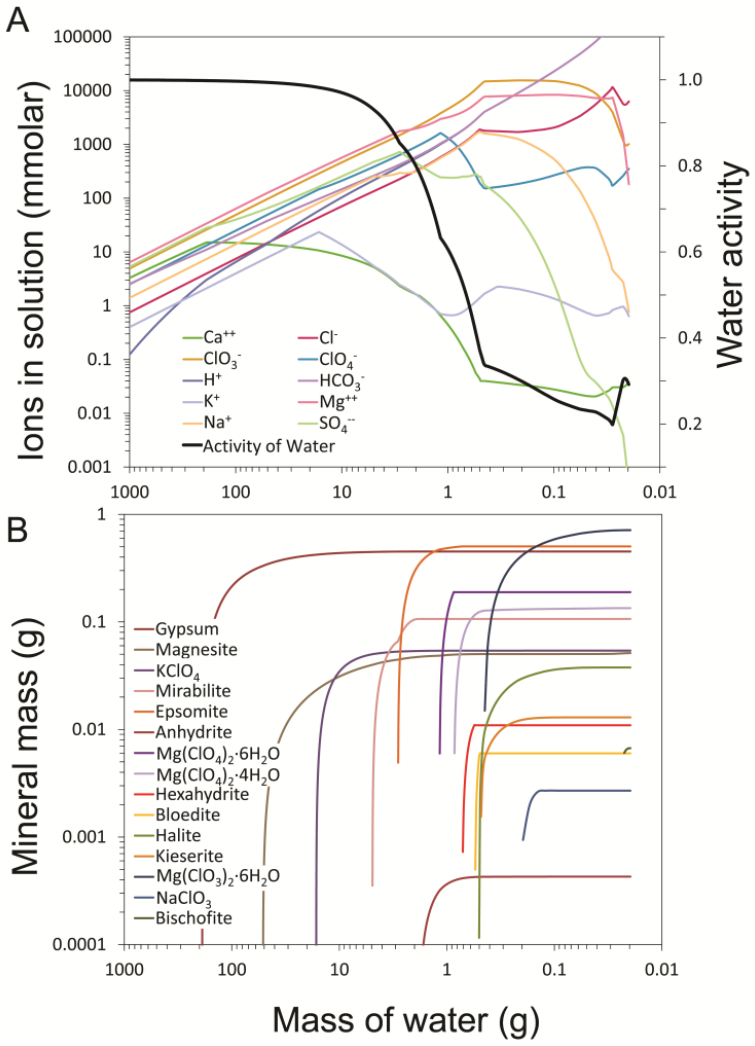

Figure 3-4. Modeled evaporation of 1 kg solution with initial ion concentrations taken from the Phoenix WCL data [Hecht et al., 2009; Kounaves et al., 2010b], with the addition of chlorate as charge balance. The model was run at 7°C, initial pH of 7.7 and a fixed amount of calcite (4.5 wt% (Boynton et al., 2009)). Evaporation progresses from left to right. (A) Concentration of ions in solution plus activity of water. (B) Precipitated minerals. Note that $Mg(ClO_3)_2 \cdot 6H_2O$ is the highest precipitated salt.

3.8 Acknowledgments

The authors acknowledge funding from NASA's Mars Data Analysis Program Grant #NNX10AN81G. The authors also thank two anonymous reviewers for helping improve the manuscript.

3.9 References

Boynton, W. V., et al. (2009), Evidence for Calcium Carbonate at the Mars Phoenix Landing Site, Science, 325(5936), 61-64.

Catling, D. C., et al. (2010), Atmospheric origins of perchlorate on Mars and in the Atacama, J. Geophys. Res., 115(E1), E00E11.

Chevrier, V. F., and T. S. Altheide (2008), Low Temperature Aqueous Ferric Sulfate Solutions on the Surface of Mars, Geophys. Res. Lett., 35(L22101).

Chevrier, V. F., and J. Hanley (2009), Thermodynamic Properties of Oxidized Forms of Chloride and Applications to the Phoenix Surface Chemistry #8009, paper presented at The New Martian Chemistry Workshop, LPI, Medford, Massachusetts.

Chevrier, V. F., et al. (2009), Stability of perchlorate hydrates and their liquid solutions at the Phoenix landing site, Mars, Geophys. Res. Lett., 36(10), L10202.

Copperthwaite, R. G., and J. Lloyd (1977), Photoinduced decomposition of sodium perchlorate and sodium chlorate when studied by X-ray photoelectron spectroscopy, Journal of the Chemical Society, Dalton Transactions(11), 1117-1121.

CRC (2005-2006), CRC Handbook of Chemistry and Physics, 86th Edition, CRC Press, Taylor & Francis Group Boca Raton, Florida.

Cull, S. C., et al. (2010), Concentrated perchlorate at the Mars Phoenix landing site: Evidence for thin film liquid water on Mars, Geophys. Res. Lett., 37(22), L22203.

Dasgupta, P. K., et al. (2005), The Origin of Naturally Occurring Perchlorate: The Role of Atmospheric Processes, Environ. Sci. Tech., 39(6), 1569-1575.

Forget, F., et al. (1999), Improved general circulation models of the Martian atmosphere from the surface to above 80 km, J. Geophys. Res., 104(E10), 24,155-124,175.

Hecht, M. H., et al. (2009), Detection of Perchlorate and the Soluble Chemistry of Martian Soil at the Phoenix Lander Site, Science, 325(5936), 64-67.

Ingersoll, A. P. (1970), Mars: Occurrence of liquid water, Science, 168(3934), 972-973.

Jackson, W. A., et al. (2010), Isotopic Composition and Origin of Indigenous Natural Perchlorate and Co-Occurring Nitrate in the Southwestern United States, Environ. Sci. Tech., 44(13), 4869-4876.

Kang, N., et al. (2006), Photochemical formation of perchlorate from aqueous oxychlorine anions, Anal. Chim. Acta, 567(1), 48-56.

Kang, N., et al. (2009), Characteristics of perchlorate formation via photodissociation of aqueous chlorite, Environmental Chemistry, 6(1), 53-59.

Kounaves, S. P., et al. (2009), The MECA Wet Chemistry Laboratory on the 2007 Phoenix Mars Scout Lander, J. Geophys. Res., 114(E3), E00A19.

Kounaves, S. P., et al. (2010a), Wet Chemistry experiments on the 2007 Phoenix Mars Scout Lander mission: Data analysis and results, J. Geophys. Res., 115(E1), E00E10.

Kounaves, S. P., et al. (2010b), Soluble sulfate in the martian soil at the Phoenix landing site, Geophys. Res. Lett., 37(9), L09201.

Kounaves, S. P., et al. (2010c), Discovery of Natural Perchlorate in the Antarctic Dry Valleys and Its Global Implications, Environ. Sci. Tech., 44(7), 2360-2364.

Linke, W. F. (1965), Solubilities: inorganic and metal-organic compounds, 4 ed., 1914 pp., D. Van Nostrand.

Marion, G. M., et al. (2010), Modeling aqueous perchlorate chemistries with applications to Mars, Icarus, 207(2), 675-685.

Mellor, J. W. (1922), A comprehensive treatise on inorganic and theoretical chemistry, Longmans, Green.

Murphy, D. M., and T. Koop (2005), Review of the vapour pressures of ice and supercooled water for atmospheric applications, Quart. J. R. Meteor. Soc., 131, 1539-1565.

Pitzer, K. S. (1991), Chapter 3. Ion interaction approach: theory and data correlation, in Activity coefficients in Electrolyte Solutions. 2nd Edition, edited by K. S. Pitzer, pp. 75-154, CRC Press.

Rajagopalan, S., et al. (2008), Perchlorate in Wet Deposition Across North America, Environ. Sci. Tech., 43(3), 616-622.

Rao, B., et al. (2010a), Perchlorate Formation by Ozone Oxidation of Aqueous Chlorine/Oxy-Chlorine Species: Role of ClxOy Radicals, Environ. Sci. Tech., 44(8), 2961-2967.

Rao, B., et al. (2010b), Natural Chlorate in the Environment: Application of a New IC-ESI/MS/MS Method with a Cl18O3- Internal Standard, Environ. Sci. Tech., 44(22), 8429-8434.

Rennó, N. O., et al. (2009), Possible physical and thermodynamical evidence for liquid water at the Phoenix landing site, J. Geophys. Res., 114(E1), E00E03.

Sears, D. W. G., and S. R. Moore (2005), On laboratory simulation and the evaporation rate of water on Mars, Geophys. Res. Lett., 32(L16202).

Zorzano, M. P., et al. (2009), Stability of liquid saline water on present day Mars, Geophys. Res. Lett., 36(20), L20201.

3.10 Supplementary Information

3.10.1 Determination of Evaporation Rates

The evaporation rate E (in mm h^{-1}) was determined from mass loss (in grams) using the formula:

$$E = \frac{\Delta m / \Delta t \, S}{\rho_{sol}} \tag{3.1}$$

where $\Delta m/\Delta t$ is the mass loss rate, S is the surface area (cm^2) of the sample and ρ_{sol} is the density (g cm^{-3}) of the solution, which was measured for each concentration.

It has been previously demonstrated that the evaporation rate of liquid water in the martian atmosphere is well described by a diffusion equation (Fick's theory) modified by the buoyancy of water molecules into the heavier CO_2 atmosphere (Ingersoll, 1970; Sears and Chittenden, 2005):

$$E = 0.17 D_{H_2O/CO_2} a_{H_2O} \frac{\rho_{sat}}{\rho_{sol}} \left[\frac{\Delta\rho / \rho \, g}{\nu^2} \right]^{\frac{1}{3}} \tag{3.2}$$

where D_{H_2O/CO_2} is the interdiffusion coefficient of $H_2O_{(g)}$ and $CO_{2(g)}$, a_{H_2O} is the activity of water in the solution, ρ_{sat} is the saturation density of water vapor in equilibrium with pure liquid water, ρ_{sol} is the density of the solution, $\Delta\rho/\rho$ is the relative difference in density of the gas mixture between the surface of the liquid and the atmosphere, g is the gravitational acceleration, and ν is the kinematic viscosity of CO_2.

Temperature has a strong effect on the saturation pressure p_{sat} (in bars) of water through the following equations:

For liquid water (Murphy and Koop, 2005)

$$p_{sat,liq} = 10^{-5} \exp\left[\begin{array}{l} 54.842763 - \dfrac{6763.22}{T} - 4.210\ln(T) + 0.000367T \\ + \tanh[0.0415(T-218.8)] \times \left(\begin{array}{l} 53.878 - \dfrac{1331.22}{T} \\ - 9.44523\ln(T) + 0.014025T \end{array}\right) \end{array}\right] \quad (3.3)$$

and for water ice (Murphy and Koop, 2005)

$$p_{sat,ice} = 10^{-5} \exp\left[9.550426 - \frac{5723.265}{T} + 3.53068\ln(T) - 0.00728332T\right] \quad (3.4)$$

From the saturation pressure, the gas density ρ_{sat} is defined as follows:

$$\rho_{sat} = \frac{p_{sat}}{M_{H_2O}T} \quad (3.5)$$

The relative density difference between the surface (ρ_{surf}) and the atmosphere (ρ_{atm}), $\Delta\rho/\rho$, is defined as:

$$\frac{\Delta\rho}{\rho} = \frac{\rho_{atm} - \rho_{surf}}{\rho_{surf}} = \frac{p_{sat}\left(M_{CO_2} - M_{H_2O}\right)}{PM_{CO_2} - p_{sat}\left(M_{CO_2} - M_{H_2O}\right)} \quad (3.6)$$

where P is the total atmospheric pressure, M_{H_2O} and M_{CO_2} are the molecular masses of water and CO_2, respectively. In addition, the kinetic parameters are also temperature dependant. The diffusion coefficient is defined as follow (Boynton and Brattain, 1929):

$$D_{H_2O/CO_2} = 1.387 \times 10^{-5} \left(\frac{T}{273.15} \right)^{\frac{3}{2}} \left(\frac{1}{P} \right) \tag{3.7}$$

In this case P is in bar. The kinetic viscosity ν is defined as follows (Crane, 1988):

$$\nu = 1.48 \times 10^{-5} \frac{RT}{M_{CO_2} P} \left(\frac{240 + 293.15}{240 + T} \right) \left(\frac{T}{293.15} \right)^{\frac{3}{2}} \tag{3.8}$$

where R is the ideal gas constant. Most of the data necessary to calculate the evaporation rates are summarized in Table 3-1. However, a_{H_2O} is usually calculated using the Pitzer ion interaction model (see section 3.10.2) (Grenthe and Plyasunov, 1997; Pitzer, 1991), but they are absent in the literature for all the chlorate salts except $NaClO_3$. For $Mg(ClO_3)_2$ we used Goal Seek in Microsoft Excel to attain the value of a_{H_2O} that when used in eq. (3.2) matched our experimental evaporation rates.

3.10.2 Determination of Pitzer Parameters from Water Activity and the Ice Line

High concentrations of chlorate create strong interactions between ions and water molecules. The kinetic eq. (3.9) includes the liquid water activity (a_{H_2O}), which can be calculated using the Pitzer ion interaction model (Grenthe and Plyasunov, 1997; Pitzer, 1991). This model accounts for electrostatic, non-specific, long-range interactions, as described by the Debye-Hückel theory, but also includes terms of short-range non-electrostatic interactions that become effective at very high concentrations. In this case the formula of the electrolyte is

modeled as $N_{v+}^{z+}X_{v-}^{z-}$, where z_+ and z_- are the charges of the ions, and υ_+ and υ_- are the number of ions in the salt formula. In the case of $NaClO_3$ and $KClO_3$, $z_+ = 1$, $\upsilon_+ = 1$, $z_- = -1$, and $\upsilon_- = 1$, and for $Mg(ClO_3)_2$ and $Ca(ClO_3)_2$, $z_+ = 2$, $\upsilon_+ = 1$, $z_- = -1$, and $\upsilon_- = 2$,. The activity of water is calculated through the following equation:

$$\ln(a_{H_2O}) = \frac{-\Phi_{H_2O}\sum_k m_k}{55.51} \tag{3.9}$$

where m_k is the molality of the ion k in the solution (in mol kg^{-1}). This can also be rewritten as:

$$\ln(a_{H_2O}) = \frac{-\Phi_{H_2O}(\upsilon_+ + \upsilon_-)m_{NX}}{55.51} \tag{3.10}$$

Where m_{NX} is the molality of the salt. The osmotic coefficient $\boldsymbol{\Phi}_{H2O}$ is calculated as follows (Pitzer, 1991):

$$\Phi_{H_2O} - 1 = |z_+ z_-| f + m_{NX}\left(\frac{2\upsilon_+\upsilon_-}{\upsilon_+ + \upsilon_-}\right)B_{NX} + m_{NX}^2\left(\frac{2(\upsilon_+\upsilon_-)^{\frac{3}{2}}}{\upsilon_+ + \upsilon_-}\right)C^{\phi} \tag{3.11}$$

where m_{NX} is the molality of the salt, B_{NX} and C^{ϕ} are constants representing specific interactions between the ions in the solution, where B_{NX} is calculated using the following equation:

$$B_{NX} = \beta^0 + \beta^1 e^{(-\alpha\sqrt{I_m})} \tag{3.12}$$

and β^0, β^1 and C^{ϕ} are the unknown Pitzer parameters. f is the extended form of the Debye-Hückel coefficient equivalent to

$$f = -\frac{A\sqrt{I_m}}{1+b\sqrt{I_m}} \tag{3.13}$$

Here A is the temperature-dependent Debye-Hückel coefficient:

$$A = 0.13422 \times \left(0.0368329 \times T - 14.62718 \times \ln(T) - \frac{1530.1474}{T} + 80.40631\right) \tag{3.14}$$

and b is a universal parameter with a value of 1.2 $kg^{1/2}$ $mol^{-1/2}$ and I_m is the ionic strength calculated as

$$I_m = \frac{1}{2}\sum_{i=1}^{n} m_i z_i^2 \tag{3.15}$$

The ionic strength can be rewritten as

$$I_m = \frac{1}{2}\left[m_N z_+^2 + m_X z_-^2\right] \tag{3.16}$$

And since $m_N = \upsilon_+ m_{NX}$ and $m_X = \upsilon_- m_{NX}$

$$I_m = \frac{1}{2} m_{NX}\left[\upsilon_+ z_+^2 + \upsilon_- z_-^2\right] \tag{3.17}$$

But to maintain the charge neutrality, we must have: $\upsilon_+ = |z\text{-}|$ and $\upsilon_- = z_+$, thus

$$I_m = \frac{1}{2} m_{NX}\left[z_- z_+^2 + z_+ z_-^2\right] = \frac{1}{2} m_{NX}\left[\left|z_-\right| \cdot z_+\right]\left[z_+ + \left|z_-\right|\right] \tag{3.18}$$

We also know that $|z_+ z_-| = \upsilon_+ \upsilon_-$ and $z_+ + |z_-| = \upsilon_+ + \upsilon_-$, therefore we define two parameters $P = |z_+ z_-| = \upsilon_+ \upsilon_-$ (product) and $S = z_+ + |z_-| = \upsilon_+ + \upsilon_-$ (sum).

For a 1-1 salt, $S = 2$, $P = 1$.

For a 2-1 salt, $S = 3$, $P = 2$

For a 2-2 salt, $S = 4$, $P = 4$

For a 3-2 salt, $S = 5$, $P = 6$

For a 3-3 salt, S = 6, P = 9

Therefore, eq. (3.17) becomes simply

$$I_m = ½\, m_{NX}.P.S \tag{3.19}$$

and $$m_{NX} = \frac{2I_m}{P \cdot S} \tag{3.20}$$

This allows to easily changing from the molality to the ionic strength for any salt. Thus, rewritten for the osmotic coefficient, eq. (3.10) becomes

$$\Phi_{H_2O} = -\frac{55.51 \ln\left(a_{H_2O}\right)}{S \cdot m_{NX}} \tag{3.21}$$

and the Pitzer formulation for the same osmotic coefficient becomes

$$\Phi_{H_2O} - 1 = P \cdot f + \frac{2P}{S} B_{NX} m_{NX} + \frac{2P^{\frac{3}{2}}}{S} C^{\phi} m_{NX}^2 \tag{3.22}$$

Since B_{NX} and f are both functions of m_{NX} through the square root of the ionic strength, i.e. eq. (3.12) and eq (3.13), we define a new variable

$\gamma = \sqrt{I_m}$, so $I_m = \gamma^2$ and $m_{NX} = \frac{2\gamma}{P \times S}$

In this case, eq. 3.21 becomes

$$\phi = -\frac{55.51 P \cdot \ln\left(a_{H_2O}\right)}{2\gamma^2} \tag{3.23}$$

And eq. (3.22) becomes

$$\phi - 1 = -\frac{P \cdot A \cdot \gamma}{1 + b \cdot \gamma} + \frac{4\gamma^2}{S^2}\left[\beta^0 + \beta^1 \exp\left(-2\gamma\right)\right] + \frac{8\gamma^4}{S^3 P^{1/2}} C^{\phi} \tag{3.24}$$

Finally, combining equations (3.21) and (3.22) and reordering gives the fitting equation to obtain the Pitzer parameters:

$$-55.51 \cdot P \cdot \ln(a_{H_2O}) - 2\gamma^2\left[1 - \frac{P \cdot A \cdot \gamma}{1 + b \cdot \gamma}\right] = \frac{8\gamma^4}{S^2}\left[\beta^0 + \beta^1 \exp\left(-2\gamma\right)\right] + \frac{16\gamma^6}{S^3 P^{1/2}} C^{\phi} \tag{3.25}$$

Or in a simplified form:

$$-\frac{55.51}{2} P \ln(a_{H_2O}) - I_m\left[1 + P \cdot f\right] = \frac{4I_m^2}{S^2}\left[\beta^0 + \beta^1 \exp\left(-2\sqrt{I_m}\right)\right] + \frac{8I_m^3}{S^3 P^{1/2}} C^{\phi} \tag{3.26}$$

From here a fit was performed using Origin Lab. An example is shown in Figure 3-5.

Finally, this assumes that C^{ϕ} is a constant. If it were not, it would just require replacing the C^{ϕ} parameter by its expression before fitting.

3.10.3 Determination of Eutectic Temperature and Concentration

We calculated the stability diagrams using a combination of theoretical calculations and data analysis. In this paper we are mostly interested in the eutectic temperature. This temperature corresponds to the intersection of the equilibrium line between water ice and liquid solution and the equilibrium line between the precipitating salt and the solution.

The first step is to determine the water ice – liquid curve. For any solution, the activity of water is determined from the eutectic temperature by integrating the Gibbs-Helmholtz equation between the freezing temperature for pure water (273.16 K) and the eutectic temperature of the solution. (Stokes, 1991):

$$\ln\left(a_{H_2O}\right)=\frac{\Delta H_f^0}{R}\left(\frac{1}{T_0}-\frac{1}{T_E}\right)+\frac{\Delta C_P}{R}\left(\ln\left(\frac{T_0}{T_E}\right)+\frac{T_0}{T_E}-1\right) \tag{3.27}$$

where ΔH^0_f is the latent heat of fusion (ΔH^0_f = 6003.9 J mol^{-1}) at T_0 = 273.16 K and ΔC_P is the specific heat capacity, which in the case of eq. (3.27) is supposed to remain constant with temperature. However, in our case ΔC_P is unknown, and is also probably itself a function of the temperature. Therefore we adopted an alternative approach and simplified eq. (3.27) into

$$T_E=\frac{1}{\frac{1}{T_0}-\frac{R\ln a_{H_2O}}{\Delta H_f}} \tag{3.28}$$

where ΔH_f is the temperature dependent enthalpy of fusion. We used an empirical fit to determine the variation of ΔH_f with a_{H_2O} (Chevrier and Altheide, 2008; Chevrier et al., 2009):

$$\Delta H_f = 3.34768 - \frac{1.85714}{1+\exp\left[\frac{a_{H_2O}-0.53822}{0.05031}\right]} + 1.85921 \cdot a_{H_2O} + 2.51524 \cdot a_{H_2O}^2 - 1.72933 \cdot a_{H_2O}^3 \quad (3.29)$$

Using the Pitzer model we calculated the water activity (see section 3.10.2), which is in turn converted into freezing point depression using eq. (3.28). Then the temperature is represented as a function of the concentration used to calculate the water activity. The result is the equilibrium line between the water ice and the liquid solution in Figure 3-3.

To determine the salt equilibrium lines, we need the hydration state of each salt at a given temperature and concentration. For this purpose we used solubility results from the literature, which unfortunately are scarce for most chlorates: (Bell, 1923; Billiter, 1920; Carlson, 1910; Le Blanc and Schmandt, 1911; Linke, 1965) for $NaClO_3$, (Linke, 1965) for $KClO_3$, (CRC, 2005-2006; Meusser, 1902) for $Mg(ClO_3)_2$, and (CRC, 2005-2006; Linke, 1965) for $Ca(ClO_3)_2$. Best fit curves were plotted according to the data.

We determine the eutectic temperature and concentration from the intercept of both curves. Therefore, we estimate the eutectic conditions to be: C_E = 39.0 wt% and T_E = 250 K for $NaClO_3$; 3 wt% and 270 K for $KClO_3$, 46.5 ± 1wt% and 204 ± 3 K for $Mg(ClO_3)_2$, and 45 wt% and 232 K for $Ca(ClO_3)_2$. The larger error on the temperature on the magnesium chlorate comes from the large variation of temperature with concentration close to the eutectic.

3.10.4 Determination of Thermodynamic Reaction Constants K(T)

Along each equilibrium line, the reaction between the salt hydrate and the solution can be written as follows (Altheide et al., 2009; Chevrier et al., 2009):

$$N_{\upsilon^+}^{z^+} X_{\upsilon^-}^{z^-} .nH_2O \leftrightarrow \upsilon^+ N^{z^+} + \upsilon^- X^{z^-} + nH_2O \quad (3.30)$$

where *NX* is the salt, *n* the number of water molecules in the structure of the salt, z^+ and z^- are the charges of the ions, and υ^+ and υ^- are the number of ions in the salt formula. The thermodynamic reaction constant *K* is defined as:

$$K(T) = \left(a_{N^{z+}}\right)^{\upsilon^+} \left(a_{X^{z-}}\right)^{\upsilon^-} \left(a_{H_2O}\right)^n \tag{3.31}$$

where *a* is the activity of each ion and water molecule in the solution. a_{N+}, a_{X-} and a_{H_2O} are calculated for each relevant temperature used in the GWB database using the Pitzer equations and the corresponding concentrations from experimental data. Then K(T) is determined using equation (3.31).

3.10.5 References

Altheide, T., et al. (2009), Experimental investigation of the stability and evaporation of sulfate and chloride brines on Mars, Earth Planet. Sci. Lett., 282(1-4), 69-78.

Bell, H. C. (1923), Solubility of Sodium Chlorate, 2713-2714.

Billiter, J. (1920), Löslichkeitsbeeinflussung von Chlorat durch Chlorid und ihre AbhÄngigkeit von der Temperatur, Monatshefte für Chemie / Chemical Monthly, 41(4), 287-295.

Boynton, W. P., and W. H. Brattain (1929), Interdiffusion of gases and vapors, International Critical Tables, 5.

Carlson, C. E. (1910), Eine neue Methode zum leichten Nachweis und zur raschen Ausscheidung von Arsen und gewissen Metallsalzen aus Flüssigkeiten, Hoppe-Seyler's Zeitschrift für physiologische Chemie, 68(3-4), 243-262.

Chevrier, V. F., and T. S. Altheide (2008), Low Temperature Aqueous Ferric Sulfate Solutions on the Surface of Mars, Geophys. Res. Lett., 35(L22101).

Chevrier, V. F., et al. (2009), Stability of perchlorate hydrates and their liquid solutions at the Phoenix landing site, Mars, Geophys. Res. Lett., 36(10), L10202.

Crane (1988), Flow of fluids through valves, fittings, and pipe, in Technical Paper No. 410, edited, Crane Company, Joliet, Il.

CRC (2005-2006), CRC Handbook of Chemistry and Physics, 86th Edition, CRC Press, Taylor & Francis Group Boca Raton, Florida.

Grenthe, I., and A. Plyasunov (1997), On the use of semiempirical electrolyte theories for the modeling of solution chemical data, Pure and Applied Chemistry, 69(5), 951-958.

Ingersoll, A. P. (1970), Mars: Occurrence of liquid water, Science, 168(3934), 972-973.

Le Blanc, M., and W. Schmandt (1911), Über Kristallisation und Auflösung in wässeriger Lösung, Zeitschrift für physikalische Chemie, 77.

Linke, W. F. (1965), Solubilities: inorganic and metal-organic compounds, 4 ed., 1914 pp., D. Van Nostrand.

Meusser, A. (1902), Metallchlorate. Studien über die Löslichkeit der Salze. X, Berichte der deutschen chemischen Gesellschaft, 35(2), 1414-1424.

Murphy, D. M., and T. Koop (2005), Review of the vapour pressures of ice and supercooled water for atmospheric applications, Quart. J. R. Meteor. Soc., 131, 1539-1565.

Pitzer, K. S. (1991), Chapter 3. Ion interaction approach: theory and data correlation, in Activity coefficients in Electrolyte Solutions. 2nd Edition, edited by K. S. Pitzer, pp. 75-154, CRC Press.

Sears, D. W. G., and J. D. Chittenden (2005), On laboratory simulation and the temperature dependence of evaporation rate of brine on Mars, Geophys. Res. Lett., 32(L23203).

Stokes, R. H. (1991), Chapter 1. Thermodynamics of solutions, in Activity coefficients in Electrolyte Solutions. 2nd Edition, edited by K. S. Pitzer, pp. 1-28, CRC Press.

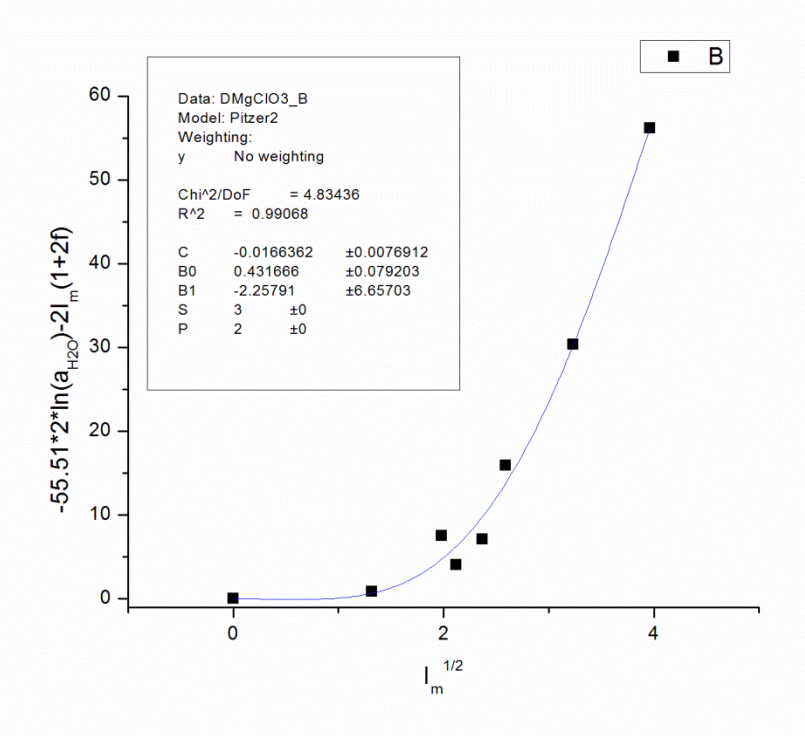

Figure 3-5. Plot of eq (3.26) as a function of ionic strength (I_m) for $Mg(ClO_3)_2$ values. The values obtained for C, B0 and B1 correspond to the Pitzer parameters C^{ϕ}, β^0 and β^1, respectively.

Table 3-1. Data obtained during evaporation experiments of chlorate solutions.

Concentration (g g^{-1})	Density (g cm^{-3})	Evaporation Rate (mm h^{-1})	Avg Sample Temp (K)	Avg Chamber Temp (K)	Avg Rh (%)	Total Pressure (mbar)	a_{H2O}
$NaClO_3$							
0.2	1.14	0.443	264.89 ± 1.44	277.75 ± 0.20	0.67 ± 0.10	7.00 ± 0.01	
0.2	1.14	0.394	262.60 ± 0.26	277.76 ± 0.21	0.48 ± 0.03	7.00 ± 0.01	
0.2	1.14	0.312	260.61 ± 0.79	270.63 ± 0.24	0.16 ± 0.03	6.99 ± 0.03	
0.2	1.14	0.226	258.28 ± 0.90	262.60 ± 0.24	0.75 ± 0.17	7.01 ± 0.01	
0.3	1.213	0.404	265.59 ± 1.22	277.93 ± 0.20	0.34 ± 0.02	7.00 ± 0.01	
0.3	1.213	0.341	263.63 ± 0.32	277.96 ± 0.20	0.16 ± 0.03	7.01 ± 0.00	
0.3	1.213	0.351	263.72 ± 1.66	270.63 ± 0.24	0.51 ± 0.25	7.00 ± 0.01	
0.3	1.213	0.269	260.59 ± 0.52	270.70 ± 0.23	0.16 ± 0.04	6.99 ± 0.00	
0.3	1.213	0.215	260.97 ± 2.02	262.63 ± 0.24	0.44 ± 0.18	7.00 ± 0.01	
0.3	1.213	0.183	256.85 ± 0.71	262.56 ± 0.24	0.14 ± 0.03	7.00 ± 0.01	
0.4	1.3095	0.340	266.98 ± 1.28	277.53 ± 0.20	0.43 ± 0.10	7.00 ± 0.01	
0.4	1.3095	0.291	264.87 ± 0.32	277.54 ± 0.20	0.26 ± 0.01	6.99 ± 0.01	
0.4	1.3095	0.252	264.58 ± 1.53	270.76 ± 0.23	0.28 ± 0.09	7.00 ± 0.01	
0.4	1.3095	0.218	261.76 ± 0.63	270.76 ± 0.23	0.13 ± 0.02	7.00 ± 0.01	
0.4	1.3095	0.182	260.34 ± 1.49	262.54 ± 0.24	0.54 ± 0.23	6.99 ± 0.01	
0.4	1.3095	0.150	257.29 ± 0.51	262.63 ± 0.24	0.16 ± 0.05	6.99 ± 0.00	
0.5	1.387	0.325	267.45 ± 1.21	277.60 ± 0.20	0.20 ± 0.05	7.00 ± 0.01	
0.5	1.387	0.284	265.85 ± 0.94	277.63 ± 0.20	0.10 ± 0.02	7.00 ± 0.01	
0.5	1.387	0.270	263.33 ± 1.05	270.65 ± 0.25	0.51 ± 0.13	7.01 ± 0.01	
0.5	1.387	0.227	261.31 ± 0.57	270.72 ± 0.22	0.30 ± 0.03	6.99 ± 0.01	
0.5	1.387	0.169	262.50 ± 2.00	262.82 ± 0.23	0.67 ± 0.21	7.00 ± 0.01	
0.5	1.387	0.141	258.35 ± 0.66	262.76 ± 0.22	0.28 ± 0.05	6.99 ± 0.01	
$Mg(ClO_3)_2$							
0.1	1.013	0.67358	268.26 ± 0.76	269.63 ± 0.40	0.90 ± 0.08	7.00 ± 0.01	0.9825009
0.1	1.013	0.45457	266.13 ± 1.38	277.63 ± 0.49	0.60 ± 0.06	7.00 ± 0.01	0.916499
0.1	1.013	0.41040	264.17 ± 0.31	277.63 ± 0.47	0.49 ± 0.02	7.00 ± 0.00	1.0018854
0.1	1.013	0.88890	269.03 ± 0.28	267.75 ± 1.48	1.52 ± 0.09	6.99 ± 0.01	1.1011984
0.1	1.013	0.70118	268.12 ± 0.48	268.26 ± 1.61	1.28 ± 0.04	6.99 ± 0.01	1.0134019
0.1	1.013	0.59444	268.21 ± 0.80	258.71 ± 1.56	1.70 ± 0.20	7.00 ± 0.01	0.8696881
0.1	1.013	0.44169	264.71 ± 1.51	258.40 ± 1.38	1.31 ± 0.11	7.00 ± 0.00	0.9289941
0.2	1.0998	0.33069	264.79 ± 1.00	277.48 ± 0.25	1.01 ± 0.12	7.00 ± 0.01	0.8951966
0.2	1.0998	0.31373	263.44 ± 0.33	277.26 ± 0.21	0.82 ± 0.03	6.99 ± 0.01	0.9506074
0.2	1.0998	0.41209	264.38 ± 1.19	275.73 ± 0.80	0.65 ± 0.10	7.01 ± 0.00	1.0360393
0.2	1.0998	0.37478	262.96 ± 0.34	276.67 ± 0.79	0.52 ± 0.02	7.00 ± 0.00	1.0953405
0.2	1.0998	0.20181	260.70 ± 1.15	267.69 ± 0.30	0.81 ± 0.14	7.00 ± 0.01	0.8364018
0.2	1.0998	0.27134	263.19 ± 0.73	267.60 ± 0.30	0.81 ± 0.04	6.99 ± 0.01	0.8295956
0.2	1.0998	0.24759	263.65 ± 0.78	259.87 ± 2.29	0.89 ± 0.04	7.00 ± 0.01	0.7142956
0.2	1.0998	0.23233	261.16 ± 0.74	259.50 ± 2.06	0.88 ± 0.02	6.99 ± 0.01	0.8371818
0.2	1.0998	0.21707	264.39 ± 0.75	261.82 ± 1.10	4.41 ± 0.33	7.00 ± 0.01	0.6498899
0.3	1.178	0.31499	265.67 ± 1.11	276.93 ± 0.81	0.58 ± 0.04	7.00 ± 0.01	0.8376427
0.3	1.178	0.29600	264.16 ± 0.36	277.06 ± 0.80	0.50 ± 0.01	7.00 ± 0.00	0.8929689
0.3	1.178	0.25801	264.13 ± 1.14	268.77 ± 1.18	0.52 ± 0.05	7.00 ± 0.00	0.7795833
0.3	1.178	0.20261	260.51 ± 1.22	268.70 ± 1.15	0.40 ± 0.02	7.00 ± 0.01	0.8914734
0.3	1.178	0.14721	259.53 ± 0.69	260.65 ± 1.80	0.65 ± 0.09	7.00 ± 0.01	0.7344125
0.3	1.178	0.11238	257.06 ± 1.15	260.10 ± 1.58	0.37 ± 0.06	7.00 ± 0.01	0.7481703

Table 3-1. Continued

Concentration (g g^{-1})	Density (g cm^{-3})	Evaporation Rate (mm h^{-1})	Avg Sample Temp (K)	Avg Chamber Temp (K)	Avg Rh (%)	Total Pressure (mbar)	a_{H2O}
0.4	1.249	0.28969	267.39 ± 1.18	277.23 ± 0.95	0.55 ± 0.07	7.01 ± 0.01	0.7174746
0.4	1.249	0.25983	265.72 ± 0.29	277.31 ± 0.96	0.43 ± 0.02	7.01 ± 0.01	0.750879
0.4	1.249	0.13589	263.43 ± 1.09	268.15 ± 1.18	0.85 ± 0.02	7.00 ± 0.01	0.555826
0.4	1.249	0.15231	261.51 ± 0.35	267.96 ± 1.14	0.80 ± 0.04	7.00 ± 0.01	0.7045028
0.4	1.249	0.13589	260.98 ± 2.19	260.81 ± 0.23	1.29 ± 0.32	6.99 ± 0.01	0.6453407
0.4	1.249	0.10304	256.42 ± 0.50	260.87 ± 0.30	0.78 ± 0.03	7.00 ± 0.01	0.7903189
0.5	1.351	0.17533	266.55 ± 0.56	274.55 ± 0.74	0.45 ± 0.05	7.00 ± 0.01	0.5655041
0.5	1.351	0.18499	266.67 ± 0.29	275.86 ± 0.81	0.38 ± 0.03	7.00 ± 0.00	0.5786898
0.5	1.351	0.10630	263.87 ± 1.60	268.83 ± 0.26	0.59 ± 0.09	7.00 ± 0.01	0.4771263
0.5	1.351	0.11734	261.74 ± 0.35	268.83 ± 0.24	0.47 ± 0.02	7.00 ± 0.00	0.6106084
0.5	1.351	0.05108	260.30 ± 1.57	261.98 ± 0.40	0.05 ± 0.09	7.00 ± 0.01	0.3599013
0.5	1.351	0.06765	257.17 ± 0.53	261.59 ± 0.27	0.01 ± 0.01	7.00 ± 0.02	0.5774161

Table 3-2. Pitzer Parameters for likely chlorate species at the Phoenix landing site.

Chem_sys	Beta(0)	Beta(1)	C(phi)
Na^+ - ClO_3^-	0.01908	0.27932	0.00181
K^+ - ClO_3^-	0.17059	0.22944	-0.00524
Mg^{2+} - ClO_3^-	0.4317 ± 0.0792	-2.258 ± 6.657	-0.0166 ± 0.0077
Ca^{2+} - ClO_3^-	0.2434 ± 0.0178	2.6812 ± 0.8059	0.0018 ± 0.0025
H^+ - ClO_3^-	0.1314 ± 0.0643	1.4577 ± 0.7616	-7.408×10^{-5} ± 0.0125

Table 3-3. Initial Composition of the Solution modeled in Figure 3-4.

Ion	Concentration (mmolar)
Na^+	1.4
K^+	0.4
Ca^{2+}	0.75
Mg^{2+}	6.4
Cl^-	0.75
ClO_4^-	2.5
SO_4^{2-}	5.3
ClO_3^-	2.25

4 Near- and Mid-Infrared Reflectance Spectra of Hydrated Chloride Salts

4.1 Abstract

The presence and distribution of chlorides on Mars has implications for the stability of water. To date, chlorine has been measured by all lander missions, but detection by remote sensing has been limited to deposits of anhydrous chlorides. Given that chlorides can form myriad hydrated phases, we have measured their near-and mid-infrared spectra from 1-22 μm. As expected, anhydrous chlorides show almost no features, except for small bands of adsorbed water. However, the hydrated chlorides show many features at less than ~6 μm, all attributable to water. Given their distinctive features, hydrated chlorides should be detectable by remote sensing, but their spectra are very similar to other hydrated salts, making them difficult to identify in mixed salt deposits.

4.2 Introduction

Chlorides have been suggested as the major constituents of some spectrally distinct units in Mars Odyssey THEMIS mid-infrared observations (Glotch et al., 2010; Glotch et al., 2013; Osterloo et al., 2008) and Mars Express OMEGA (Ruesch et al., 2012). Along with other geomorphologic arguments for their existence in the martian regolith, the discovery of chlorides and perchlorates in the north subpolar latitudes by NASA's Phoenix Lander (Hecht et al., 2009) reinforced the potential for the global distribution of chlorides on Mars.

On Earth, chlorides form as precipitates from saline waters, and during volcanic outgassing. Finding chlorides present on Mars is important for understanding the geological and chemical history of the planet. It is also important for the potential presence of water since chloride salts can form aqueous solutions in present day martian conditions because of their low

temperature eutectics and related lower evaporation rates (Altheide et al., 2009; Brass, 1980; Marion et al., 2003; Marion et al., 2008).

Chlorine, presumed to be mostly in the form of chlorides, have been directly detected on the surface of Mars by the two Viking landers (Clark et al., 1976; Clark et al., 1982) , Pathfinder rover (Wänke et al., 2001), Spirit and Opportunity rovers (Gellert et al., 2004; Rieder et al., 2004) and Phoenix lander (Hecht et al., 2009); however orbital detection of chlorides has been scarce. Osterloo et al. (2010; 2008) identified spectrally distinct units in Terra Sirenum, using Mars Odyssey Thermal Emission Imaging System (THEMIS) that resembled chloride-bearing minerals. Jensen and Glotch (2011) demonstrate that some of the featureless terrain with a red sloping spectrum seen by CRISM could indeed be anhydrous sodium chloride mixed with labradorite/flood basalts. However, many chloride salts form multiple hydration phases, e.g. NaCl forms $NaCl{\cdot}2H_2O$, and $MgCl_2$ forms phases with 2, 4, 6, 8 and 12 water molecules, with the hexahydrate being stable at standard Earth temperatures.

Although the martian atmosphere is very dry, it can reach 100% RH at night (Zent et al., 2010) and is also quite cold (average ~218 K), making higher hydration states stable for longer periods of time. All chlorides will form hydrates in the presence of water at sufficiently low temperatures (see Figure 4-1 for stability diagrams of the chlorides studied in this paper). While there have been studies into playa evaporites (e.g. Crowley, 1991; Hunt et al., 1972), many of these are field samples not available in current digital spectral libraries. Laboratory spectra of each chloride at each hydration state would be beneficial to obtain for analysis of remote sensing data.

This purpose of this paper is to supplement existing spectral libraries and thereby enhance the ability for remote detection of chlorides. For this study, we focused on the near-

infrared (NIR) from 1-2.5 μm due to the large number of missions spectroscopically observing this range around planetary bodies other than Earth: e.g. CRISM (Compact Reconnaissance Imaging Spectrometer) on board the Mars Reconnaissance Orbiter and OMEGA (Visible and Infrared Mineralogical Mapping Spectrometer) on board Mars Express, both orbiting Mars; NIMS (Near-Infrared Mapping Spectrometer) on board Galileo around the Jupiter system; VIMS (Visual and Infrared Mapping Spectrometer) on board Cassini around the Saturn system; and LEISA (Linear Etalon Imaging Spectral Array) on the New Horizons mission. This region of the spectrum is dominated by water absorption overtones, making it extremely sensitive to hydrated minerals. Analysis of the water bands shows distortion and shifting depending on how the water is bound to the molecule, as well as the number of the hydrates. Since the absorption modes of water fall in the mid-infrared (MIR), we also collected reflectance spectra from 2.5-22 μm for a few hydrated phases stable at room temperature. A companion paper regarding spectra of chlorine oxyanions (hypochlorites, chlorites, chlorates and perchlorates) is in preparation as well.

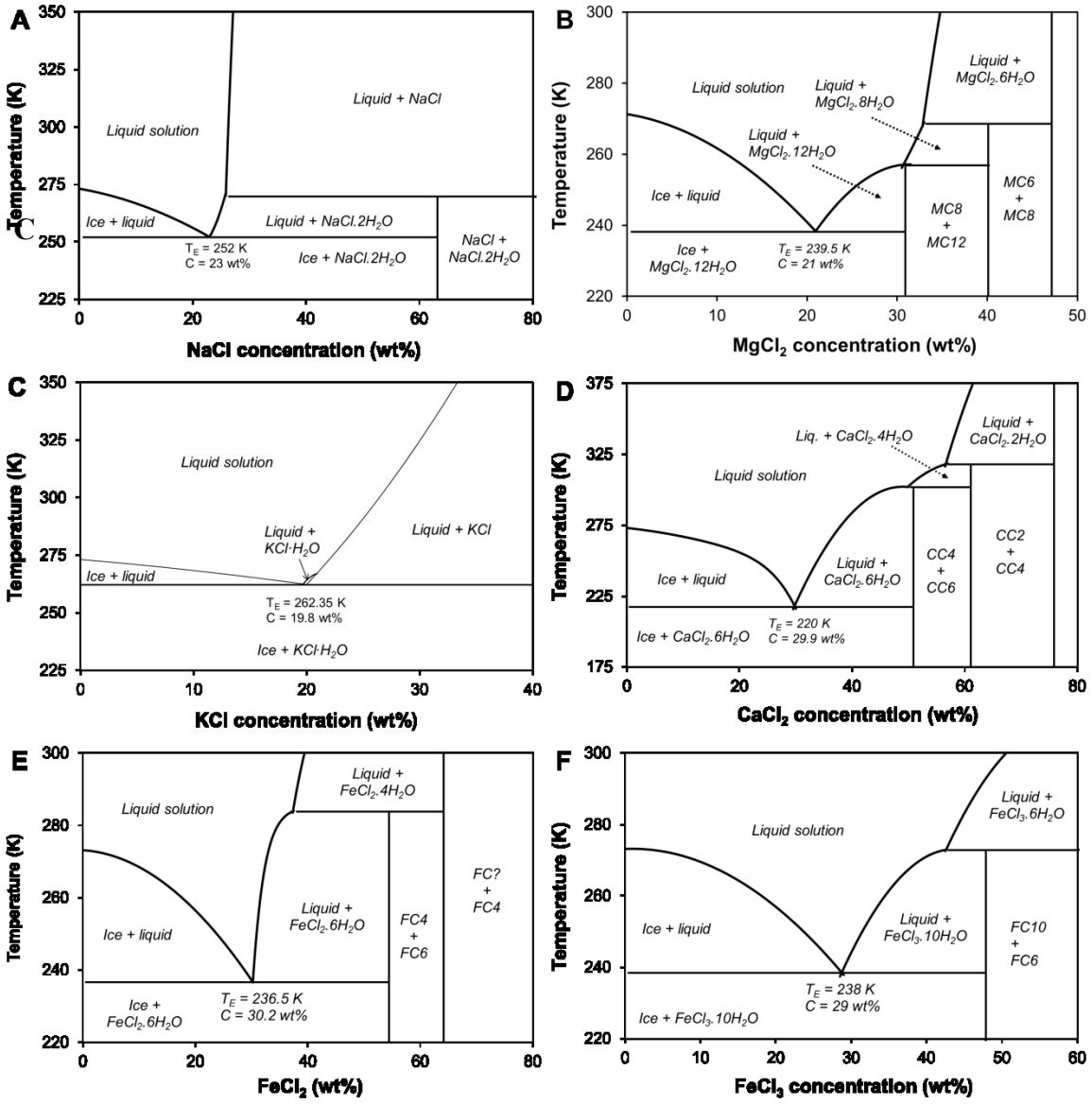

Figure 4-1. Stability diagrams for (A) NaCl, (B) $MgCl_2$, (C) KCl, (D) $CaCl_2$, (E) $FeCl_2$ and (F) $FeCl_3$, which were created using solubility data from Linke (1965), Fialkov and Chernogorenko (1955), Shul'gina et al (1955), and Marion (2003; 2008). Notice that all chlorides form a hydrated phase, though some are only stable in a small range of temperatures. Samples were prepared by precipitating saturated solutions at the appropriate temperatures from these figures, as described in Table 4-1.

4.3 Methods

Table 4-1 lists the salts and their hydrates which we synthesized for our study. Salts stable at room temperature were sieved to 63 μm and measured. Higher hydrates were prepared by precipitating saturated solutions at the appropriate temperatures, using the stability diagrams in Figure 4-1. Stability diagrams were created based on solubility data (Fialkov and Chernogorenko, 1955; Linke, 1965; Marion et al., 2003; Marion et al., 2008; Shul'gina et al., 1955). Lower hydrates were synthesized by heating to the appropriate temperature. For $MgCl_2$, heating directions were followed from Gurevich et al. (1978). Truly anhydrous phases were difficult to obtain; these salts are extremely hygroscopic. Anhydrous phases of magnesium and ferric chlorides cannot be synthesized directly from their hydrated phases, as they will release chlorine gas (HCl) and form oxidized states instead. However, based on their ionic bonds, they are likely to be featureless in the NIR like NaCl and KCl. The exceptions to this are the iron chlorides, which might exhibit electronic transitions. To remove as much water as possible, anhydrous spectra were collected on a hot plate set to 120°C, under nitrogen flow for two hours.

Reflectance spectra were taken using a Nicolet 6700 FTIR Spectrometer. For NIR reflectance, the spectrometer was equipped with fiber optics and a SmartNIR accessory to allow analysis in the range 1.0-2.5 μm. White light was the source, TEC was the detector, with a CaF_2 beamsplitter. KBr was used as a background. For MIR reflectance, DTGS was the detector, with a KBr beamsplitter, and standard gold was used for the background.

Table 4-1. Minerals/Salts prepared for this study.

Mineral/Salt Name	Formula	Source/Method of Preparation
--	$MgCl_2 \cdot 2H_2O$	Dehydrated $MgCl_2 \cdot 6H_2O$ at 120°C
--	$MgCl_2 \cdot 4H_2O$	Dehydrated $MgCl_2 \cdot 6H_2O$ at 100°C
Bischofite	$MgCl_2 \cdot 6H_2O$	BDH $MgCl_2 \cdot 6H_2O$ powder
--	$MgCl_2 \cdot 8H_2O$	Precipitated saturated solution at -4°C
Hydrophilite	$CaCl_2$	Alfa Aesar $CaCl_2$ powder
Sinjarite	$CaCl_2 \cdot 2H_2O$	Alfa Aesar $CaCl_2 \cdot 2H_2O$ powder
Antarcticite	$CaCl_2 \cdot 6H_2O$	Precipitated saturated solution at 30°C
--	$FeCl_2 \cdot 4H_2O$	Dehydrated $FeCl_2 \cdot 6H_2O$ at 100°C
--	$FeCl_2 \cdot 6H_2O$	Alfa Aesar
Hydromolysite	$FeCl_3 \cdot 6H_2O$	Alfa Aesar
--	$FeCl_3 \cdot 10H_2O$	Precipitated saturated solution at -10°C

4.4 Results

Numerous absorption features are found in the NIR for almost all compounds measured. Table 4-2 lists the minima positions for each band. All hydrates have the characteristic water bands at ~1.4 and ~1.9 μm. Overtones of water are also seen at ~1.19 (1.17-1.21) and ~1.77 (1.75-1.80) μm. Hydrated $MgCl_2$ salts demonstrate myriad spectral features in the 2, 4 and $6H_2O$ forms (Figure 4-2). Numerous hydration bands are also seen in the other chlorides. Ferric and ferrous chlorides (Figure 4-3) yield asymmetric hydration bands, particularly in the 1.9 μm band of $FeCl_2 \cdot 4H_2O$. It is unique in that the asymmetry favors the shorter wavelengths, unlike other bands. Although the powder for $CaCl_2$ was labeled as anhydrous, there are clearly features of hydration, and not just from adsorbed water (Figure 4-4). We would conclude that this is in fact a hydrated form, although it does not resemble $CaCl_2 \cdot 2H_2O$, the next known hydration state, therefore it may contain a monohydrate or hydroxyl molecule.

Overall, a trend is seen where these features are affected by the level of hydration, which controls the depth, breadth and number of absorption bands. Specifically, increasing hydration states broadens and deepens the bands, while reducing the number of individual, resolvable

bands. This is because the more water molecules there are, the more blended each feature becomes, especially when looking at combinations and overtones.

In the MIR, fundamentals of water ice are expected at 2.94 µm, 3.1 µm and 6.06 µm (Cloutis et al., 2006). In the magnesium chlorides (Figure 4-5), as expected, no features are seen except those due to water of hydration. Our features match the water fundamentals, which compare closely to those found in Gurevich et al. (1978). No features were seen at longer than ~6 µm in the $2H_2O$ and $4H_2O$ hydrates. In the hexahydrate, there is an increase around 16 µm and a dip at 18 µm, which could be due to the rotational fundamental of water (Bayly et al., 1963).

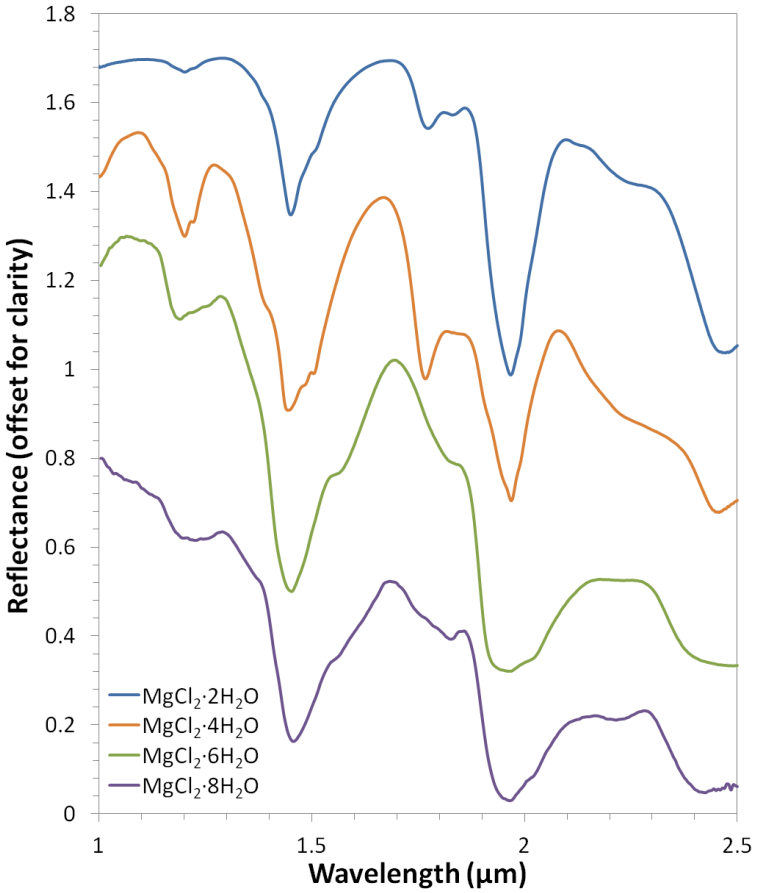

Figure 4-2. NIR reflectance spectra of magnesium chloride hydrates.

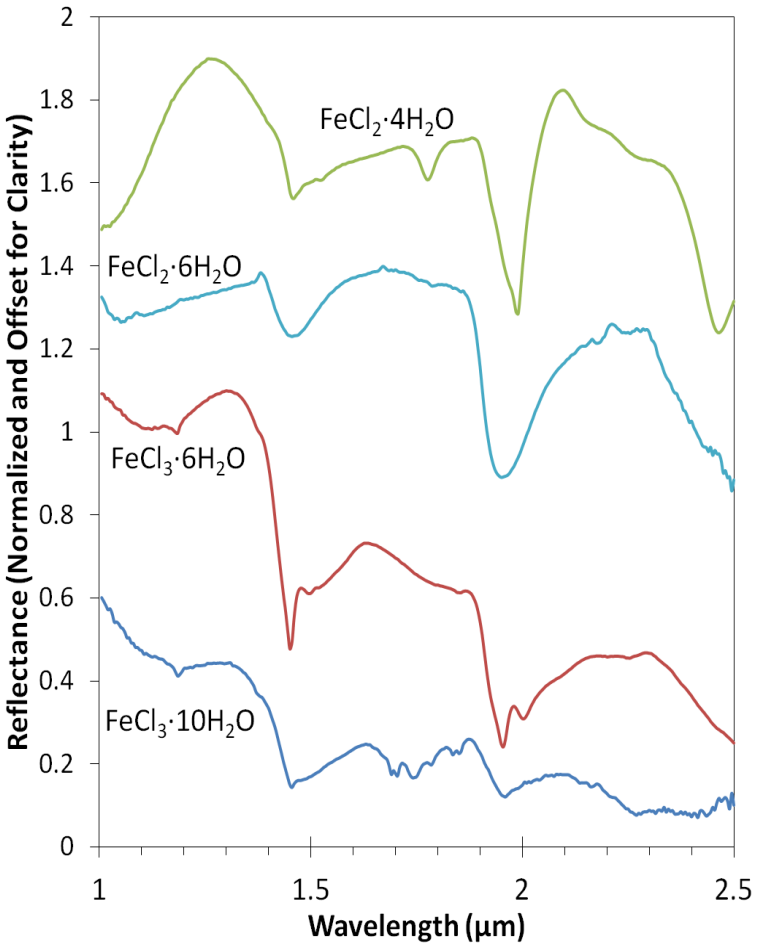

Figure 4-3. NIR reflectance spectra of iron chloride hydrates.

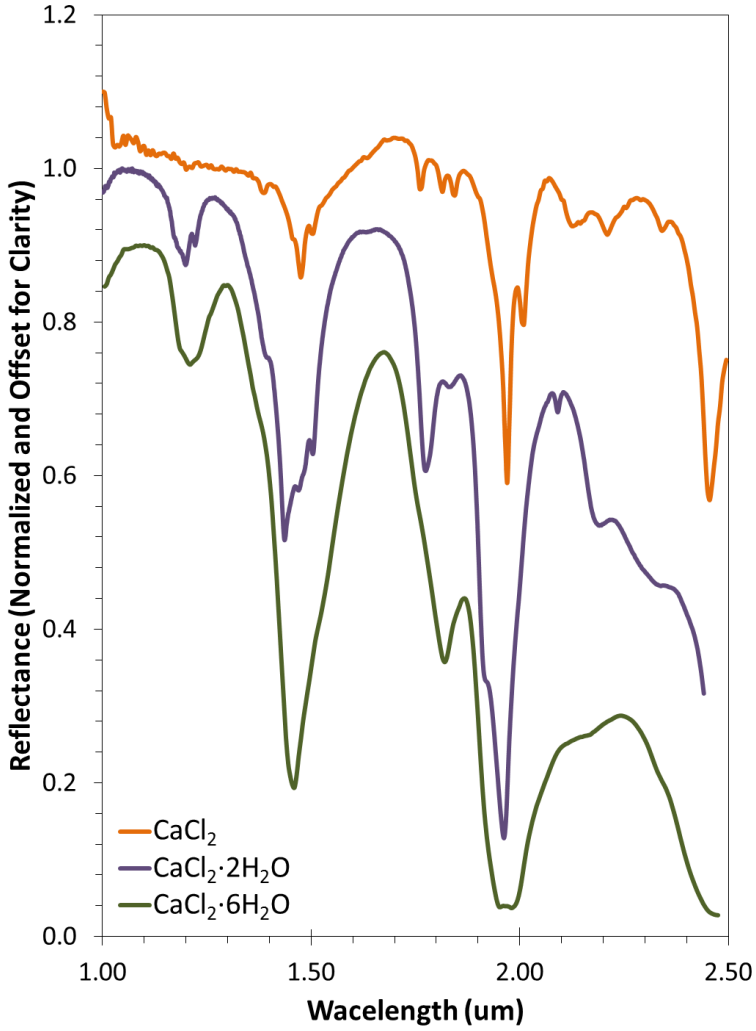

Figure 4-4. NIR reflectance of calcium chloride hydrates. $CaCl_2$ (top) is clearly not anhydrous, though its hydration state remains unknown.

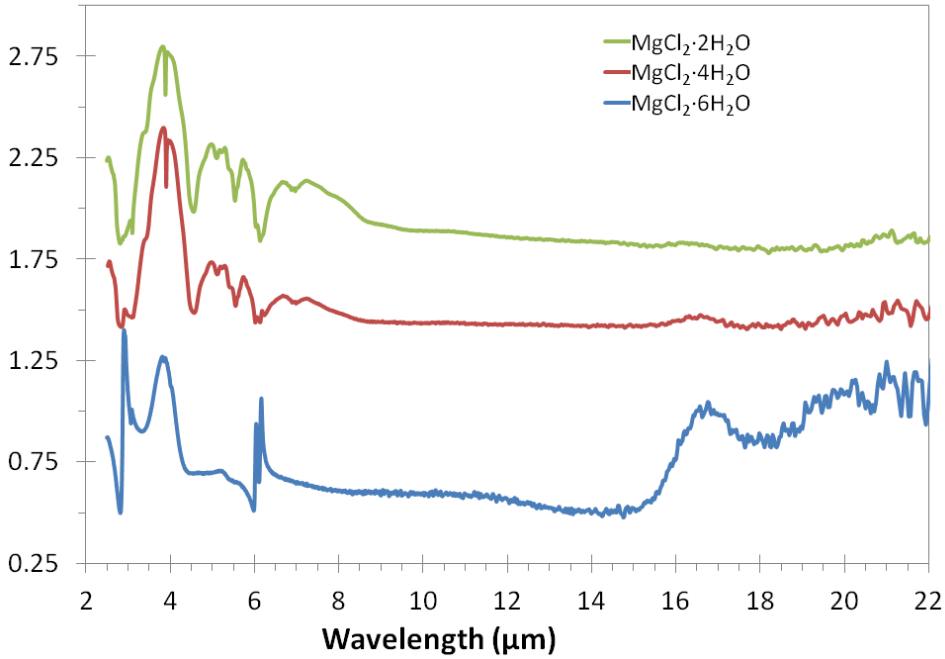

Figure 4-5. MIR reflectance spectra of $MgCl_2$ hydrates.

Table 4-2. NIR reflectance minima positions for measured chlorides (all in μm), grouped by wavelength, highlighting the characteristic water bands at ~1.4 and ~1.9 μm.

		~1.4 H_2O		~1.9 H_2O	
$CaCl_2$		1.48	1.76, 1.82, 1.84	1.97, 2.01	2.13, 2.21, 2.45
$CaCl_2 \cdot 2H_2O$	1.20	1.44	1.78	1.96	
$CaCl_2 \cdot 6H_2O$	1.21	1.46	1.82	1.98	
$MgCl_2 \cdot 2H_2O$	1.22	1.47	1.77, 1.81	1.98	2.46
$MgCl_2 \cdot 4H_2O$	1.21	1.44	1.78	1.96	2.45
$MgCl_2 \cdot 6H_2O$	1.19	1.45		1.96	2.42
$MgCl_2 \cdot 8H_2O$	1.20	1.46		1.97	2.41
$FeCl_2 \cdot 4H_2O$		1.46	1.78	1.99	2.46
$FeCl_2 \cdot 6H_2O$		1.47		1.96	
$FeCl_3 \cdot 6H_2O$	1.18	1.45		1.95, 2.00	
$FeCl_3 \cdot 10H_2O$	1.19	1.46	1.75	1.96	2.27, 2.42

4.5 Discussion

The salts used in our analysis are all extremely hygroscopic. For instance, grains of $MgCl_2 \cdot 6H_2O$ at room temperature and high relative humidity (~60%) will form liquid droplets on the lab bench. Even NaCl has remnants of water adsorption bands present at ~1.9 μm (Figure 4-6), even though they it does not form hydrates at room temperature. Even heating at 120°C for 2 hours under nitrogen flow is not sufficient to remove all water in some instances. This has implications for the amount of water present as hydrated chlorides on the martian surface.

Most hydrated salts exhibit features in the NIR that are primarily due to water. This is evidenced by comparing the hydrates to their anhydrous forms. This comes as no surprise, as the major fundamentals and overtones of water are in the NIR, e.g. 1.04, 1.25, 1.5-1.6, and 1.96-2 μm (Clark et al., 1990; Cloutis et al., 2006).

It is interesting to note that for all the salts studied thus far, all of the absorption bands appear to result from the presence of water. It is likely that the band at ~1.2 μm is a distortion of the combination band $v_1 + v_2 + v_3$, however it is unclear what the 1.75-1.82 μm band is caused by. It is possible that it is from the cation-water interaction; this is a significant effect which must be

taken into account, as the structure for $MgCl_2 \cdot 6H_2O$ is actually Mg(6OH, H)+2Cl. The same is true for the iron and calcium chlorides; the water molecules are bound to the cation, while the chloride ions are situated outside the first coordination sphere.

The cation will also control the number and quantity of hydration states. For example, potassium and sodium salts form only a few (if any) hydration states (Figure 4-1). Magnesium salts are extremely hygroscopic; under terrestrial conditions of temperature, pressure and humidity their hydration states are likely to be hexahydrate (Figure 4-1), but can be hydrated up to $12H_2O$.

4.5.1 Comparison to Other Hydrated Spectra

To date, the only chloride salts in the USGS spectral library are carnallite ($MgCl_2 \cdot KCl \cdot 6H_2O$) and halite (NaCl). In the CRISM library, they have measured sal-ammoniac (NH_4Cl) and an evaporite mixture composed primarily of halite, sylvite and kieserite. These are all shown in Figure 4-6.

Halite does not have any spectral features in the NIR, except for a little band of adsorbed water at ~1.9 μm, as would be expected of an anhydrous halide. Sal-ammoniac is the only salt to exhibit features not due to water.

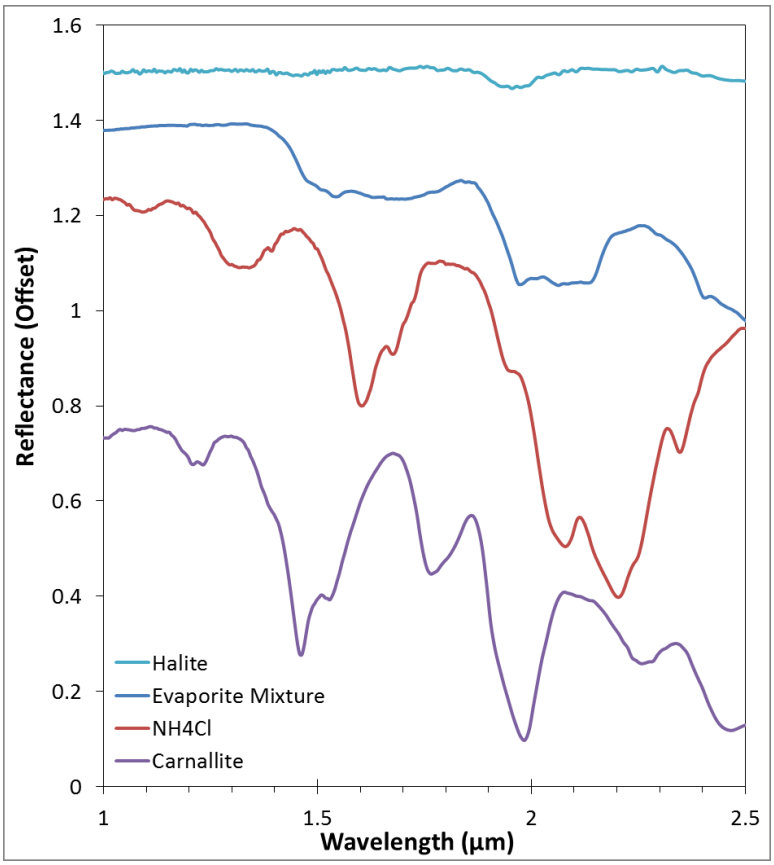

Figure 4-6. Chlorides present in CRISM and USGS databases. Evaporite Mixture C1MS45 and NH_4Cl CACL49 from CRISM spectral library. Carnallite NMNH98011 and Halite HS433.3B from Clark et al. (2007).

It is interesting to compare the chloride spectra to other hydrated minerals that have been detected on Mars from remote sensing (Figure 4-7, Murchie et al., 2009). Those salts include gypsum ($CaSO_4 \cdot 2H_2O$), bassanite ($2CaSO_4 \cdot H_2O$), kieserite ($MgSO_4 \cdot H_2O$) and epsomite ($MgSO_4 \cdot 7H_2O$). Phyllosilicates include nontronite, montmorillonite and saponite. The spectrum of epsomite is particularly similar to that of $MgCl_2 \cdot 6H_2O$.

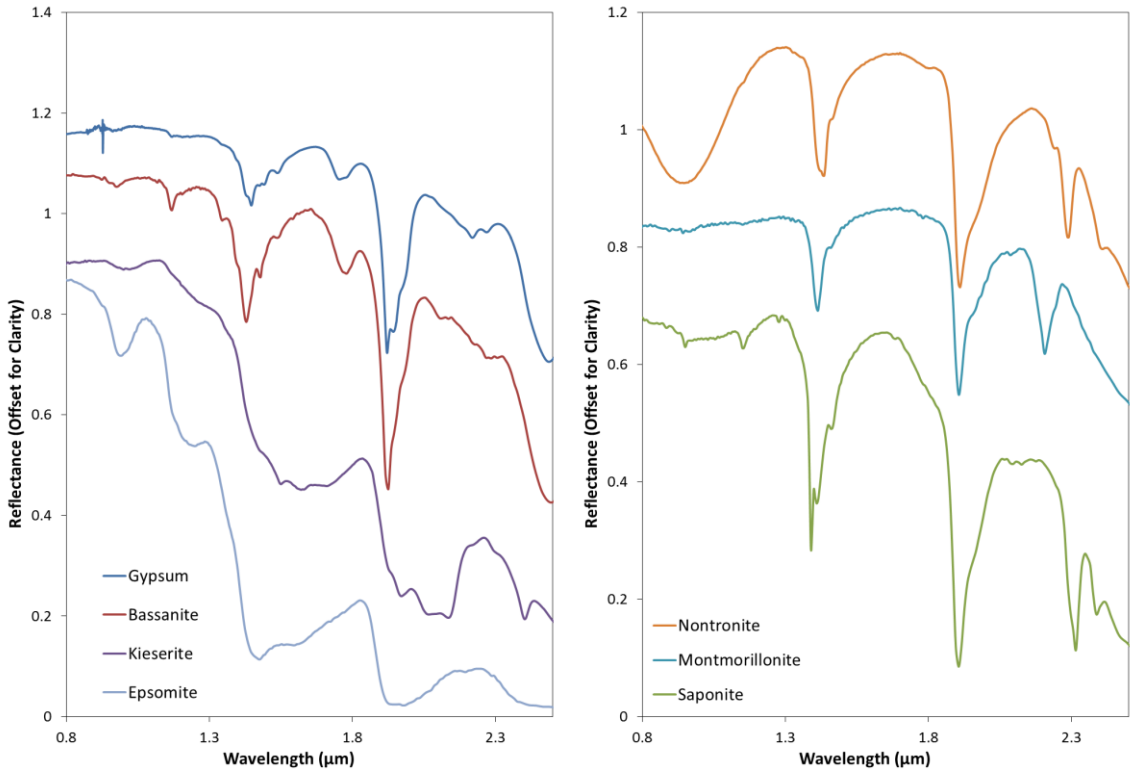

Figure 4-7. Reflectance spectra of hydrated minerals commonly found on Mars (Murchie et al., 2009). From the CRISM library: Gypsum BKR1JB556, Kieserite C1CC15, Nontronite CBJB26. From the USGS Library (Clark et al., 2007): Bassanite GDS145, Epsomite GDS149, Montmorillonite SWy-1, Saponite SapCa-1.AcB.

4.6 Conclusions

Hydrated chlorides show significant spectral features that should allow for their identification on the surface of Mars. All hydrates exhibit diagnostic bands characteristic of hydrated phases (1.4 and 1.9 µm). Hydration band depth and width both increase with increasing hydration state. The cation-water interaction can generate spectral features that enable differentiation between various chlorides.

Other factors that can affect the reflectance spectra include whether the water of hydration is heavy (Guillermet and Novak, 1969), grain size (Pommerol and Schmitt, 2008b),

observing angle (Pommerol and Schmitt, 2008a) and temperature (Dalton, 2007; Grundy and Schmitt, 1998). Much more work is needed to acquire a complete library of these salts under the appropriate conditions needed for planetary comparisons. In particular, the low temperature hydrates are difficult to synthesize without having liquid water or ice also present. Having an environmental chamber capable of synthesizing each hydrate at the appropriate temperature and humidity, and measuring the spectra in situ would be beneficial.

Although many hydrate phases might be metastable, the spectral database should include all known hydration states for each compound. The biggest hurdle to unique identification of hydrated chlorides is that polyhydrated salts have many similar features depending on hydration state; some unidentified hydrates in planetary remote sensing observations could in fact be chlorides. Therefore care must be taken to distinguish between highly hydrated salts.

4.7 References

Altheide, T., Chevrier, V., Nicholson, C., Denson, J., 2009. Experimental investigation of the stability and evaporation of sulfate and chloride brines on Mars. Earth and Planetary Science Letters. 282**,** 69-78.

Bayly, J. G., Kartha, V. B., Stevens, W. H., 1963. The absorption spectra of liquid phase H2O, HDO and D2O from 0·7 μm to 10 μm. Infrared Physics. 3**,** 211-222.

Brass, G. W., 1980. The stability of brines on Mars. Icarus. 42**,** 20-28.

Clark, B. C., et al., 1976. Inorganic Analyses of Martian Surface Samples at the Viking Landing Sites. Science. 194**,** 1283-1288.

Clark, B. C., Baird, A. K., Weldon, R. J., Tsusaki, D. M., Schnabel, L., Candelaria, M. P., 1982. Chemical Composition of Martian Fines. Journal of Geophysical Research. 87**,** 10059-10,067.

Clark, R. N., King, T. V. V., Klejwa, M., Swayze, G. A., Vergo, N., 1990. High Spectral Resolution Reflectance Spectroscopy of Minerals. Journal of Geophysical Research. 95**,** 12653-12680.

Clark, R. N., et al., 2007. USGS digital spectral library splib06a. Digital Data Series 231. U.S. Geological Survey.

Cloutis, E. A., et al., 2006. Detection and discrimination of sulfate minerals using reflectance spectroscopy. Icarus. 184**,** 121-157.

Crowley, J. K., 1991. Visible and Near-Infrared (0.4-2.5 μm) Reflectance Spectra of Playa Evaporite Minerals. Journal of Geophysical Research. 96**,** 16231-16240.

Dalton, J. B., III, 2007. Linear mixture modeling of Europa's non-ice material based on cryogenic laboratory spectroscopy. Geophysical Research Letters. 34**,** L21205.

Fialkov, Y. A., Chernogorenko, V. B., 1955. Potassium chloride hydrate. Dokl. Akad. Nauk SSSR, Vol. 102, pp. 759-762.

Gellert, R., et al., 2004. Chemistry of rocks and soils in Gusev Crater from the Alpha Particle X-ray Spectrometer. Science. 305**,** 829-832.

Glotch, T. D., Bandfield, J. L., Tornabene, L. L., Jensen, H. B., Seelos, F. P., 2010. Distribution and formation of chlorides and phyllosilicates in Terra Sirenum, Mars. Geophysical Research Letters. 37**,** L16202.

Glotch, T. D., Bandfield, J. L., Wolff, M. J., Arnold, J. A., 2013. Chloride Salt Deposits on Mars - No Longer "Putative". 44th Lunar and Planetary Science Conference. Lunar and Planetary Institute, Houston, pp. Abstract #1549.

Grundy, W. M., Schmitt, B., 1998. The temperature-dependent near-infrared absorption spectrum of hexagonal H2O ice. Journal of Geophysical Research: Planets. 103**,** 25809-25822.

Guillermet, J., Novak, A., 1969. Spectres infrarouges des chlorures et des bromures de magnésium hydratés. J. Chim. Phys. Physiochim. Biol. 66**,** 68-80.

Gurevich, L., Rommel, I., Polyakov, Y., 1978. Infrared spectra and characteristic structural features of the hydrates of magnesium chloride. Journal of Structural Chemistry. 18**,** 683-687.

Hecht, M. H., et al., 2009. Detection of Perchlorate and the Soluble Chemistry of Martian Soil at the Phoenix Lander Site. Science. 325**,** 64-67.

Hunt, G. R., Salisbury, J. W., Lenhoff, C. J., 1972. Visible and near-infrared spectra of minerals and rocks: V. Halides, phosphates, arsenates and borates. Modern Geology. 3**,** 121-132.

Jensen, H. B., Glotch, T. D., 2011. Investigation of the near-infrared spectral character of putative Martian chloride deposits. Journal of Geophysical Research. 116**,** E00J03.

Linke, W. F., 1965. Solubilities: inorganic and metal-organic compounds. D. Van Nostrand.

Marion, G. M., Catling, D. C., Kargel, J. S., 2003. Modeling aqueous ferrous iron chemistry at low temperatures with application to Mars. Geochimica et Cosmochimica Acta. 67**,** 4251-4266.

Marion, G. M., Kargel, J. S., Catling, D. C., 2008. Modeling ferrous–ferric iron chemistry with application to martian surface geochemistry. Geochimica et Cosmochimica Acta. 72**,** 242-266.

Murchie, S. L., et al., 2009. A synthesis of Martian aqueous mineralogy after 1 Mars year of observations from the Mars Reconnaissance Orbiter. Journal of Geophysical Research: Planets. 114**,** n/a-n/a.

Osterloo, M. M., Anderson, F. S., Hamilton, V. E., Hynek, B. M., 2010. Geologic context of proposed chloride-bearing materials on Mars. Journal of Geophysical Research. 115**,** E10012.

Osterloo, M. M., et al., 2008. Chloride-Bearing Materials in the Southern Highlands of Mars. Science. 319**,** 1651-1654.

Pommerol, A., Schmitt, B., 2008a. Strength of the H2O near-infrared absorption bands in hydrated minerals: Effects of measurement geometry. Journal of Geophysical Research. 113**,** E12008.

Pommerol, A., Schmitt, B., 2008b. Strength of the H2O near-infrared absorption bands in hydrated minerals: Effects of particle size and correlation with albedo. Journal of Geophysical Research. 113**,** E10009.

Rieder, R., et al., 2004. Chemistry of Rocks and Soils at Meridiani Planum from the Alpha Particle X-ray Spectrometer. Science. 306**,** 1746-1749.

Ruesch, O., et al., 2012. Compositional investigation of the proposed chloride-bearing materials on Mars using near-infrared orbital data from OMEGA/MEx. Journal of Geophysical Research: Planets. 117.

Shul'gina, M. P., Kharchuk, O. S., Yanat'eva, O. K., 1955. New Solid Phases in the System KCl-K2SO4-H2O. Izv. Akad. Nauk SSSR, Sektor Fiz-Khim Analiza. 26**,** 198–210.

Wänke, H., Brückner, J., Dreibus, G., Rieder, R., Ryabchikov, I., 2001. Chemical Composition of Rocks and Soils at the Pathfinder Site. Space Science Reviews. 96**,** 317-330.

Zent, A. P., et al., 2010. Initial results from the thermal and electrical conductivity probe (TECP) on Phoenix. Journal of Geophysical Research. 115**,** E00E14.

5 Near- and Mid-Infrared Reflectance Spectra of Hydrated Chlorine Oxyanion Salts

5.1 Abstract

The presence and distribution of oxychlorine salts (e.g. chlorates and perchlorates) on Mars has implications for the stability of water. To date, chlorine has been measured by all lander missions, but detection by remote sensing has been limited to deposits of anhydrous chlorides. Given that oxychlorine salts can form myriad hydrated phases, we have measured their near-infrared (NIR) and mid-infrared (MIR) spectra from 1-24 μm. As expected, anhydrous oxychlorine salts show almost no features in the NIR, except for small bands of adsorbed water. Hydrated oxychlorine salts show numerous features due to water in the NIR, specifically at ~1.4 and ~1.9 μm. Chlorates exhibit an additional feature at ~2.2 μm. All salts show features in the MIR, due to the fundamental vibrations of Cl-O longward of ~9 μm. Given their distinctive features, oxychlorine salts should be detectable by remote sensing, but their features in the NIR are very similar to other hydrated salts, making them difficult to identify in mixed salt deposits.

5.2 Introduction

Perchlorates were discovered in the north subpolar latitudes by NASA's Phoenix Lander (Hecht et al., 2009), and potentially by the Curiosity rover (Archer et al., 2013). On Mars, as on Earth, perchlorates are thought to form through atmospheric oxidation of chlorine molecules (Catling et al., 2010; Ericksen, 1981; Rao et al., 2010). Intermediate oxyanions between chloride (Cl^-) and perchlorate (ClO_4^-) are chlorate (ClO_3^-), chlorite (ClO_2^-) and hypochlorite (ClO^-). These salts are of special interest since chlorates and perchlorates present on Mars can form aqueous solutions because of their low temperature eutectics (Chevrier et al., 2009; Hanley et al., 2012). Due to the oxidizing nature of the martian surface, perchlorates and chlorates may in fact account

for a significant fraction of the known chlorine concentrations measured by previous landers and orbiters (Clark et al., 1976; Gellert et al., 2004; Keller et al., 2006; Rieder et al., 2004; Wänke et al., 2001). However, at present, no perchlorate spectra are available in any databases, making detection via remote sensing difficult. In order to understand the global distribution, laboratory spectra of each salt at each hydration state need to be obtained.

Vibrational modes for chlorates and perchlorates occur in the MIR (Table 5-1). ClO_X^- possesses 4 normal modes, where ν_1 and ν_3 are bond stretches and ν_2 and ν_4 are bends, all of which are observed at longer than ~8.5 μm (Decius and Hexter, 1977). The 3 fundamental modes for water ice also occur in the MIR: ν_1 (ν_{OH}) at 3.1 μm, ν_2 at 6.06 μm, and ν_3 at 2.94 μm. However there exist many combinations and overtones detectable in the near-infrared (NIR). In particular, they are expected at 1.04 μm ($2\nu_1 + \nu_3$), 1.25 μm ($\nu_1 + \nu_2 + \nu_3$), 1.50-1.66 μm ($2\nu_2 + \nu_3$, $\nu_1 + \nu_3$), 1.55 μm ($2\nu_{OH}$), and 1.96-2.05 μm ($\nu_2 + \nu_3$) (Cloutis et al., 2006).

For this study, we focused primarily on the NIR from 1-2.5 μm due to the large number of missions spectroscopically observing this wavelength range around other planetary bodies: e.g. CRISM (Compact Reconnaissance Imaging Spectrometer) on board the Mars Reconnaissance Orbiter and OMEGA (Visible and Infrared Mineralogical Mapping Spectrometer) on board Mars Express, both around Mars; NIMS (Near-Infrared Mapping Spectrometer) on board Galileo around the Jupiter system; VIMS (Visual and Infrared Mapping Spectrometer) on board Cassini around the Saturn system; and LEISA (Linear Etalon Imaging Spectral Array) on the New Horizons mission. This region of the spectrum is dominated by water absorption bands, making it sensitive to hydrated minerals. Analysis of the water bands shows distortion and shifting depending on how the water is bound to the molecule, as well as the number of the hydrates (Crowley, 1991; Hunt, 1977). Although the martian atmosphere is very

dry, it is also quite cold, making higher hydration states stable for longer periods of time. In general, chlorine salts will form hydrates in the presence of water at low enough temperatures. The purpose of this paper is to supplement existing spectral libraries to enhance the ability for remote detection of chlorates and perchlorates. This will be accomplished by measuring the NIR and MIR reflectance spectra of these salts. Our study will serve to alleviate the lack of data in the current spectral libraries for hydrates that exist on Mars. A companion paper regarding spectra of chlorides is in preparation as well.

Table 5-1. Chlorate infrared rotational and vibrational modes (Decius and Hexter, 1977).

Molecular Mode	**ClO_2^- (gas)**			**ClO_3^-**		**ClO_4^-**	
	(cm^{-1})	**(µm)**		**(cm^{-1})**	**(µm)**	**(cm^{-1})**	**(µm)**
v_1	943	10.60		910	10.99	928	10.78
v_2	445	22.47		617	16.21	459	21.79
v_3	1111	9.00		960	10.42	1119	8.94
v_4				493	20.28	625	16.00
Molecular Mode	**$NaClO_3$**			**$KClO_4$**		**$NaClO_2$ (aq)**	
	(cm^{-1})	**(µm)**		**(cm^{-1})**	**(µm)**	**(cm^{-1})**	**(µm)**
v_1	937.5	10.67	T			790	12.66
v_2	624	16.03	T			400	25.00
v_3	966.4	10.35	L	1170	8.55	840	11.90
	983.5	10.17	T	1050	9.52		
	987.2	10.13	L	(1170-1050)			
	1027	9.74	T				
v_4	481.5	20.77	T	935	10.70		
	485.2	20.61	L				

5.3 Methods

The following salts and some of their hydrates were synthesized and their reflectance spectra were measured: $NaClO_2$, $NaClO_3$, $NaClO_4$, $Ca(ClO)_2$, $Ca(ClO_4)_2$, $KClO_3$, $KClO_4$, $Mg(ClO_3)_2$ and $Mg(ClO_4)_2$ (Table 5-2). Salts stable at room temperature were sieved to 63 μm and measured. For anhydrous salts, the sample was heated to 120°C under constant flow of N_2 for two hours to remove adsorbed water. $NaClO_3$, $KClO_3$, and $KClO_4$ do not form any known hydrates.

Hydrates were prepared by using the stability diagrams prepared by Chevrier et al. (2009) for $NaClO_4$ and $Mg(ClO_4)_2$, and by Hanley et al. (2012) for $Mg(ClO_3)_2$. Stability diagrams were created for the other salts studied from solubility data (Linke, 1965). $Mg(ClO_4)_2 \cdot 6H_2O$ has been shown to be stable over a wide range of temperatures (Robertson and Bish, 2011), and is thus the only phase of $Mg(ClO_4)_2$ studied in this investigation.

$Mg(ClO_3)_2$ was synthesized using the method from Hanley et al. (2012): $Ba(ClO_3)_2$ was mixed in solution with $MgSO_4$, which precipitated $BaSO_4$ but left $Mg(ClO_3)_2$ in solution. Water was slowly evaporated at 100°C to avoid the 112°C melting point of $Mg(ClO_3)_2$. Not all water was able to be removed, leading us to suspect it was $Mg(ClO_3)_2 \cdot 2H_2O$, which stoichiometric calculations confirmed. At room temperature, the salt changed to a more translucent color, and considering its stability diagram, it is likely the hexahydrate. We measured both the dried salt, presumed to be the dihydrate, and the hexahydrate.

Reflectance spectra were taken using a Nicolet 6700 FTIR Spectrometer. For NIR reflectance, the spectrometer was equipped with fiber optics and a SmartNIR accessory to allow analysis in the range 1.0-2.5 μm. White light was the source, TEC was the detector, with a CaF_2

beamsplitter. KBr was used as a background. For MIR reflectance, DTGS was the detector, with a KBr beamsplitter, and standard gold was used for the background.

Table 5-2. Minerals/Salts prepared for this study.

Mineral/Salt Formula	Source/Method of Preparation
$NaClO_2$	Alfa Aesar
$NaClO_3$	Alfa Aesar
$NaClO_4$	Dehydration of monohydrate at 110°C
$NaClO_4 \cdot H_2O$	EMD
$NaClO_4 \cdot 2H_2O$	Monohydrate at 23°C and high humidity
$KClO_3$	Alfa Aesar
$KClO_4$	Alfa Aesar
$Mg(ClO_3)_2 \cdot 2H_2O$	Hanley et al (2012), heated to 112°C
$Mg(ClO_3)_2 \cdot 6H_2O$	Hanley et al (2012), room temperature
$Mg(ClO_4)_2 \cdot 6H_2O$	Alfa Aesar
$Ca(ClO)_2$	JT Baker
$Ca(ClO_4)_2 \cdot nH_2O$	Alfa Aesar

5.4 Results and Discussion

Numerous absorption features are found in the NIR for all compounds measured. These features can be explained by examining three characteristics of the salt being studied: its cation, anion and hydration state. Table 5-3 lists the minima positions for each band, sorted by anion, with features grouped as they relate to the characteristic hydration features at ~1.4 and ~1.9 μm.

All hydrates have the characteristic water bands at ~1.4 and ~1.9 μm. Combinations and overtones of water are also seen at ~1.19 (1.17-1.21) and ~1.77 (1.75-1.80) μm. With the exception of anhydrous $KClO_4$, all salts show bands at ~1.42 and ~1.92 μm. This is true even for the other anhydrous salts, even though some do not form hydrates at room temperature: $NaClO_4$, $NaClO_3$ (Figure 5-1) and $KClO_3$ (Figure 5-2) show bands at 1.9 μm, even after heating at 120°C for 2 hours under nitrogen. This is because these salts are extremely hygroscopic. For instance, $Mg(ClO_4)_2 \cdot 6H_2O$ at room temperature and high relative humidity (~60%) will form a liquid.

Table 5-3. NIR minima positions, grouped according to wavelength (μm), with the typical ~1.4 and ~1.9 μm water absorption bands marked accordingly

		~1.4 H_2O		**~1.9 H_2O**	
Perchlorates					
$Mg(ClO_4)_2 \cdot 6H_2O$	1.16, 1.32	1.42, 1.47	1.73	1.92	2.11, 2.22, 2.39, 2.48
$NaClO_4$		1.42	1.77	1.92	2.21
$NaClO_4 \cdot H_2O$	1.17, 1.33	1.43, 1.47	1.74, 1.80	1.92	2.14, 2.23, 2.42
$NaClO_4 \cdot 2H_2O$	1.17, 1.34, 1.37	1.42	1.56, 1.64, 1.69, 1.78	1.92	2.19, 2.22, 2.27, 2.30, 2.43, 2.48
$KClO_4$	1.25, 1.39		1.55		2.02, 2.12
$Ca(ClO_4)_2 \cdot nH2O$	1.17	1.42	1.75, 1.80	1.92	2.19, 2.23, 2.45
Chlorates					
$Mg(ClO_3)_2 \cdot 2H_2O$		1.43, 1.47	1.54, 1.75	1.92, 1.97	2.22, 2.45
$Mg(ClO_3)_2 \cdot 6H_2O$	1.19	1.44	1.75	1.95	2.27
$NaClO_3$		1.43		1.92	2.23
$KClO_3$	1.12, 1.23	1.43		1.94	2.23, 2.49
Chlorites					
$NaClO_2$	1.19	1.43		1.93	2.20, 2.49
Hypochlorites					
$Ca(ClO)_2$	1.17	1.41, 1.43		1.92	2.36

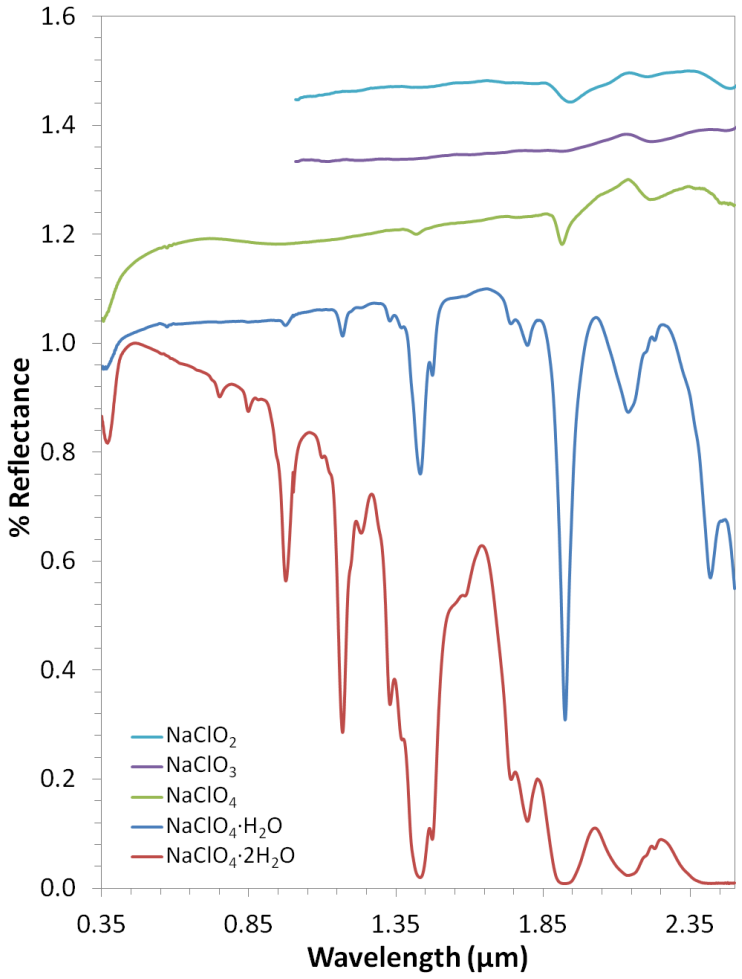

Figure 5-1. NIR reflectance spectra of $NaClO_2$, $NaClO_3$, and $NaClO_4$ anhydrous, monohydrate and dihydrate. The anhydrous salts show remnant adsorbed water bands. The monohydrate and dihydrate have similar bands, due to water, but in the dihydrate the bands are deeper and wider.

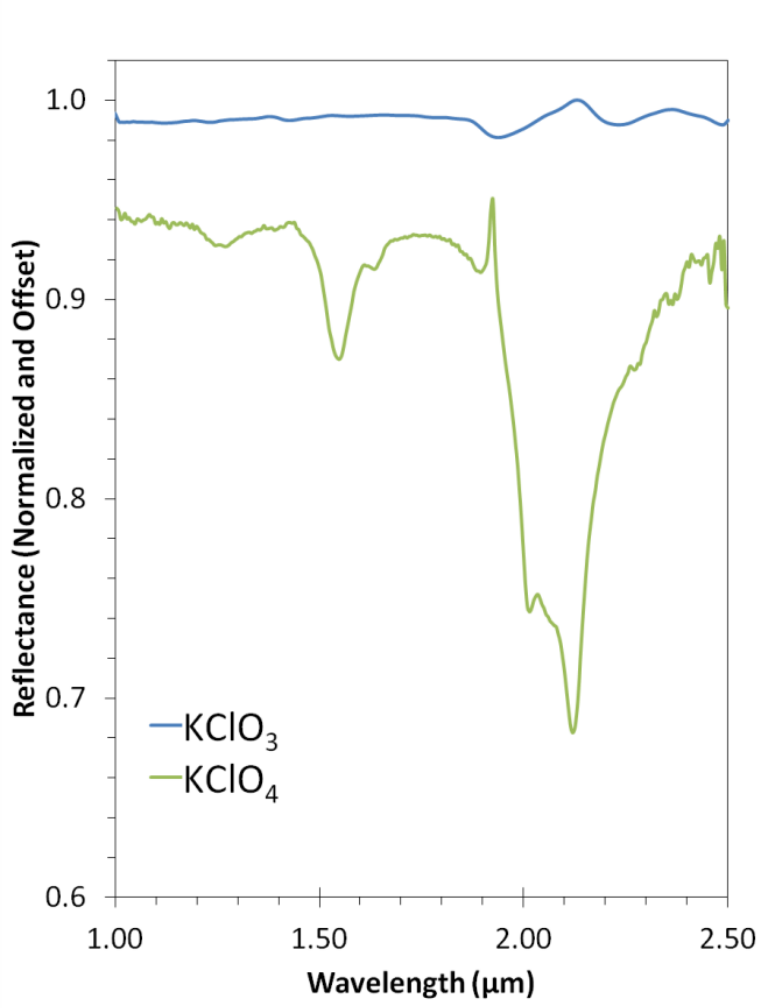

Figure 5-2. NIR reflectance spectra of potassium chlorate and potassium perchlorate. Though neither form hydrates, there are interesting features in both. $KClO_3$ has a remnant water band at ~1.9, and a broad band at 2.2 µm that is seen in other chlorates. $KClO_4$ has features at ~1.55 and 2.0-2.1 µm, possibly due to Cl-O overtones or combinations.

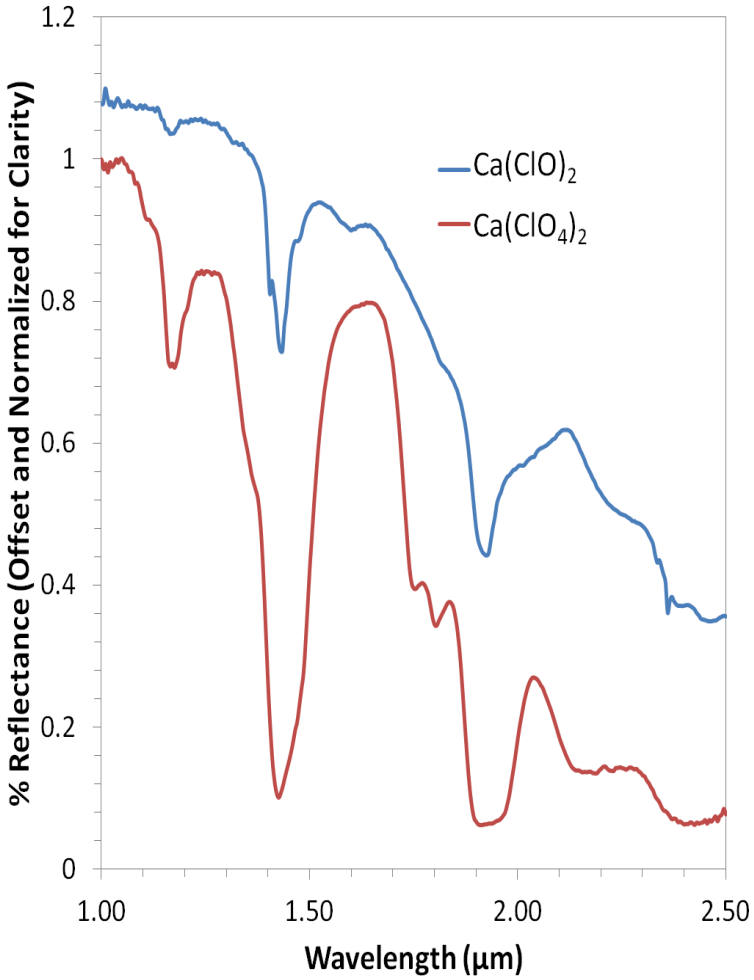

Figure 5-3. NIR reflectance spectra of $Ca(ClO)_2$ and $Ca(ClO_4)_2 \cdot nH_2O$. Both salts show features due to water at ~1.17, ~1.47 and ~1.97 µm.

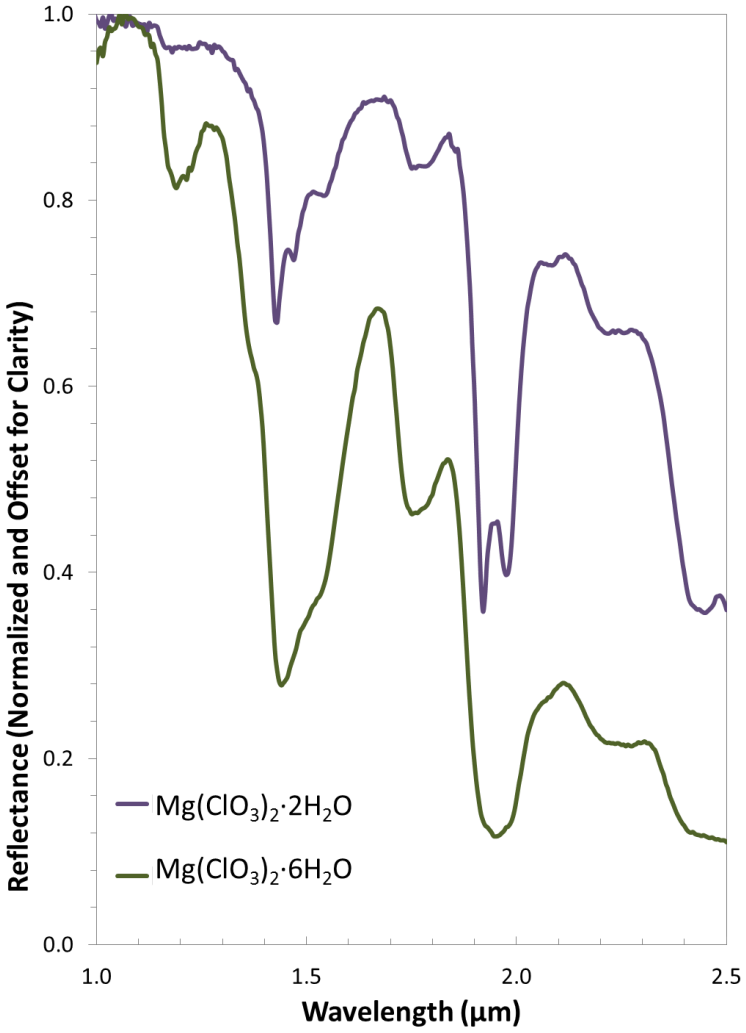

Figure 5-4. NIR reflectance spectra of magnesium chlorate dihydrate and hexahydrate. The water bands are shallower and narrower in the dihydrate than the hexhydrate. There is also a band at ~2.2 µm that is seen in other chlorates as well.

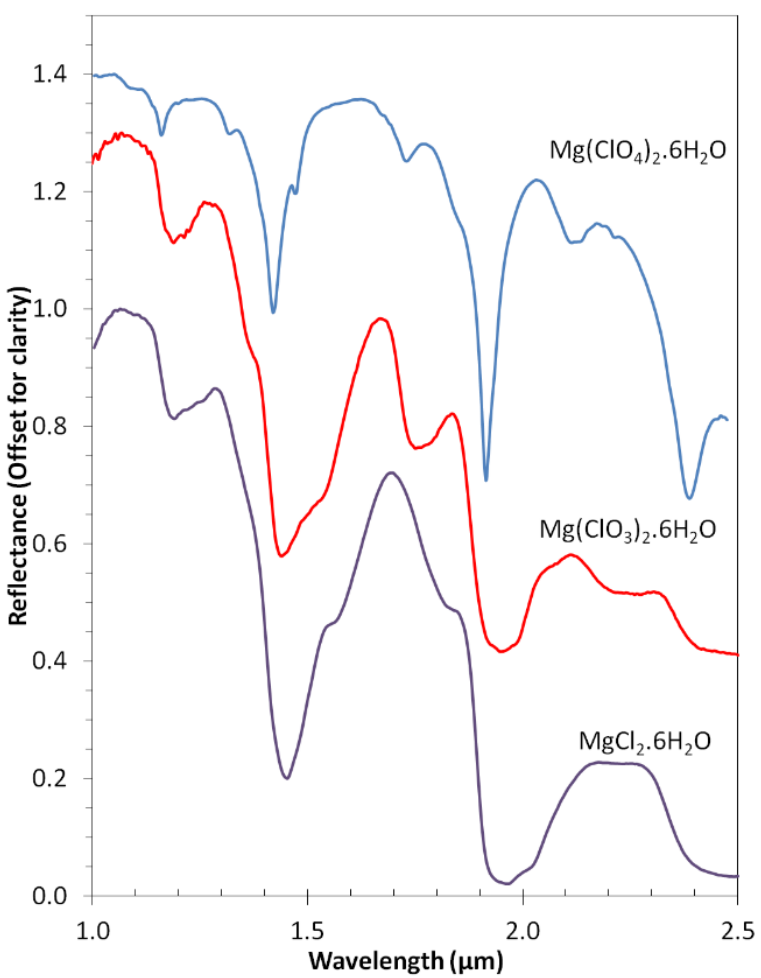

Figure 5-5. NIR reflectance spectra of magnesium perchlorate and chlorate, with $MgCl_2$ shown for comparison from Hanley et al., (in prep). Overall the features are characteristic of many hydrated salts, with bands at ~1.4 and ~1.9 µm, though $Mg(ClO_4)_2$ has much narrower bands than the chlorate and chloride hydrates.

The rest of the hydrated salts, $NaClO_4 \cdot xH_2O$ (Figure 5-1), $Ca(ClO_x)_2 \cdot nH_2O$ (Figure 5-3), $Mg(ClO_3)_2 \cdot xH_2O$ (Figure 5-4) and $Mg(ClO_4)_2 \cdot 6H_2O$ (Figure 5-5), all show features that are due to water. As seen in other hydrated salts (Hanley et al, in prep), band depth and width increase with increasing hydration state. Conversely, at lower hydration states, more individual features are resolved, likely because higher hydration results in increased blending of the features.

In addition, a band appears at ~2.14 μm (possibly due to the Cl-O bond in the perchlorate ion) in each spectrum. The chlorates also exhibit a band at ~2.22 μm, which is present in each of the chlorate salts $NaClO_2$, $NaClO_3$ (Figure 5-1), $KClO_3$ (Figure 5-2) and $Mg(ClO_3)_2 \cdot xH_2O$ (Figure 5-4).

It comes as no surprise that water features dominate the spectral characteristics of the hydrated salts, as the major combinations and overtones of water are in the NIR. However, the anion does have an effect on the reflectance spectra, as evidenced by comparing the spectra of magnesium chloride, chlorate and perchlorate (Figure 5-5). Even though each salt in this case has six water molecules, the features in the perchlorate salt are much narrower, with the chloride features being the widest.

The cation also will affect the spectral features. It is interesting to note that in the structure for these salts the water is actually coordinated with the cation. For instance, $MgClO_4 \cdot 6H_2O$ is actually Mg(6OH, H)+2ClO_4. This in turn controls the hydration states. For example, potassium and sodium salts form only a few (if any) hydration states, while calcium and magnesium salts can be hydrated up to $12H_2O$ ($MgCl_2 \cdot 12H_2O$).

Numerous absorption features are found in the MIR for all compounds measured. In the sodium and magnesium perchlorates (Figure 5-6), there are features that represent the fundamental modes of Cl-O vibration at ~9, 10, 16 and 20 μm (see Table 5-1). There also exists features <6 μm that represent water bands. As expected, these are seen in the sodium and magnesium chlorates as well (Figure 5-7).

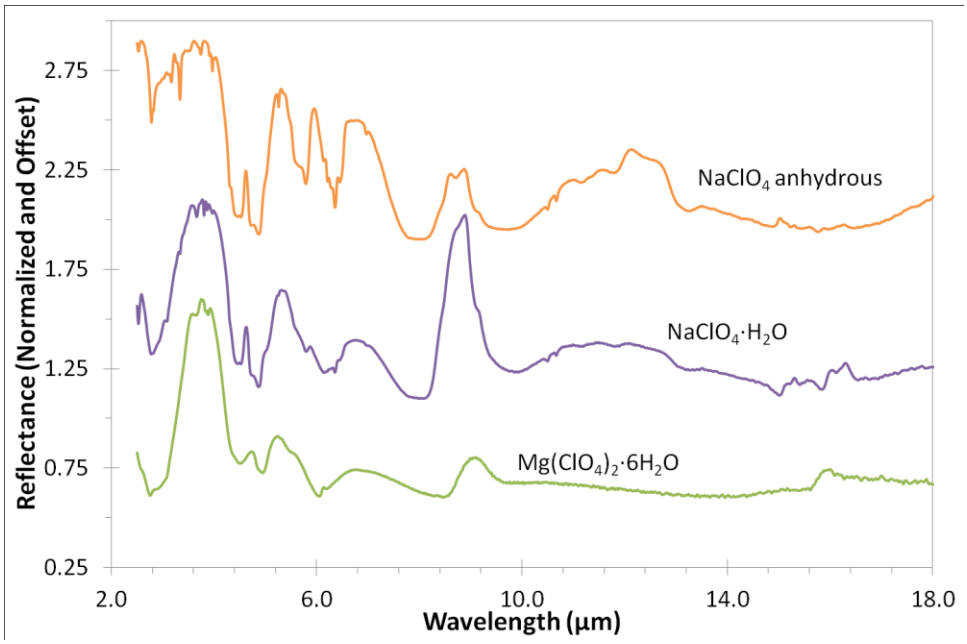

Figure 5-6. MIR reflectance spectra of $NaClO_4$, $NaClO_4 \cdot H_2O$ and $Mg(ClO_4)_2 \cdot 6H_2O$. Fundamentals of water are seen at <6 µm, and fundamentals of ClO_2 are seen at >9 µm.

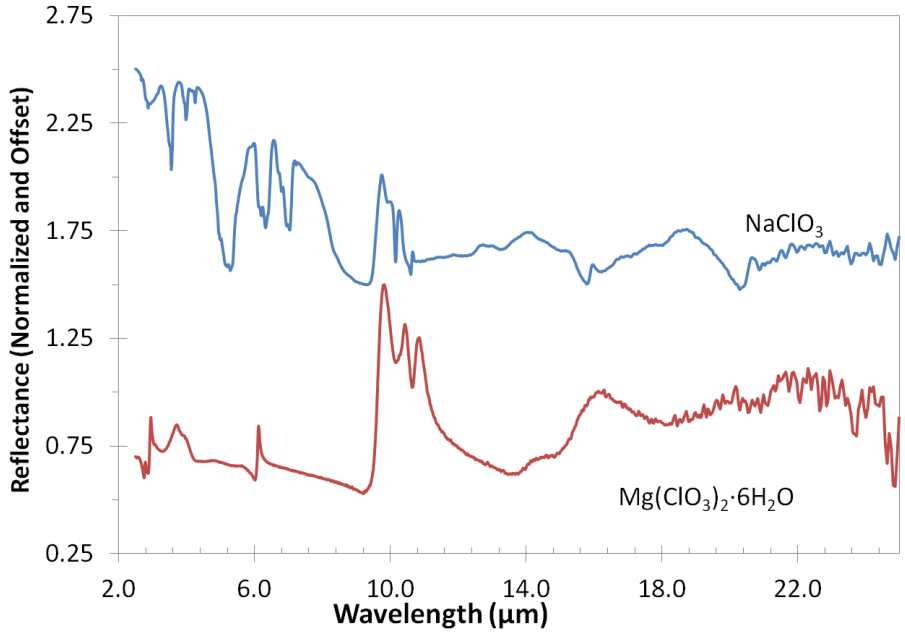

Figure 5-7. MIR reflectance spectra of $NaClO_3$ and $Mg(ClO_3)_2 \cdot 6H_2O$. Fundamentals of water are seen at <6 µm, and fundamentals of ClO_2 are seen at >9 µm.

5.5 Conclusions

Oxidized chlorine salts exhibit many spectral features in both the near- and mid-infrared that should allow for their detection by remote sensing on other planetary bodies. The features are predominantly caused by two molecules, H_2O and ClO_x, though the cation will affect the hydration state.

Water features are seen only <6 μm, while the fundamental modes of ClO_x are seen at >9 μm; however, combinations and overtones of these molecules are seen at shorter wavelengths. Water bands are seen at ~1.4 and ~1.9 μm. In chlorate salts, an additional band is seen at ~2.2 μm. The water bands are affected by the hydration state of the molecule. With increasing water, both the band depth and band width increase. More water also causes blending of the features; at lower hydration states individual bands become more resolvable.

More work is needed to acquire a complete library of these salts at the appropriate temperatures and pressures needed for planetary comparisons. In particular, the low temperature hydrates are difficult to synthesize without having liquid water or ice also present. The lower hydration states (i.e. higher temperatures) are also unstable due to the extreme hygroscopic nature of these salts. However, these are important to understand since they could be relevant to the dry environments on Mars.

5.6 References

Archer, P. D., et al., Possible Detection of Perchlorates by Evolved Gas Analysis of Rocknest Soils: Global Implications. LPSC XLIV, Vol. #2168, The Woodlands, TX, USA, 2013.

Catling, D. C., et al., 2010. Atmospheric origins of perchlorate on Mars and in the Atacama. Journal of Geophysical Research. 115**,** E00E11.

Chevrier, V. F., et al., 2009. Stability of perchlorate hydrates and their liquid solutions at the Phoenix landing site, Mars. Geophysical Research Letters. 36**,** L10202.

Clark, B. C., et al., 1976. Inorganic Analyses of Martian Surface Samples at the Viking Landing Sites. Science. 194**,** 1283-1288.

Cloutis, E. A., et al., 2006. Detection and discrimination of sulfate minerals using reflectance spectroscopy. Icarus. 184**,** 121-157.

Crowley, J. K., 1991. Visible and Near-Infrared (0.4-2.5 μm) Reflectance Spectra of Playa Evaporite Minerals. Journal of Geophysical Research. 96**,** 16231-16240.

Decius, J. C., Hexter, R. M., 1977. Molecular Vibrations in Crystals. McGraw-Hill Inc.

Ericksen, G. E., 1981. Geology and origin of the Chilean nitrate deposits. Geological Survey Professional Paper #1188.

Gellert, R., et al., 2004. Chemistry of rocks and soils in Gusev Crater from the Alpha Particle X-ray Spectrometer. Science. 305**,** 829-832.

Hanley, J., et al., 2012. Chlorate salts and solutions on Mars. Geophysical Research Letters. 39**,** L08201.

Hecht, M. H., et al., 2009. Detection of Perchlorate and the Soluble Chemistry of Martian Soil at the Phoenix Lander Site. Science. 325**,** 64-67.

Hunt, G. R., 1977. Spectral Signatures of Particulate Minerals in the Visible and Near Infrared. Geophysics. 42**,** 501-513.

Keller, J. M., et al., 2006. Equatorial and midlatitude distribution of chlorine measured by Mars Odyssey GRS. J. Geophys. Res. 111**,** E03S08.

Linke, W. F., 1965. Solubilities: inorganic and metal-organic compounds. D. Van Nostrand.

Rao, B., et al., 2010. Perchlorate Formation by Ozone Oxidation of Aqueous Chlorine/Oxy-Chlorine Species: Role of ClxOy Radicals. Environmental Science & Technology. 44**,** 2961-2967.

Rieder, R., et al., 2004. Chemistry of Rocks and Soils at Meridiani Planum from the Alpha Particle X-ray Spectrometer. Science. 306**,** 1746-1749.

Robertson, K., Bish, D., 2011. Stability of phases in the Mg(ClO4)2·nH2O system and implications for perchlorate occurrences on Mars. Journal of Geophysical Research: Planets. 116.

Wänke, H., et al., 2001. Chemical Composition of Rocks and Soils at the Pathfinder Site. Space Science Reviews. 96**,** 317-330.

6 Reflectance Spectra of Hydrated Chlorine Salts: The Effect of Temperature

6.1 Abstract

Hydrated chlorine salts are expected to exist on a variety of planetary bodies, ranging from nearby planets such as Mars to outer moons such as Europa; however, detection by remote sensing has been limited by a lack of comparison data in spectral libraries. In addition, most spectra are acquired at room temperature while most other planetary bodies are much colder than Earth. Thus, we acquired spectra of NaCl, $NaClO_4 \cdot xH_2O$, $MgCl_2 \cdot xH_2O$, $Mg(ClO_4)_2 \cdot 6H_2O$, and $Mg(ClO_3)_2 \cdot 6H_2O$ from 0.5-2.5 μm at both 298 and 80 K to observe the effects of temperature. In the near-infrared (NIR), spectra only show absorption features due to water molecules. Increasing hydration states increases the depth and width of water bands. At low temperature the bands become narrower with sharper, more well-defined minima, allowing individual bands to be more easily resolved. We find these features to be distinct enough to be resolvable by many remote sensing instruments, making them useful for comparison. We also measured frozen eutectic solutions of NaCl, $MgCl_2$, and KCl, and compared the NIR spectra to that of Galileo's NIMS. Although in each of these cases the salts form a hydrated phase in addition to the water ice present, the overall shape was very similar to that of pure water ice, making the distinction between these salts and pure ice difficult. This has implications for the detection of certain minerals on Mars and Europa and suggests that care must be taken to confirm their presence.

6.2 Introduction

Chlorine salts, e.g. chlorides (Cl^-), chlorates (ClO_3^-) and perchlorates (ClO_4^-), play an important role in the stability of liquid water (Altheide et al., 2009; Chevrier et al., 2009; Hanley et al., 2012; Zolotov and Shock, 2001; Zorzano et al., 2009). In particular, chlorine salts depress

the freezing point of water down to 204 K (Chevrier et al., 2009; Hanley et al., 2012). Therefore, identifying chlorine salts on other bodies would indicate a wider range of temperature stability for water. The primary method of detection is through remote sensing; however, laboratory data does not exist for many of the chlorine salts hydrates. In companion papers, we have measured the mid-infrared (MIR) and near-infrared (NIR) reflectance spectral properties of chlorides (in prep) and oxidized chlorine salts (in prep) with respect to Mars. Any planetary body that has a chondritic starting composition, and has had contact with liquid water in the past (whether through hydrothermal or otherwise), is likely to form chlorine salts; therefore, these salts are expected to exist throughout the solar system. Although most studies of chlorides focus on their anhydrous forms, all known chlorides form hydrates (Hanley et al., in prep). In the case of Europa, given the abundance of water on the surface and its low surface temperature, any chlorine salts present would almost certainly be in a highly hydrated form.

If found on the surface of Europa, chlorine salts would serve as a window to the interior, and support the existence of a liquid ocean beneath the icy crust. Galileo's magnetometer indicates that Europa has an induced magnetic field as a result of an interaction with Jupiter's magnetic field (Khurana et al., 1998; Kivelson et al., 2000), implying a conducting liquid, likely a salty ocean (Carr et al., 1998). If an ocean exists, the question remains whether that ocean interacts with both the surface above and the silicate mantle below.

The ice shell thickness has direct implications for the composition of the surface: if the crust is constantly being resurfaced by deposits from the salty ocean, then the surface composition will indicate the makeup of the ocean below, which in turn can constrain mixing with the mantle and possible organic reactions. Some surface features, such as ridges and chaotic terrain, suggest a thinner ice layer with possible surface contact with the ocean (Greenberg,

2005; Schmidt et al., 2011). If the ocean is salty, the materials likely came from interactions with the silicate mantle, in which case gases (e.g. CO_2 and CH_4) may also have been released from the rock and traveled to the water-ice interface. Gas build up may have been enough to fracture the ice, if thin, causing an eruption of gas and salty water, leading to salty deposits (Greeley et al., 2004).

Europa can be broken down into two regions of NIR spectral distinctness: icy and non-icy. In general, the leading hemisphere and the poles are predominantly water ice, while the trailing hemisphere is darker, i.e. non-icy "dark material" (Grundy et al., 2007). Most of the non-ice spectra are very similar (McCord et al., 1999).

Temperature is known to influence the spectral reflectance of a material (Dalton et al., 2005; Grundy and Schmitt, 1998). In general, the temperature effect is reversible within a given crystal phase. With colder temperatures, thermal contraction of the crystal shifts spectral features toward longer wavelengths. Absorption bands shift up to 0.02 μm longer from 270 to 40 K, and band-width generally decreases with lower temperatures (Grundy and Schmitt 1998). NIR ice spectra at different temperatures indicate that the 1.65 μm band is strongly temperature dependent, being more pronounced at lower temperatures, yet almost non-existent at room temperature (Schmitt et al., 1998).

Therefore, based on the likelihood of finding chlorine salts on Europa, we have conducted an investigation into the temperature dependence of hydrated chlorine salts. In this project we measured some of the chlorine salts at low temperature (80 K) and compared them to the room temperature spectra from our companion papers.

6.3 Methods

The following salts and some of their hydrates were synthesized: NaCl, $MgCl_2$, $Mg(ClO_3)_2$, $NaClO_4$, and $Mg(ClO_4)_2$, as described in Hanley et al (in prep). Anhydrous compounds were heated to 120°C for two days to drive off excess water. Salts were stored in a desiccator under low humidity, since these salts are extremely hygroscopic. Reflectance spectra of the above compounds were taken using an ASD FieldSpec Pro in the range 0.3-2.5 μm. The spectra were measured at two temperatures: 298 K (room temperature, RT) and 80 K. Spectra were measured at RT, then the apparatus was cooled to 80 K with liquid nitrogen and spectra were reacquired. Another spectrum was measured once the sample returned to RT to ensure that no phase changes occurred during cooling. Twenty-five measurements were taken at spectral resolution of 1 nm and then averaged to obtain the final spectrum.

Eutectic compositions of $MgCl_2$, NaCl, and KCl were frozen at -30°C overnight. Spectra for eutectic mixtures were measured with a Nicolet 6700 FTIR Spectrometer equipped with fiber optics to allow analysis in the range 1.0-2.5 μm. Samples were placed in a container with dry ice to keep cool during spectral measurements. Smart NIR accessory was used with TEC detector and a fiber optic probe. KBr was used as a background with a white light source and CaF_2 beam splitter.

6.4 Results

As expected, hydration state is the primary driver of spectral features in the NIR, with absorption bands due to water being the only features. These hydrated salts demonstrate myriad spectral features in their hydrated forms. For example, $NaClO_4 \cdot 2H_2O$ (Figure 6-1) shows features that are mostly due to water. Additionally, hydrated $MgCl_2$ shows features due to the 2,

4, and 6 H_2O forms (Figure 6-2) and $Mg(ClO_4)_2 \cdot 6H_2O$ and $Mg(ClO_3)_2 \cdot 6H_2O$ (Figure 6-3) show several prominent water features. Other major bands of $NaClO_4 \cdot 2H_2O$ are located at 1.17, 1.42, 1.46, and 1.93 μm, the latter three corresponding to the usual hydration bands observed in all the hydrated phases.

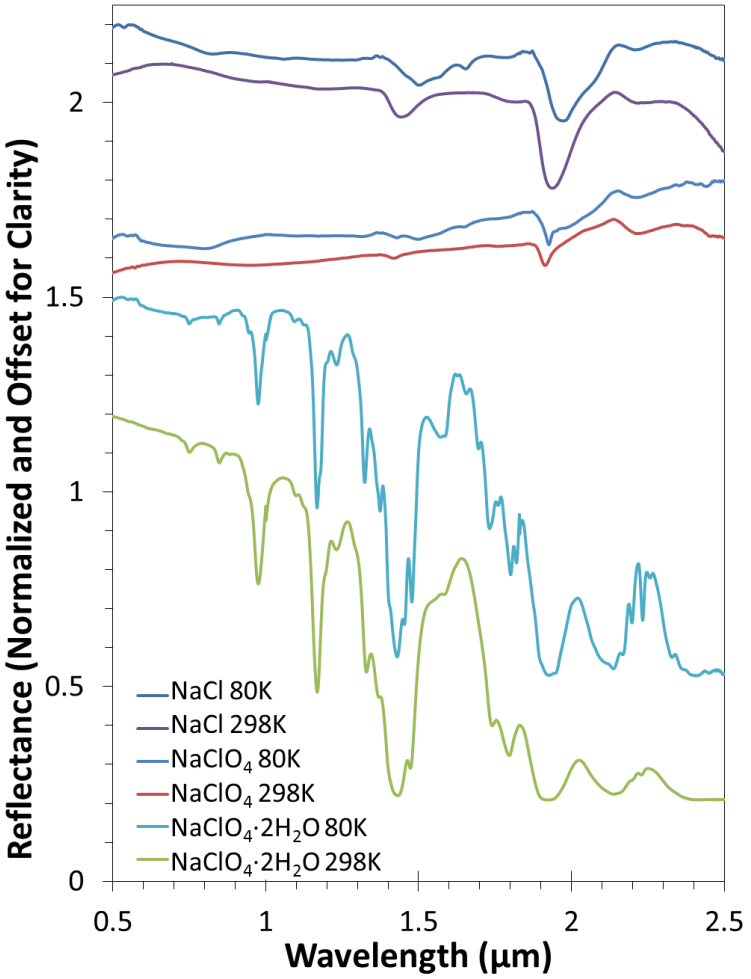

Figure 6-1. NIR reflectance spectra of NaCl, $NaClO_4$ anhydrous, and $NaClO_4 \cdot 2H_2O$ at 298 and 80K.

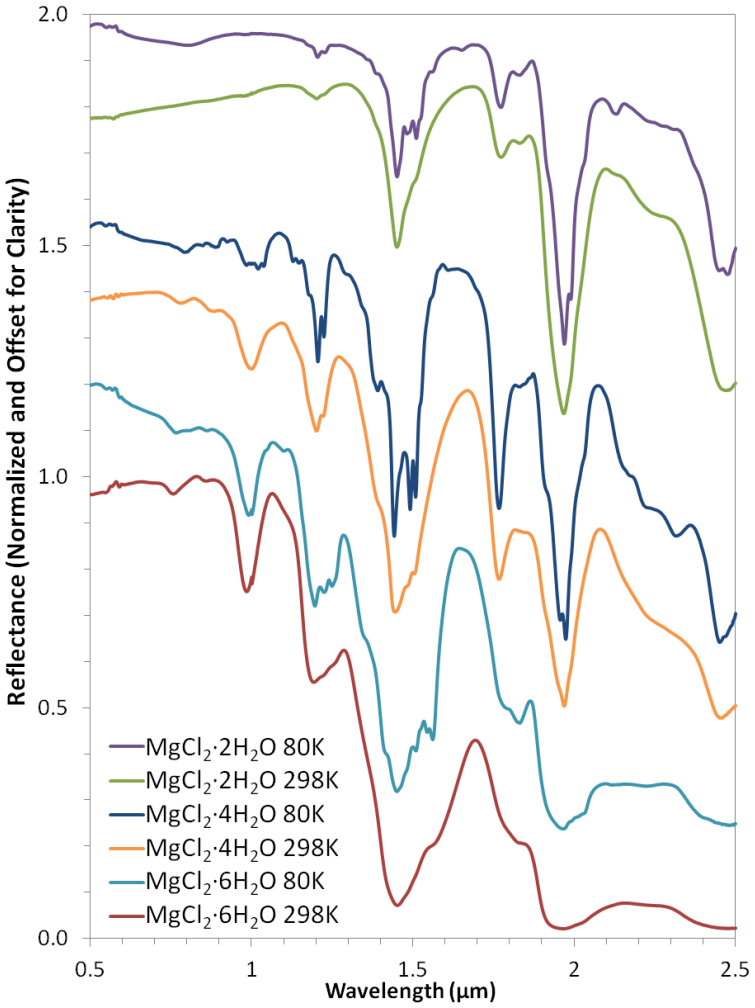

Figure 6-2. NIR reflectance spectra of $MgCl_2$ hydrates at 298 and 80K.

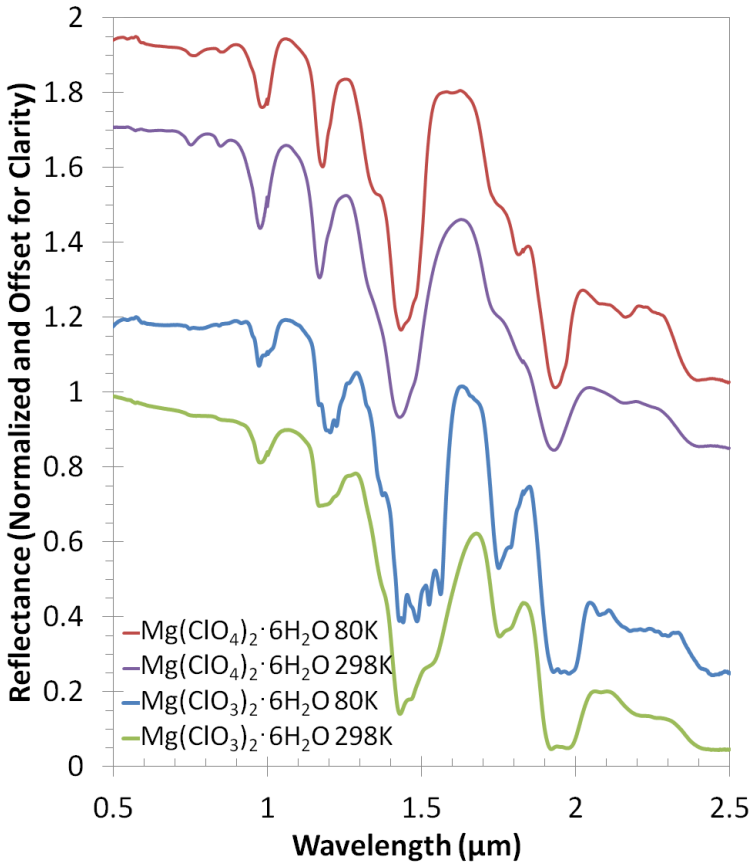

Figure 6-3. NIR reflectance spectra of $Mg(ClO_4)_2 \cdot 6H_2O$ and $Mg(ClO_3)_2 \cdot 6H_2O$ at 298 and 80K.

To determine relative changes between each mineral's spectra, we performed spectral modeling using SPECFIT (Kriss, 1994), a line-fitting program that finds the best-fit model by minimizing the χ^2 statistic. We modeled each individual feature in the spectrum with as many Gaussians as were necessary to obtain a satisfactory fit. We assumed a baseline of 1 (100% reflectance) since this is what would be expected from a pure anhydrous chloride salt. An example of the fit is shown in Figure 6-4.

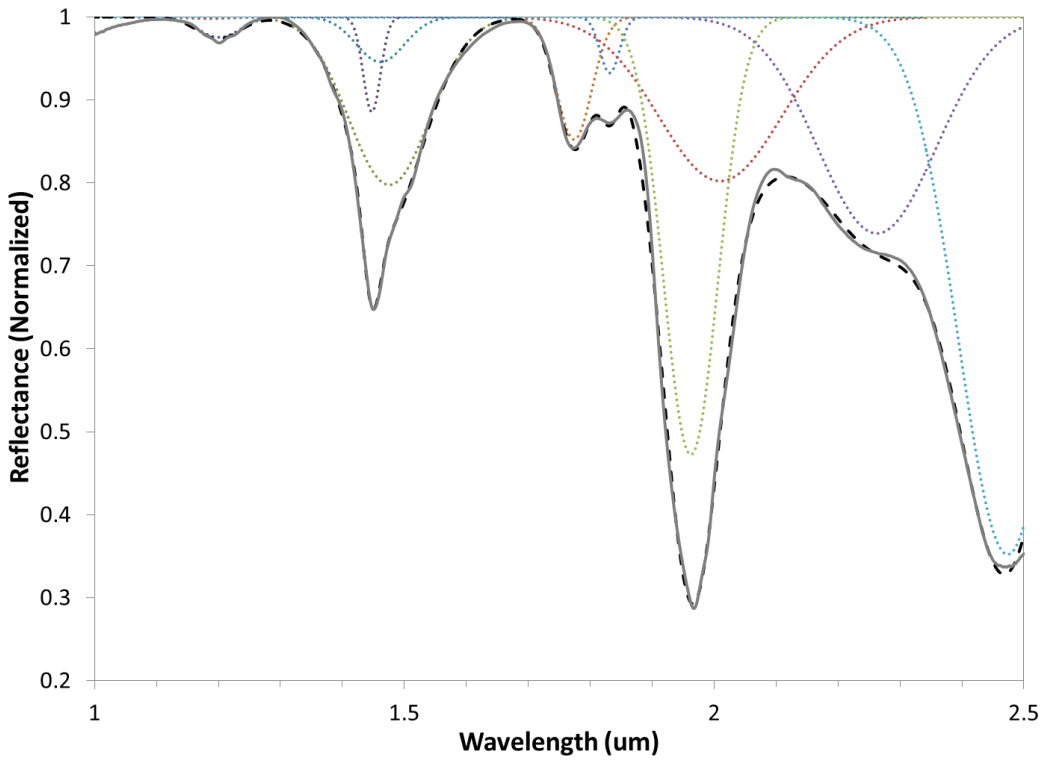

Figure 6-4. Spectrum of $MgCl_2 \cdot 2H_2O$ 298 K (gray), model sum (black dash) and best fit Gaussians (colored dots).

The level of hydration controls the depth, width, and number of absorption bands, which all increase with water content. For example, in the $2H_2O$, the full-width at half maximum (FWHM) for the ~1.4 μm water band is 0.103±0.003 μm, with the minima position at 1.450±0.0013 μm and a band depth of 0.349±0.0016. Comparing to the $6H_2O$, the FWHM was 0.302±0.0052 μm, minima position was located at 1.455±0.002 μm, and the band depth was 0.926±0.032.

The interesting result is how the hydration band changes with temperature. Changes in temperature produce a number of effects. For example, the band for $MgCl_2 \cdot 6H_2O$ at ~1.25 μm splits into a triplet at the lower temperature. The same band splits into a doublet in the $4H_2O$ and $2H_2O$ hydrates. Overall, bands tend to become narrower, shallower and some shift toward longer

wavelengths. For example, comparing the $MgCl_2 \cdot 6H_2O$ RT ~1.4 μm band to 80 K, at the lower temperature the new values are: FWHM of 0.253±0.004 μm (compared to 0.303 μm) and band depth of 0.880±0.039 (compared to 0.93). Although the model sum minima position for the 1.4 μm feature at 80 K (1.455±0.002 μm) is consistent, within error, with the minima position at RT, when looking at individual features there is a shift toward longer wavelengths (on the order of nm). These effects are seen in almost all absorption bands, which become narrower and have sharper minima at lower temperature, perhaps due to resolving individual water molecules.

When mixed with water at eutectic concentrations, chloride salts show little difference from pure water ice, even though they will form a hydrated phase; however, the bands appear broader than for those in pure water ice (Figure 6-5). When comparing to the Galileo NIMS spectrum of "dark material," the general shape is similar, though this is to be expected since Europa is a giant ice ball.

6.5 Discussion

Most hydrated salts exhibit features in the NIR that are due to water. This is confirmed by comparing the hydrated salts to their anhydrous forms. It is very difficult, though, to synthesize some of the anhydrous forms due to the extreme hygroscopic nature of these salts. Many remain slightly hydrated even after heating. Note that even anhydrous NaCl and anhydrous $NaClO_4$ (Figure 6-1) show remnant water bands at 1.4 and 1.9 μm after heating for several days.

Assigning specific modes to each feature is difficult due to the blending of individual bands. Even when considering which modes are responsible for which features in pure water ice, exact locations are difficult to determine (Cloutis et al., 2006; Grundy and Schmitt, 1998). Hydrated salts still possess many similar absorption features due to overtones and combinations

of the fundamental modes of water. In particular, they are expected at 1.04 μm ($2v_1 + v_3$), 1.25 μm ($v_1 + v_2 + v_3$), 1.50-1.66 μm ($2v_2 + v_3$, $v_1 + v_3$), 1.55 μm ($2v_{OH}$), and 1.96-2.05 μm ($v_2 + v_3$) (Cloutis et al., 2006). Our results have shown that temperature significantly affects the hydration features. In general, water bands become narrower and the minima become sharper, with individual features more easily identified.

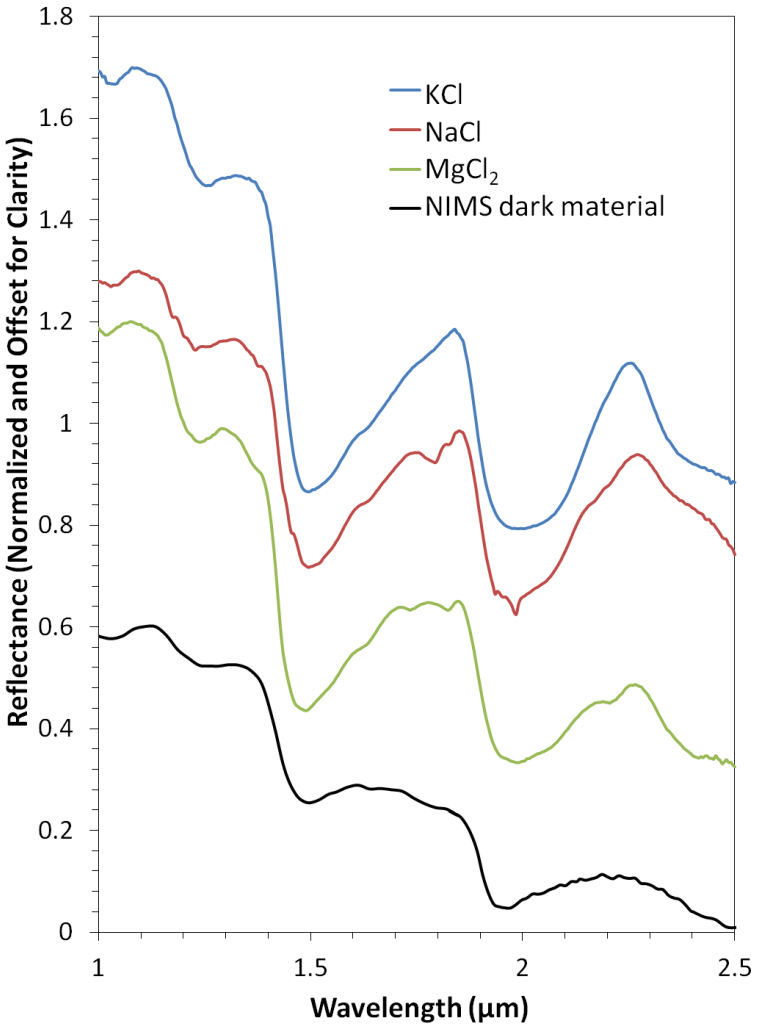

Figure 6-5. NIR reflectance spectra of frozen eutectic $MgCl_2$, NaCl, KCl at -30°C. For comparison, we also show NIMS "non-icy" or "dark" spectrum.

The differences between RT and 80 K are just enough to be resolvable by most current NIR spectrometers in orbit around other planetary bodies, e.g. MRO CRISM's 6.55 nm (Murchie et al., 2007), MEx OMEGA's 13nm (Ryskin, 1974), and Galileo NIMS's 25 nm (Carlson et al., 1992) spectral resolutions. For instance, in the 1.25 band of $MgCl_2 \cdot 6H_2O$, where the feature splits in to a triplet, the individual bands are separated by approximately 30 nm each (1.190, 1.226 and 1.255 μm). Depending on observing conditions, this may not be discernible; however, the fact that this feature changes from more of a "shoulder" at 298 K to a proper "band" at 80 K would be perceptible. In addition, the general narrowing of the bands would be evident even given the relatively poor resolution of NIMS.

Europa's temperature ranges from 86 to 132 K (Spencer et al., 1999), with spectroscopic evidence suggesting an average temperature of 95 ± 10 K (Fink and Larson, 1975), therefore, our 80 K spectra are reasonably well-suited to compare with NIMS data. This data would also be relevant to other icy satellites in the outer solar system, such as Iapetus (80-130 K), Enceladus (average 75 K (Spencer et al., 2006b)), and Pluto (40 ± 2 K; Tryka et al., 1994), among others. Mars, on the other hand, ranges from ~130 K at the winter poles to ~273 K at the equator in the summer, with an average of ~218 K. Based on these temperatures, the spectra would fall somewhere in between RT and 80 K. The large temperature variations in locations where chlorine salts might be present necessitate a broader study of chlorine salts at all temperatures.

6.5.1 Analysis of Europa Spectra

When analyzing the absorption features in the NIMS non-icy spectrum, water bands are distorted and broadened when compared to pure water-ice, which suggests heavily hydrated minerals. The strength of the 1.9 μm band indicates that H_2O must be present, not just OH

(Crowley, 1991). Clays such as montmorillonite and sepiolite have structural water, as evidenced by their 1.4 and 1.9 μm bands; however, the bands are not broadened like the NIMS spectrum, due to the very specific binding sites allowed by these minerals. In addition, they have metal-OH bands (2.2- to 2.4-μm), which are not present in the NIMS spectrum (Figure 6-5).

Hydrated phases of borates, sulfates, and carbonates were suggested as possible candidates that might produce the observed features on Europa. Borates, though, are unlikely due to the low solar abundance of boron. On the other hand, sulfates and carbonates are more likely, especially if models predicting a chondritic composition are accurate. Studies show that hydrous alteration of chondrites could produce sulfate salts (Kargel et al., 2000; Zolotov and Shock, 2001). Mg- and Na-sulfates and Na-carbonates match the spectra reasonably well (McCord et al., 1998). In addition, hydrated salts appear to be more stable to the harsh radiation environment of Jupiter than pure water-ice (McCord et al., 2001).

Because no single material spectrum provides a satisfactory fit to the NIMS data, mixtures of salts have been suggested. More work is required to acquire spectra at appropriate pressures and temperatures of these mixtures, not just single salt components, because there may be interactions between the salts that affect their spectral features. Many groups have attempted to address this issue, with the consensus being that sulfates are the most likely salts to be present both at the surface and dissolved in the ocean. It is suggested that no crystalline salt matches the spectra well (Spencer et al., 2006a), arguing for either brine mixtures (McCord et al., 2002) and/or hydrated sulfuric acid (Carlson et al., 1999b).

Recent studies have acquired higher resolution spectral imaging of Europa's surface, finding new evidence to support magnesium sulfate on the trailing hemisphere (Brown and Hand, 2013). This is suggested to be due to radiolysis by sulfur implantation from Io's torus.

Since the feature associated with $MgSO_4$ (a band at 2.07 μm) is not seen on the leading hemisphere, it is suggested that the magnesium is originally brought to the surface as magnesium chloride. Given the relative abundance of Na, K, and Mg, the authors suggest that all three are associated with chloride on the leading hemisphere, but Na and K were preferentially sputtered off the surface at the same timescales as necessary to implant the sulfur; however, they were unable to detect the chloride salts because the spectra on the leading hemisphere look only like distorted water.

Comparing the NIMS spectrum to our eutectic mixtures of NaCl, $MgCl_2$, KCl, and H_2O (Figure 6-5), this is exactly what we see: distorted water ice. When frozen these eutectic mixtures consist of the highest hydrate ($NaCl \cdot 2H_2O$, $MgCl_2 \cdot 12H_2O$, and $KCl \cdot H_2O$, respectively) and ice, consistent with results that the material of the Europa spectrum is a flash frozen brine (McCord et al., 2002). Further studies of other materials flash frozen in brines might suggest a similar result.

Kargel et al. (2000) suggest the possibility of a salty ocean with a NaCl crust, but rule this out due to spectral reasons, namely the presence of hydration bands. We suggest that it may in fact be possible to identify chlorine salts on the surface of Europa, given the similarities of hydrated chloride spectra to ice and other hydrated salts, such as sulfates. If there is chlorine in the system, as models predict (Kargel et al., 2000), chloride salts would be likely to form. Also, considering the highly oxidizing conditions on the surface (Carlson et al., 1999a), perchlorates and chlorates should exist as well. UV radiation is also abundant, which is a possible formation mechanism for perchlorate (Catling et al., 2010). Any detection of chlorine salts at the surface would further constrain that the "dark" surface material might in fact be due to movement of the

ice sheet and possible subsurface ocean interaction, rather than implantation from Io's torus, as could be the case for sulfates.

6.5.2 Limitations

Synthesizing and measuring each hydration state is difficult due to the hygroscopic nature of these salts. Due to the instability of many of the hydrates at room temperature, ensuring a consistent grain size was difficult. McCord et al. (1999) suggest, though, the effects are not sufficient to account for the differences between the icy and non-icy end-members of Europa spectra. Still, grain size is known to affect reflectance spectra, and future work will address the issue of grain size. We would like to characterize each hydration state of each chlorine salt at steps of 25 K from 0-300 K.

6.6 Conclusions

The effect of temperature on the hydrated chlorine salts is significant. At low temperatures, many features change. Hydration bands became narrower, the minima become sharper, shoulders turn in to true bands, multiple peaks are present where before only a broad band was apparent (i.e. individual features are more easily resolved), and the minima shift toward longer wavelengths. Clearly it is important to use laboratory spectra taken under the expected conditions of the planetary body being studied. This is especially true for the outer solar system bodies, which experience very low temperatures. Obtaining reflectance spectra at various temperatures is important not only to understand the spectral properties of Europa, but all other planetary bodies. Spectra acquired at 80 K are relevant to other icy satellites and outer solar system bodies, and in the case of Mars, which has temperatures between approximately 130 and

273 K, spectral features would likely exhibit features that are in between the two studied temperature profiles, including sharper, narrower bands. This study confirms the need to build a complete spectral library to be used for remote sensing. It is important that spectra be acquired for all known hydrates of various salts, and that their temperature matches the expected conditions of the planetary body being studied.

6.7 References

Altheide, T., et al., 2009. Experimental investigation of the stability and evaporation of sulfate and chloride brines on Mars. Earth and Planetary Science Letters. 282**,** 69-78.

Brown, M. E., Hand, K. P., 2013. Salts and Radiation Products on the Surface of Europa. Astrophysical Journal. in press.

Carlson, R. W., et al., 1999a. Hydrogen Peroxide on the Surface of Europa. Science. 283**,** 2062-2064.

Carlson, R. W., et al., 1999b. Sulfuric Acid on Europa and the Radiolytic Sulfur Cycle. Science. 286**,** 97-99.

Carlson, R. W., et al., 1992. Near-Infrared Mapping Spectrometer experiment on Galileo. Space Science Reviews. 60**,** 457-502.

Carr, M. H., et al., 1998. Evidence for a subsurface ocean on Europa. Nature. 391**,** 363-365.

Catling, D. C., et al., 2010. Atmospheric origins of perchlorate on Mars and in the Atacama. Journal of Geophysical Research. 115**,** E00E11.

Chevrier, V. F., et al., 2009. Stability of perchlorate hydrates and their liquid solutions at the Phoenix landing site, Mars. Geophysical Research Letters. 36**,** L10202.

Cloutis, E. A., et al., 2006. Detection and discrimination of sulfate minerals using reflectance spectroscopy. Icarus. 184**,** 121-157.

Crowley, J. K., 1991. Visible and Near-Infrared (0.4-2.5 μm) Reflectance Spectra of Playa Evaporite Minerals. Journal of Geophysical Research. 96**,** 16231-16240.

Dalton, J. B., et al., 2005. Spectral comparison of heavily hydrated salts with disrupted terrains on Europa. Icarus. 177**,** 472-490.

Fink, U., Larson, H. P., 1975. Temperature dependence of the water-ice spectrum between 1 and 4 microns: Application to Europa, Ganymede and Saturn's rings. Icarus. 24**,** 411-420.

Greeley, R., et al., Geology of Europa. In: F. Bagenal, et al., (Eds.), Jupiter: The Planet, Satellites and Magnetosphere. Cambridge University Press, 2004.

Greenberg, R., 2005. Europa - The Ocean Moon: Search for an Alien Biosphere. Praxis Publishing Ltd.

Grundy, W. M., et al., 2007. New Horizons Mapping of Europa and Ganymede. Science. 318**,** 234-237.

Grundy, W. M., Schmitt, B., 1998. The temperature-dependent near-infrared absorption spectrum of hexagonal H2O ice. Journal of Geophysical Research: Planets. 103**,** 25809-25822.

Hanley, J., et al., 2012. Chlorate salts and solutions on Mars. Geophysical Research Letters. 39**,** L08201.

Kargel, J. S., et al., 2000. Europa's Crust and Ocean: Origin, Composition, and the Prospects for Life. Icarus. 148**,** 226-265.

Khurana, K. K., et al., 1998. Induced magnetic fields as evidence for subsurface oceans in Europa and Callisto. Nature. 395**,** 777-780.

Kivelson, M. G., et al., 2000. Galileo Magnetometer Measurements: A Stronger Case for a Subsurface Ocean at Europa. Science. 289**,** 1340-1343.

Kriss, G., 1994. Fitting models to UV and optical spectral data. Astronomical Data Analysis Software and Systems. 3**,** 437.

McCord, T. B., et al., 1998. Salts on Europa's Surface Detected by Galileo's Near Infrared Mapping Spectrometer. Science. 280**,** 1242-1245.

McCord, T. B., et al., 1999. Hydrated salt minerals on Europa's Surface from the Galileo near-infrared mapping spectrometer (NIMS) investigation. Journal of Geophysical Research. 104**,** 11827-11851.

McCord, T. B., et al., 2001. Thermal and radiation stability of the hydrated salt minerals epsomite, mirabilite, and natron under Europa environmental conditions. Journal of Geophysical Research. 106**,** 3311-3319.

McCord, T. B., et al., 2002. Brines exposed to Europa surface conditions. Journal of Geophysical Research. 107**,** 5004.

Murchie, S., et al., 2007. Compact Reconnaissance Imaging Spectrometer for Mars (CRISM) on Mars Reconnaissance Orbiter (MRO). Journal of Geophysical Research: Planets. 112**,** E05S03.

Ryskin, Y. I., 1974. The vibrations of protons in minerals: hydroxyl, water and ammonium. The infrared spectra of minerals. 137-181.

Schmidt, B. E., et al., 2011. Active formation of 'chaos terrain' over shallow subsurface water on Europa. Nature. 479**,** 502-505.

Schmitt, B., et al., Optical Properties of Ices from UV to Infrared. In: B. Schmitt, et al., (Eds.), Solar System Ices. Kluwer Academic Publishers, 1998, pp. 199-240.

Spencer, J. R., et al., 2006a. The nature of Europa's dark non-ice surface material: Spatially-resolved high spectral resolution spectroscopy from the Keck telescope. Icarus. 182**,** 202-210.

Spencer, J. R., et al., 2006b. Cassini Encounters Enceladus: Background and the Discovery of a South Polar Hot Spot. Science. 311**,** 1401-1405.

Spencer, J. R., et al., 1999. Temperatures on Europa from Galileo Photopolarimeter-Radiometer: Nighttime Thermal Anomalies. Science. 284**,** 1514-1516.

Tryka, K. A., et al., 1994. Temperature of Nitrogen Ice on Pluto and Its Implications for Flux Measurements. Icarus. 112**,** 513-527.

Zolotov, M. Y., Shock, E. L., 2001. Composition and stability of salts on the surface of Europa and their oceanic origin. Journal of Geophysical Research. 106**,** 32815-32827.

Zorzano, M. P., et al., 2009. Stability of liquid saline water on present day Mars. Geophysical Research Letters. 36**,** L20201.

7 Summary and Conclusions

7.1 Stability of Water

Chlorine salts are expected to exist throughout the solar system, and have been detected on the surface of Mars. A thorough investigation is needed to quantify the effect of these salts on the stability of water. We have shown that these salts can be stable under present day conditions on the surface of Mars by measuring the evaporation rates of perchlorate (Chevrier et al., 2009) and chlorate (Hanley et al., 2012) solutions in a simulated martian environment (CO_2 atmosphere, <1% RH, -20° to 0°C).

Another important consideration is that humidity plays a significant role in the stability of these salts, in both their liquid and solid phases (Gough et al., 2011). Humidity is directly related to the activity of water (a_{H2O}) of these solutions. Under high enough relative humidity, the solid salts will deliquesce, forming a liquid solution. High relative humidity will also slow the evaporation rate of the solution. For example, in the right conditions at the Phoenix landing site magnesium perchlorate solutions can be stable, neither frozen nor evaporating, for a few hours each day. Identifying and quantifying the compositions of these salts on other planets would increase our understanding of the stability of water at those locations.

Extrapolating to other locations on Mars, in order to form gullies or lakes at present day temperatures, much more salt is needed than is reported from remote observations or bulk analysis on the ground (generally around 1 wt%). Given the amount of chlorine salts detected, there would only be small amounts of actual liquid formation at the eutectic temperature. For example, for a eutectic $Mg(ClO_4)_2$ solution, 44 wt% is needed: from a 1 kg sample at the Phoenix landing site, and 0.6 wt% perchlorate (Hecht et al., 2009), we can assume a maximum of 3 g $Mg(ClO_4)_2$, meaning only ~7 g liquid solution over 1 kg regolith. This is not enough for

running water, but it may be enough to alter the landscape and geochemical makeup of the regolith through freeze-thaw cycles.

7.2 Detection

Identifying these chlorine salts throughout the solar system would establish the stability of water in that location. Unfortunately, most attempts to detect chlorine salts have focused on chlorides, which are anhydrous at typical Earth temperatures and therefore are featureless in the near-infrared (NIR). Here we acquired laboratory reflectance spectra of various chlorine salts (including chlorides, chlorates and perchlorates) at different hydration states. These spectra show distinct features that should allow for their detection by remote sensing. Most features seen in the NIR are due to overtones and combinations of water's fundamental modes, which exist in the mid-infrared (MIR). With increasing hydration state the absorption bands become deeper, wider, and generally more blended together. ClO_x also has fundamentals in the MIR, which might be a better range to uniquely identify oxychlorines if present.

Furthermore, compared to spectra taken at 298 K, those taken at 80 K showed significant differences: bands became shallower and narrower at the lower temperature. Our work shows that each hydration state should be measured at a range of temperatures relevant to the planetary body being studied.

7.3 Implications for Life

In order to achieve freezing temperatures down to ~204 K, the water must be at $a_{H2O} = 0.5$ (Hanley et al., 2012). Even chlorine salts in mixtures will lower the activity of water enough to achieve liquid at present day conditions (Hanley et al., 2012), and almost certainly in the past, as

evidenced by possible paloelakes (Rivera-Valentin et al., 2013; Wray et al., 2011). Though halophiles can survive down to low activities, life as we know it in general does not thrive at low water activity. The organism with the lowest know water activity is a form of yeast, which has been demonstrated to survive down to $a_{H2O} = 0.61$ (Grant, 2004).

Numerous examples of life have been found in the martian analogue site of the Atacama Desert in Chile, which is one of the driest places on Earth. Photosynthetic cyanobacteria were found within crusts of halite (Wierzchos et al., 2006), a result of the hygroscopic properties of the salt, allowing deliquescence at relative humidities too low to otherwise produce liquid water events (Davila et al., 2008). Additionally, these halite crusts can scatter UV-light while being transparent to photosynthetically active radiation (Cockell and Raven, 2004).

Another martian analogue is Antarctica, where salt lakes provide a cold alternative to the dry but hot conditions in the Atacama desert. Lake Vida supports a diverse ecosystem, primarily composed of anoxic bacteria, which are metabolically active at -13°C (Murray et al., 2012). *Planococcus halocryophilus Or1* can grow and divide down to -15°C at 18% NaCl, and is metabolically active at -25°C in frozen permafrost (Mykytczuk et al., 2013).

Extrapolating the survival of these organisms to other planets is problematic, as they might be salt- or temperature-tolerant, but may be limited by conditions such as radiation and water availability. Indeed, there are other organisms that can survive harsh radiation environments and/or desiccation, e.g. *Deinococcus radiodurans* (Battista, 1997) and *Methanosarcina barkeri* (Anderson et al., 2012). These examples demonstrate that biologic activity at low temperatures and low activities is not unheard of even on Earth, suggesting that life might be able to survive throughout the solar system.

7.4 References

Anderson, K. L., et al., 2012. Desiccation as a Long-Term Survival Mechanism for the Archaeon Methanosarcina barkeri. Applied and Environmental Microbiology. 78**,** 1473-1479.

Battista, J., 1997. Against all odds: the survival strategies of Deinococcus radiodurans. Annual Reviews in Microbiology. 51**,** 203-224.

Chevrier, V. F., et al., 2009. Stability of perchlorate hydrates and their liquid solutions at the Phoenix landing site, Mars. Geophysical Research Letters. 36**,** L10202.

Cockell, C. S., Raven, J. A., 2004. Zones of photosynthetic potential on Mars and the early Earth. Icarus. 169**,** 300-310.

Davila, A. F., et al., 2008. Facilitation of endolithic microbial survival in the hyperarid core of the Atacama Desert by mineral deliquescence. Journal of Geophysical Research: Biogeosciences. 113**,** G01028.

Gough, R. V., et al., 2011. Laboratory studies of perchlorate phase transitions: Support for metastable aqueous perchlorate solutions on Mars. Earth and Planetary Science Letters. 312**,** 371-377.

Grant, W. D., 2004. Life at low water activity. Philosophical Transactions of the Royal Society of London. Series B: Biological Sciences. 359**,** 1249-1267.

Hanley, J., et al., 2012. Chlorate salts and solutions on Mars. Geophysical Research Letters. 39**,** L08201.

Hecht, M. H., et al., 2009. Detection of Perchlorate and the Soluble Chemistry of Martian Soil at the Phoenix Lander Site. Science. 325**,** 64-67.

Murray, A. E., et al., 2012. Microbial life at −13 °C in the brine of an ice-sealed Antarctic lake. Proceedings of the National Academy of Sciences. 109**,** 20626-20631.

Mykytczuk, N. C., et al., 2013. Bacterial growth at− 15° C; molecular insights from the permafrost bacterium Planococcus halocryophilus Or1. The ISME journal.

Rivera-Valentin, E. G., et al., 2013. Journal of Geophysical Research. under review.

Wierzchos, J., et al., 2006. Endolithic cyanobacteria in halite rocks from the hyperarid core of the Atacama Desert. Astrobiology. 6**,** 415-422.

Wray, J. J., et al., 2011. Columbus crater and other possible groundwater-fed paleolakes of Terra Sirenum, Mars. Journal of Geophysical Research: Planets. 116**,** E01001.

Appendix A – Copyrights and Permissions

Copyright Clearance Center RightsLink®

Home | Account Info | Help

WILEY

Title:	Stability of perchlorate hydrates and their liquid solutions at the Phoenix landing site, Mars
Author:	Vincent F. Chevrier,Jennifer Hanley,Travis S. Altheide
Publication:	Geophysical Research Letters
Publisher:	John Wiley and Sons
Date:	May 20, 2009

Copyright 2009 by the American Geophysical Union.

Logged in as: Jennifer Hanley

LOGOUT

Order Completed

Thank you very much for your order.

This is a License Agreement between Jennifer Hanley ("You") and John Wiley and Sons ("John Wiley and Sons"). The license consists of your order details, the terms and conditions provided by John Wiley and Sons, and the payment terms and conditions.

Get the printable license.

License Number	3083370937912
License date	Feb 06, 2013
Licensed content publisher	John Wiley and Sons
Licensed content publication	Geophysical Research Letters
Licensed content title	Stability of perchlorate hydrates and their liquid solutions at the Phoenix landing site, Mars
Licensed copyright line	Copyright 2009 by the American Geophysical Union.
Licensed content author	Vincent F. Chevrier,Jennifer Hanley,Travis S. Altheide
Licensed content date	May 20, 2009
Start page	n/a
End page	n/a
Type of use	Dissertation/Thesis
Requestor type	Author of this Wiley article
Format	Electronic
Portion	Full article
Will you be translating?	No
Total	0.00 USD

ORDER MORE... | CLOSE WINDOW

Copyright © 2013 Copyright Clearance Center, Inc. All Rights Reserved. Privacy statement.
Comments? We would like to hear from you. E-mail us at customercare@copyright.com

Copyright Clearance Center RightsLink®

Home | Account Info | Help

WILEY

Title: Chlorate salts and solutions on Mars
Author: Jennifer Hanley,Vincent F. Chevrier,Deanna J. Berget,Robert D. Adams
Publication: Geophysical Research Letters
Publisher: John Wiley and Sons
Date: Apr 24, 2012
Copyright 2012 by the American Geophysical Union

Logged in as:
Jennifer Hanley
LOGOUT

Order Completed

Thank you very much for your order.

This is a License Agreement between Jennifer Hanley ("You") and John Wiley and Sons ("John Wiley and Sons"). The license consists of your order details, the terms and conditions provided by John Wiley and Sons, and the payment terms and conditions.

Get the printable license.

License Number	3083370314273
License date	Feb 06, 2013
Licensed content publisher	John Wiley and Sons
Licensed content publication	Geophysical Research Letters
Licensed content title	Chlorate salts and solutions on Mars
Licensed copyright line	Copyright 2012 by the American Geophysical Union
Licensed content author	Jennifer Hanley,Vincent F. Chevrier,Deanna J. Berget,Robert D. Adams
Licensed content date	Apr 24, 2012
Start page	n/a
End page	n/a
Type of use	Dissertation/Thesis
Requestor type	Author of this Wiley article
Format	Electronic
Portion	Full article
Will you be translating?	No
Total	0.00 USD

ORDER MORE... CLOSE WINDOW

Copyright © 2013 Copyright Clearance Center, Inc. All Rights Reserved. Privacy statement.
Comments? We would like to hear from you. E-mail us at customercare@copyright.com

Arkansas Center for Space and Planetary Sciences
FELD 202, University of Arkansas
Fayetteville, AR 72701, USA
Tel 479 575 2183
Fax 479 575 7778
E-mail vchevrie@uark.edu

Object: Letter for Jennifer Hanley's PhD thesis

To whom it may concern,

This letter is to certify that Jennifer Hanley performed more than 51% of the work presented in the following paper: *Stability of perchlorate hydrates and their liquid solutions at the Phoenix landing site, Mars*, published in Geophysical Research Letters. Jennifer performed all the experiments, analyzed the resulting data, and helped with the interpretations and model. Therefore, she can use the work in her thesis manuscript.

Sincerely,

Vincent F. Chevrier